PHYSICAL PROPERTIES OF PROPYLENE/PROPANE MIX TURES IN ZEOLITIC IMIDAZOLATE FRAMEWORKS BY DFTB AND MOLECULAR DYNAMICS SIMULATION

Miss Benjawan Kaewruksa

A Dissertation Submitted in Partial Fulfillment of the Requirements
for the Degree of Doctor of Philosophy in Chemistry
Department of Chemistry
Faculty of Science
Chulalongkorn University
Academic Year 2018

สมบัติทางกายภาพของของผสมโพรพิลีน/โพรเพนในซีโอไลติกอิมิดาโซเลตเฟรมเวิร์กโดยดีเอฟทีบีและการจำลองพลวัตเชิงโมเลกุล

น.ส.เบญจวรรณ แก้วรักษา

วิทยานิพนธ์นี้เป็นส่วนหนึ่งของการศึกษาตามหลักสูตรปริญญาวิทยาศาสตรดุษฎีบัณฑิต
สาขาวิชาเคมี ภาควิชาเคมี
คณะวิทยาศาสตร์ จุฬาลงกรณ์มหาวิทยาลัย
ปีการศึกษา 2561

Thesis Title	PHYSICAL PROPERTIES OF PROPYLENE/PROPANE MIXTURES IN ZEOLITIC IMIDAZOLATE FRAMEWORKS BY DFTB AND MOLECULAR DYNAMICS SIMULATION
By	Miss Benjawan Kaewruksa
Field of Study	Chemistry
Thesis Advisor	Professor VITHAYA RUANGPORNVISUTI, Dr.rer.nat.

Accepted by the Faculty of Science, Chulalongkorn University in Partial Fulfillment of the Requirement for the Doctor of Philosophy

..... Dean of the Faculty of Science
(Professor POLKIT SANGVANICH, Ph.D.)

DISSERTATION COMMITTEE

..... Chairman
(Associate Professor VUDHICHAI PARASUK, Ph.D.)

..... Thesis Advisor
(Professor VITHAYA RUANGPORNVISUTI, Dr.rer.nat.)

..... Examiner
(Professor THAWATCHAI TUNTULANI, Ph.D.)

..... Examiner
(Professor PORNTHEP SOMPORNPISUT, Ph.D.)

..... External Examiner
(Assistant Professor Banchob Wanno, Ph.D.)

เบญจวรรณ แก้วรักษา : สมบัติทางกายภาพของของผสมโพรพิลีน/โพรเพนในซีโอไลติกอิมิดาโซเลตเฟรมเวิร์ก โดยดีเอฟทีบีและการจำลองพลวัตเชิงโมเลกุล. (
PHYSICAL PROPERTIES OF PROPYLENE/PROPANE MIXTURES IN ZEOLITIC IMIDAZOLATE FRAMEWORKS BY DFTB AND MOLECULAR DYNAMICS SIMULATION) อ.ที่ปรึกษาหลัก : ศ.ดรวิทยา เรืองพรวิสุทธิ์

โครงข่ายซีโอไลติกอิมิดาโซเลต (ซิฟ) คือวัสดุรูพรุนที่น่าสนใจมาก ซึ่งถูกใช้ประโยชน์อย่างมากมายสำหรับการดูดซับ การคัดแยก และการกักเก็บแก๊ส เนื่องจากความคงตัวทางความร้อนและเคมีสูง ในงานนี้ศึกษาการดูดซับของโพรเพนและโพรพิลีน ภายใต้เงื่อนไขแบบพีรีออดิก วิธีเอสซีซี–ดีเอฟทีบี พบหกและสิบเอ็ดของโครงรูปการดูดซับโพรเพนและโพรพิลีนในรูพรุนซิฟ–8 ในขณะที่พบสี่โครงรูปเท่านั้นของการดูดซับโพรเพนและโพรพิลีนในรูพรุนซิฟ–67 โครงรูปที่เสถียรที่สุดขึ้นกับพลังงานการดูดซับ ค่าพลังงานการดูดซับของโพรเพนทั้งซิฟ–8 และซิฟ–67 ต่ำกว่าโพรพิลีน ผลที่ได้นี้สอดคล้องกับประสิทธิภาพของรูพรุนซิฟ–8 และซิฟ–67 ในการแยกแก๊สผสมโพรเพนและโพรพิลีน โดยอาศัยหลักการแบ่งส่วนแก๊ส–ของแข็ง เนื่องจากความสามารถในการดูดซับของรูพรุนซิฟ–8 และซิฟ–67 จะสามารถดูดซับโพรเพนได้ดีกว่าโพรพิลีน ดังนั้นฟลักซ์การแพร่ที่แตกต่างกันของโพรเพนและโพรพิลีนในรูพรุนซิฟ–8 และซิฟ–67 จึงถูกแยกผ่านช่องหกเหลี่ยม พลังงานก่อกัมมันต์ของโพรเพนและโพรพิลีนที่ผ่านช่องหกเหลี่ยมนำไปสู่ปัจจัยในการแยกโพรเพนและโพรพิลีน และพบว่ามีสองสภาวะทรานซิชันสเตตของโพรพิลีนเกิดปฏิกิริยากับกลุ่มเมทิลและเอทิลีนกับช่องหกเหลี่ยมของอิมิดาโซเลต นอกจากนี้ได้ทำการศึกษาการแพร่ของโพรเพนและโพรพิลีนในซิฟ–8 โดยใช้แบบจำลองพลวัตเชิงโมเลกุล ซึ่งจะขึ้นกับ NVT เอนเซมเบิล โดยค่าสัมประสิทธิ์การแพร่ในตัวเองของโพรเพน, โพรพิลีน และแก๊สผสมโพรเพนโพรพิลีนอยู่ในช่วงระหว่าง 1.19×10^{-9}– 6.68×10^{-9} เมตร^2/วินาที, 3.49×10^{-10} – 8.29×10^{-10} เมตร^2/วินาที และ 1.68×10^{-9}–9.82×10^{-10} เมตร^2/วินาที ตามลำดับ จากผลชี้ให้เห็นว่าซิฟอาจเป็นวัสดุที่ดีเยี่ยมสำหรับการแยกโพรพิลีนโพรเพน

สาขาวิชา เคมี ลายมือชื่อนิสิต .....
ปีการศึกษา 2561 ลายมือชื่อ อ.ที่ปรึกษาหลัก .....

5672827523 : MAJOR CHEMISTRY
KEYWORD: DFTB, ZIF-8, ZIF-67, ADSORPTION, DIFFUSION, PROPANE, PROPYLENE

Benjawan Kaewruksa : PHYSICAL PROPERTIES OF PROPYLENE/PROPANE MIXTURES IN ZEOLITIC IMIDAZOLATE FRAMEWORKS BY DFTB AND MOLECULAR DYNAMICS SIMULATION. Advisor: Prof. VITHAYA RUANGPORNVISUTI, Dr.rer.nat.

Zeolitic imidazolate frameworks (ZIFs) are fascinating porous materials which were widely utilized for gas adsorptions, separation and storage due to its high thermal and chemical stability. In this work, adsorptions of propane and propylene in ZIF−8 and ZIF−67 pores were studied under the periodic boundary condition based on the SCC−DFTB method. Six and eleven adsorption configurations of propane and propylene molecules can be observed in the ZIF−8 pore, whereas only four adsorption configurations in the ZIF−67 pore were found. Based on the most stable configurations, the adsorption energies of propane both ZIF−8 pore and ZIF−67 pore are lower than propylene. These results agree with abilities of ZIF−8 and ZIF−67 pores to separate propane/propylene mixture based on the principle of gas–solid partition. Due to adsorption abilities of ZIF−8 and ZIF−67 pores which can adsorb propane better than propylene, ZIF−8 and ZIF−67 pores, therefore, differentiate diffusion flux of propane and propylene via the hexagonal aperture. Activation energies of propane and propylene via the hexagonal aperture lead to the separation factor of the propylene/propane. As two transition–state structures of propylene interacting with methyl and ethylene groups of imidazolate belonging to the hexagonal aperture were found. In addition, diffusion of propane and propylene in the ZIF–8 were investigated using molecular dynamics simulation based on the NVE ensemble. The self–diffusivity coefficient of propane, propylene and propane/propylene mixtures were within the ranges of 1.19×10^{-9}–6.68×10^{-9} m^2/s, 3.49×10^{-10}–8.29×10^{-10} m^2/s and 1.68×10^{-9}–9.82×10^{-10} m^2/s, respectively. The results suggest that ZIFs could be an excellent material for the separation of propylene/propane.

Field of Study:	Chemistry	Student's Signature .....
Academic Year:	2018	Advisor's Signature .....

ACKNOWLEDGEMENTS

This dissertation would not be possible and completed without people who encouraged and supported me. Consequently, in this acknowledgment, I would like to declare and thank the people that have collaborated in my work.

Firstly, I would like to gratefully thank my advisor Prof. Dr. Vithaya Ruangpornvisuti for useful guidance, understanding and constant support throughout the course of this research.

I would like to take this chance to thank my dissertation committee, Assoc. Prof. Dr. Vudhichai Parasuk, Prof. Dr. Thawatchai Tuntulani, Prof. Dr. Pornthep Sompornpisut, and Asst. Prof. Dr. Banchob Wanno, who act as the thesis committee. Their sincere suggestions are definitely imperative for accomplishing my dissertation.

Special thanks to the 100th Anniversary Chulalongkorn University Fund for Doctoral scholarship for financial supporting, the Chemistry, Faculty of Science, Chulalongkorn University for research facilities and all members in Supramolecular Chemistry Research Unit for their kind help. I also would like to thank all the teaching staff and my friends for all their good suggestions, friendship, and continuous encouragement.

Finally, I would like to thank my family, all lab's members for their infinite love and for always supporting and trusting in my decisions. I am very proud to be a part of this beloved family.

Benjawan Kaewruksa

TABLE OF CONTENTS

Page

..... iii

ABSTRACT (THAI) iii

.....iv

ABSTRACT (ENGLISH).....iv

ACKNOWLEDGEMENTS.....v

TABLE OF CONTENTS.....vi

LIST OF TABLES.....ix

LIST OF FIGURES x

CHAPTER I INTRODUCTION.....1

1.1 Research rationale.....1

1.2 Zeolitic imidazolate frameworks (ZIFs) 3

1.3 Applications.....5

1.3.1 Gas adsorption.....5

1.3.2 Gas separation 5

1.3.3 Gas storage 6

1.4 Zeolitic imidazolate frameworks−8 (ZIF−8).....6

1.5 Zeolitic imidazolate frameworks−67 (ZIF−67) 7

1.6 Literature reviews 8

1.7 Scope of dissertation.....9

CHAPTER II THEORETICAL BACKGROUND.....10

2.1 *Ab Initio* Method.....10

2.1.1 Hartree–Fock Method.....11

2.2 Density functional theory (DFT) method 12

2.2.1 The Kohn–Sham Equations and the Kohn–Sham Energy.....12

2.2.1.1 The KS Equations.....13

2.3 Density functional tight–binding (DFTB) method 14
2.3.1 DFTB1 15
2.3.2 DFTB2 16
2.3.3 DFTB3 17
2.4 Molecular dynamics (MD) simulation 17
2.4.1 Classical mechanics 18
2.4.2 Integration algorithms 20
2.4.3 Canonical (NVT) ensemble 22
2.4.3.1 Andersen thermostat 22
2.4.3.2 Berendsen thermostat 22
2.4.4 Gas diffusion 22
2.4.4.1 The mean-square displacement (MSD) 23
2.4.4.2 The self–diffusion coefficient 23
2.4.4.3 The radial distribution function (RDF) 23
2.4.5 Gas adsorption 24
CHAPTER III 25
DETAILS OF THE CALCULATIONS 25
3.1 Computational method 25
3.2 MD simulations details 27
3.3 Adsorption energies of propylene and propane molecules in the ZIF–8 and ZIF–67 27
3.4 Transition–state structure of gases moving through hexagonal aperture of ZIF–8 and some related theories 27
3.5 Adsorption–based energy barrier 28
3.6 Separation factor for two gases competition 29
CHATER IV 30
RESULTS AND DISCUSSION 30
4.1 Geometry optimization of ZIF–8 and ZIF–67 30
4.1.1 Interaction energy of propane on windows of the ZIF−8 pore 31

4.1.2 Interaction energy of propylene on windows of the ZIF-8 pore 35

4.1.3 Effect of adsorption configurations on separation of propane and propylene mixture in ZIF−8 38

4.1.4 Interaction energy of propane on windows of the ZIF−67 pore.....40

4.1.5 Interaction energy of propylene on windows of the ZIF–67 pore.....42

4.1.6 Effect of adsorption configurations on separation of propane and propylene mixture in ZIF–67 44

Moreover, this research also demonstrates that adsorption behavior is determined by the containing arrangement of the guest inside the host, which in turn defines how the adsorbed gas molecules distribute inside the cavities and control the gas induced opening of both ZIF–8 and ZIF–67structures. 46

4.2 Adsorption configurations of propane and propylene in ZIF–8 46

4.3 Estimation of the separation factor from activation energy.....52

4.4 MD simulations and dynamical quantities of propane and propylene in ZIF–8 pore 55

CHAPTER V 60

CONCLUSIONS.....60

REFERENCES 62

VITA 72

LIST OF TABLES

Page

Table 1 Total energies of the SCC−DFTB−optimized structure of propane and propylene adsorbed on wall of the ZIF−8 pore and their components, and its corresponding adsorption energies. 33

Table 2 The shortest bond−distances between specific atoms of propane and the ZIF−8. 34

Table 3 The shortest bond−distances between specific atoms of propylene and the ZIF−8. 37

Table 4 Total energies of the SCC–DFTB–optimized structure of propane and propene adsorbed on windows of the ZIF–67 pore and their components, and its corresponding adsorption energies. 41

Table 5 The shortest bond−distances between specific atoms of propane and the ZIF−8. 41

Table 6 The shortest bond−distances between specific atoms of propylene and the ZIF−67. 43

Table 7 Total (E_{Total}), adsorption (ΔE_{ads}) energies of propane and propylene molecules in the ZIF–8, their energy barrier (E_{B}), and separation factor (α) of propylene from the propylene/propane. 47

Table 8 The activation energies based on various properties (adsorption, diffusion and permeance) of propane and propylene molecules in the ZIF–8 cage. 53

Table 9 Diffusion constants D_s ,for the host–guest systems of 4, 8, 12 and 16 molecules of propane, propylene and propane/propylene mixtures in ZIF–8 pore at 298.15 K. 58

LIST OF FIGURES

Page

Figure 1 The kind of imidazolate linkers used in the coordination frameworks. 3

Figure 2 The bridging angles between metal and imidazolate linkers of ZIFs (1) and zeolites structure (2) [16].....4

Figure 3 Crystal structures of ZIFs were shown in left and center columns. The largest cage in each ZIF was shown in right column [41].....4

Figure 4 The single crystal structure of ZIF–8: Zn (polyhedral), C (line), and N (sphere) [49].....6

Figure 5 The single crystal structure of ZIF–67: Co (polyhedral), C (line), and N (sphere) [50].....7

Figure 6 The DFTB optimized structures of the ZIF–8 and ZIF–67 pores and approximated pore apertures (six–membered ring window), based on ($Zn_{12}N_{48}C_{96}H_{120}$) and ($Co_{12}N_{48}C_{96}H_{120}$) periodic formulas, respectively.....26

Figure 7 The SCC−DFTB optimized structure of ZIF−8 and ZIF–67 unit−cell depicted by tube model, shown its a tetragonal aperture (TA), b hexagonal aperture (HA) and c propane (left) and propylene (right) molecules, shown by ball–stick model.....31

Figure 8 Adsorption structures of propane in the ZIF−8 pore, which the propane molecule is located close to the tetragonal aperture as configuration a PPA/ZIF-8_H, b PPA/ZIF−8_T, c PPA/ZIF−8_H/T_1, d PPA/ZIF−8_h−H, e PPA/ZIF−8_H/T_2 and f PPA/ZIF−8_h−T. “H” and “T” stand for hexagonal and tetragonal apertures, respectively, and h means at hollow position. Atoms in ZIF apertures and propane molecule, shown by tube model are the main adsorption interaction. The left and right graphics are side and top views, respectively. The adsorption energies (ΔE_{ads}), in kcal/mol are shown. 32

Figure 9 Adsorption structures of propene in the ZIF−8 pore, which the propene molecule located close to the tetragonal aperture as configuration a PPE/ZIF−8_H_1, b PPE/ZIF−8_h−H, c PPE/ZIF−8_H/T_1, d PPE/ZIF−8_H/T_2, e PPE/ZIF−8_T_1, f PPE/ZIF−8_T_2, close to the hexagonal aperture as g PPE/ZIF−8_h−H(CH_2), h PPE/ZIF−8_H_2, i PPE/ZIF−8_h−H_2(CH_3), j PPE/ZIF−8_h−H_3(CH_2) and close to the center as k PPE/ZIF−8_center. Atoms of apertures and the propane molecule, shown by tube are the main adsorption interaction. The left and right graphics are side

and top views, respectively. The adsorption energies (ΔE_{ads}), in kcal/mol are shown. 36

Figure 10 The most stable adsorption−structures of a propane and b propylene in ZIF−8 pore as configurations PPA/ZIF−8_H/T_1 and PPE/ZIF−8_T_1, respectively. Bond distances between nearest atoms of guest molecule (propane or propylene) and ZIF−8 pore are illustrated. 39

Figure 11 Adsorption structures of propane in the ZIF–67 pore, which the propane molecule is located close to the tetragonal aperture as configuration a PPA/ZIF–67_H, b PPA/ZIF–67_H/T, c PPA/ZIF–67_h–H and d PPA/ZIF–67_T. “H” and “T” stand for hexagonal and tetragonal apertures, respectively, and h means at hollow position. Atoms in ZIF apertures and propane molecule, shown by tube model are the main adsorption interaction. The left and right graphics are side and top views, respectively. The adsorption energies (ΔE_{ads}), in kcal/mol are shown. 40

Figure 12 Adsorption structures of propylene in the ZIF–67 pore, which the propylene molecule located close to the tetragonal aperture as configuration a PPE/ZIF–67_h–H_1, b ZIF–67_H/T_1, c PPE/ZIF–67_h–H_2 and d PPE/ZIF–67_T. Atoms of apertures and the propylene molecule, shown by tube are the main adsorption interaction. The left and right graphics are side and top views, respectively. The adsorption energies (ΔE_{ads}), in kcal/mol are shown.....43

Figure 13 The most stable adsorption–structures of a propane and b propylene in ZIF–67 pore as configurations PPA/ZIF–67_h–H and PPE/ZIF–67_H/T_1, respectively. Bond distances between nearest atoms of guest molecule (propane or propylene) and ZIF–67 pore are illustrated. 45

Figure 14 The optimized structure of the most stable configuration of propane molecule adsorbed on the ZIF–8 cage, (a) through–tetragonal view and (b) through–hexagonal view. All bond distances are in Å.....48

Figure 15 The optimized structure of the most stable configuration of propylene molecule adsorbed on the ZIF–8 cage, (a) through–tetragonal view and (b) through–hexagonal view. All bond distances are in Å.....49

Figure 16 The optimized transition–state structure of propane molecule adsorbed on the ZIF–8 (TS_PPA) located in between its hexagonal aperture, (a) looking through tetragonal aperture and (b) through hexagonal aperture. The right views are zoomed images of the left views. All bond distances are in Å.....50

Figure 17 The optimized transition–state structure (type I) of propylene molecule adsorbed on the ZIF–8 (TS–I_PPE) located in between its hexagonal aperture, (a)

looking through tetragonal aperture and (b) through hexagonal aperture. The right views are zoomed images of the left views. All bond distances are in Å. 51

Figure 18 The optimized transition–state structure (type II) of propylene molecule adsorbed on the ZIF–8 (TS–II_PPE) located in between its hexagonal aperture, (a) looking through tetragonal aperture and (b) through hexagonal aperture. The right views are zoomed images of the left views. All bond distances are in Å. 52

Figure 19 The energetic profile for transportation of (a) propane (PPA) molecule via transition–state structure, TS_PPA, (b) propylene (PPE) molecule via transition–state structure, TS–I_PPE by pointing its methyl group through the hexagonal aperture from inside to outside cage and (c) PPE molecule via transition–state structure, TS–II_PPE by pointing its methyl group through the hexagonal aperture from inside to outside cage. The activation energies are in kcal/mol. 54

Figure 20 The MD simulations based on the SCC–DFTB method with the Berendsen thermostat for the host–guest systems of 4, 8, 12 and 16 molecules of propane in ZIF–8 pore. 56

Figure 21 The MD simulations based on the SCC–DFTB method with the Berendsen thermostat for the host–guest systems of 4, 8, 12 and 16 molecules of propylene in ZIF–8 pore. 56

Figure 22 The MD simulations based on the SCC–DFTB method with the Berendsen thermostat for the host–guest systems of 4, 8, 12 and 16 molecules of propane/propylene mixtures in ZIF–8 pore. 57

CHAPTER I
INTRODUCTION

1.1 Research rationale

Nanoporous materials have received increasing attention for applications in several industrial processes due to their superior features such as high chemical and thermal stabilities, large surface area, small size, and high reactivity [1-3], which are the most essential factors. Hence, porous materials have wide applications as gas separation, catalysis, adsorption, and energy [4-6]. Metal–organic frameworks (MOFs) is exhibited, highlighting the significant advances in their research over the past decade. This new class of porous materials is composed of metal ions and organic linkers. Functionalities and large pore can be obtained and make this porous material for many industrial applications.

A special type of metal organic frameworks is zeolitic imidazolate frameworks (ZIFs) which constructed from tetrahedrally bonded transition metals (M = Zn, Co, Cu, Fe, etc.) linked by imidazolate (IM) ligands. ZIFs present high thermal stability, frameworks flexibility, remarkable chemical and physical properties [7-8]. This ability would be useful in many applications such as adsorption, separation, sensing catalysts, and gas storage [9-11]. Moreover, they have studied the synthesis of many types of ZIFs, such as ZIF–11 [10], ZIF–7 [12], ZIF–8 [13], ZIF–69 [14], and ZIF–67 [15].

Nowadays, many researchers have been studied the separation and adsorption of pure gases in ZIFs [16-18]. Hydrogen separations and adsorptions in various types of ZIFs such as ZIF–7 [12], ZIF–8, and ZIF–11 were widely studied. ZIF–8 has exhibited wide applications for the diffusion and adsorption of various gases (CO_2, N_2, CH_4, etc.) [19-21], catalysts [22-23], and gas storages [21, 24]. The primary applications for ZIFs in the petrochemical industry were used in purification of propylene from propylene/propane mixture [25] and the purity of propylene depends on the removal of propane in dehydrogenation reaction [26]. The ZIF–8 membranes synthesized by different methods showed excellent separation performance for propylene/propane

mixture [27-29]. Hara et al. studied on diffusive separation of propylene/propane with ZIF–8 membranes based on their performances [30-32].

The separation of propylene/propane using the ZIF–8 membranes, i.e. computed in terms of diffusivities, activation energies and adsorption properties of propane and propylene [33], and optimum separation performance of ZIF-8 membranes including its Cd^{2+}, Co^{2+} and Be^{2+} substitutes of Zn^{2+}, [34] were theoretically studied using molecular simulations. The excellent separation performance of ZIF–8 membranes for C2/C3 hydrocarbon mixtures was also found [35]. The gate opening in ZIF–8 and the self–diffusion values (Ds) of hydrocarbon molecules from for ethane and propane separation process were studied by molecular dynamics (MD) simulations based on force field parameters [36]. Investigation of the crystal size dependency of structural transitions of ZIF–8 during N_2, Ar, and *n*–butanol adsorption showed that at low pressure, isotherms of studied gases are not affected by crystal size [37]. This suggested that at low–pressure, low–loading adsorption energy is independent of crystal size, but at high–pressure, crystal downsizing suppressed the structural flexibility. Nevertheless, there are two sizes of hexagonal aperture of the ZIF–8 namely small sizes [16, 38] and large size [39]. These varied sizes resulting different performance of gas separation from its mixture have been expected. ZIF–8 and ZIF–67 have been extensively studied in terms of their separation efficiency [27, 40].

However, separation performances of membranes depend on several factors and adsorption of propylene and propane gases. ZIFs are attractive for effective factors separations of gas mixtures. Particularly ZIF–8 and ZIF–67 pores have become more specific MOF for purification in terms of adsorption and separation of propane and propylene molecules.

Even though, several publications on propylene and propane storage, adsorption and separation of their mixtures in ZIFs, the physical insight of propylene and propane gases in ZIFs has not been clarified. This becomes the main aims of this study focus on the investigation of adsorption and separation of propylene and propane mixtures in ZIF–8 and ZIF–67 pores by the density functional tight binding (DFTB) and molecular dynamic simulation methods (MD). Moreover, we have investigated interaction between single guest molecule (propane and propylene

molecules) representing low–pressure interacting with inside wall of the ZIF–8 pore using periodic density functional theory (DFT) as first–principles method. Interactions of propane and propylene gases with functional groups of the ZIF–8 and their corresponding transition–state configurations of guest molecule passing through the hexagonal aperture have been investigated. The separation factor of propylene/ propane based on their transition–state configurations have been assessed.

1.2 Zeolitic imidazolate frameworks (ZIFs)

ZIFs are a new subclass of the metal organic frameworks (MOFs) which consist of tetrahedral metal ions (M=Zn, Co, Cu, Fe, etc.) linked by imidazolate linkers or functional imidazolate ligands-based, of the kind shown in Figure 1, to make porous frameworks based on tetrahedral topologies. The angle of metal ions formed by imidazolate (IM) linkers in the metal–imidazolate–metal (namely M–IM–M) units is 145^{o}, which is similar to the Si–O–Si angle in zeolites. Therefore, ZIFs have zeolite like topologies as shown in Figure 2.

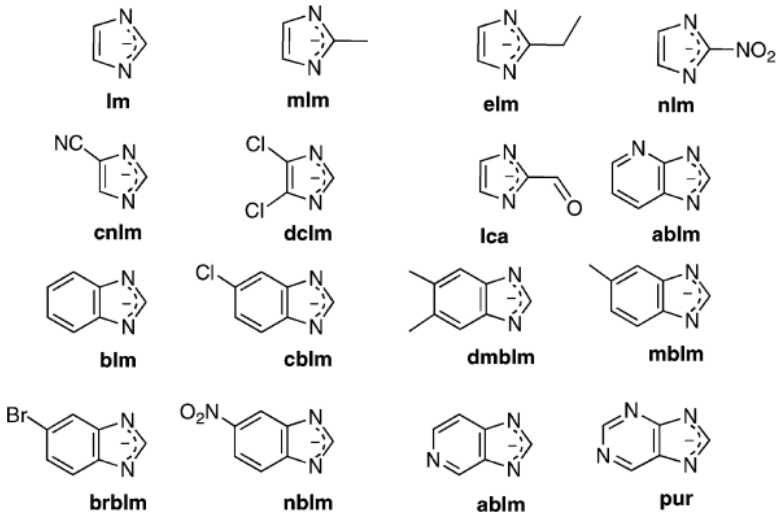

Figure 1 The kind of imidazolate linkers used in the coordination frameworks.

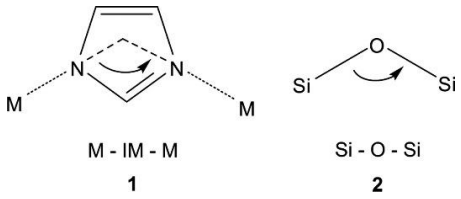

Figure 2 The bridging angles between metal and imidazolate linkers of ZIFs **(1)** and zeolites structure **(2)** [16].

Structure of ZIF is controlled by IM linkers, which have several type zeolite topologies according to the main advantages of ZIFs characteristics of both zeolites and MOFs porous materials, such as many functionalities and chemical stabilities of MOFs and catalysis, separation and sensing of zeolites. This feature confirmed the potential for a systematic approach to further developing this new category of porous crystals. The types of ZIFs with zeolitic topologies are shown in Figure 2.

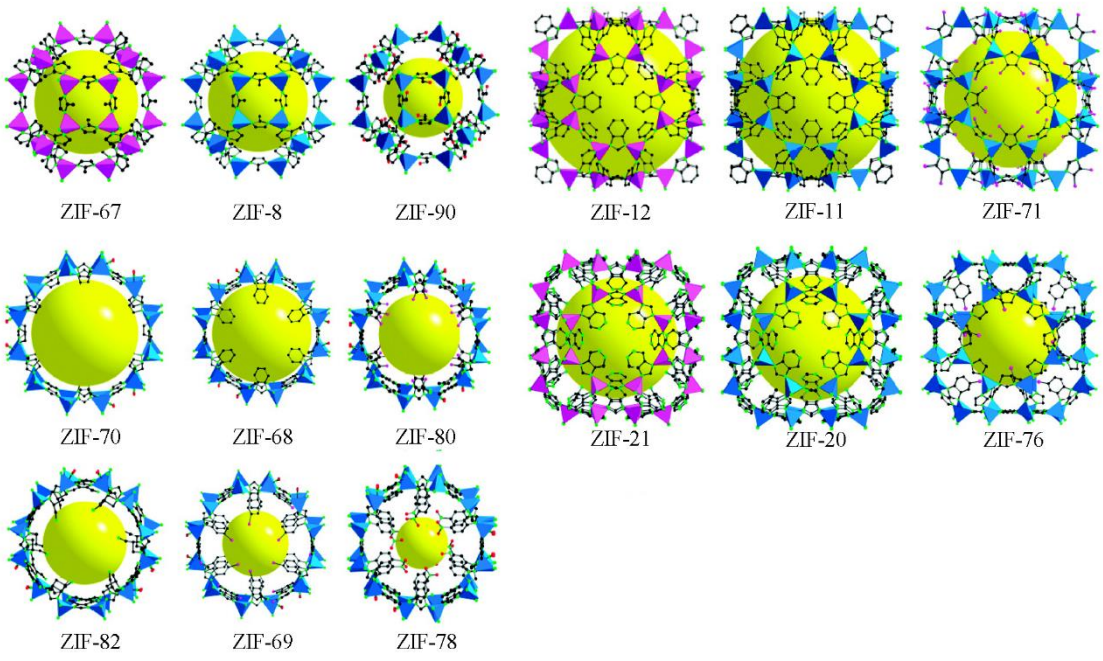

Figure 3 Crystal structures of ZIFs were shown in left and center columns. The largest cage in each ZIF was shown in right column [41].

1.3 Applications

Due to ZIFs have several classes of topologies. The key of their design was suggested by A. Phan and co−workers in 2009 [41]. They can be made for chemical properties and large surface area. ZIFs are charming candidates for various applications such as gases adsorption, separation and storage.

1.3.1 Gas adsorption

Gas adsorption processes are of outstanding excellence for developing efficient storage porous materials. The adsorption characteristics of molecules on solid surfaces have been studied many different techniques. One of the solid surfaces comes from the design to obtain numerous topologies by replacing metal and organic linkers. The result showed that ZIFs adsorbed vast amount of various gases in industrial processes [42-43].

ZIFs have been widely used for gas adsorption for light gases including hydrogen storage and light hydrocarbons [44]. In 2013, Zhang et al. [45] suggests that the post−synthetic modification of the ZIF−8 not only reforms its adsorption capacity of CO_2 considerably, but also increases its adsorption selectivity for $CO_2/N_2/H_2O$ significantly. Therefore, ZIF−8 is useful for CO_2 adsorption.

1.3.2 Gas separation

ZIFs membranes are attractive interesting for industrial gas separation applications. They have high selectivity based on strong molecular sieving behavior. The gas separation efficiency of ZIFs membranes can be considered by making the shapes and sizes of their pores and by the chemical functionalization of ZIFs membranes Krokidas et al. [46] suggested that gas mixtures can efficiently been separated with porous of ZIF−8 and ZIF−67 via the size exclusion using sub nanometer pore edges. The response of the membranes to the demonstration of diffusing molecules of different sizes from He (2.66 Å) up to n−butane (4.16 Å) has been analyzed, providing data on how huge molecules pass through the apertures that

connect the framework cages. Thus, both ZIF–8 and ZIF–67 are advantageous for gas mixtures.

1.3.3 Gas storage

The pore topology of ZIFs, which is defined by their crystal topology, is a remarkable feature in the gas storage applications. This specific surface area could lead to a new path for the design of ZIFs membranes aimed at gas storage. Ma et al. [47] indicate that ZIFs showed great agreement for the adsorptive storage of carbon dioxide, methane and hydrogen and in clean energy applications. The rising efficiency to improve pore size and pore wall functionality permits researchers to concentrate on those key factors which fixing the most promise, increasing both the high area to volume ratio utilizable for the affinity and storage of the porous network for the stored gas molecules. Remarkably, ZIFs present permanent porosity, which generate its appealing candidates for gas storage.

1.4 Zeolitic imidazolate frameworks–8 (ZIF–8)

ZIF–8 is composed of zinc ions coordinated by 2–methylimidazole forming a sodalite (SOD)–like structure which is similar to Si and Al atoms types of zeolite structures. It has large pore cavity of about 11.4 Å [48] diameter, which is composed of 4 member ring windows, 6 member ring windows and ZnN_4 clusters of 3.3 Å [48] diameter (Figure 4).

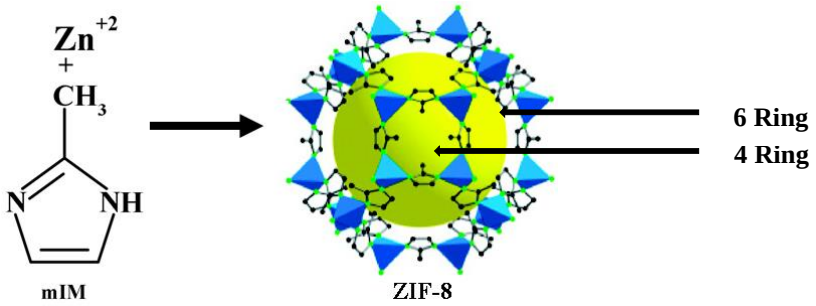

Figure 4 The single crystal structure of ZIF–8: Zn (polyhedral), C (line), and N (sphere) [49].

This structure makes ZIF–8 especially attractive as a molecular sieve. Another interesting factor is the flexibility of framework, permitting adsorption of molecules whose dimensions are abundant larger than the conventional pore diameter.

1.5 Zeolitic imidazolate frameworks–67 (ZIF–67)

ZIF–67 is consists of cobalt ion connected by 2–methylimidazole linkers to combine a three–dimensional framework with sodalite framework topology (SOD) like structure similar to ZIF–8 and a pore size of about 3.4 Å [49], which has large pore cavities about 11.6 Å as shown in Figure 5.

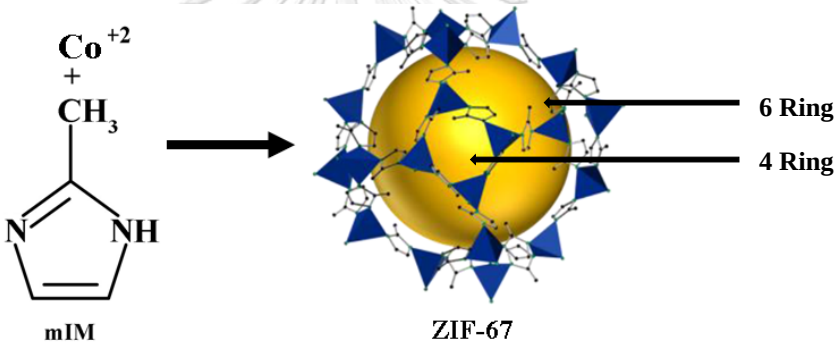

Figure 5 The single crystal structure of ZIF–67: Co (polyhedral), C (line), and N (sphere) [50].

ZIF–67 is one of the typical zeolitic imidazole frameworks ZIF–67 has potential application in gas separation, gas adsorption and gas storage due to physical characteristics and flexible pore size in the framework. In addition, it has high chemical and thermal stabilities as a function of chemical structure.

1.6 Literature reviews

The ZIF–8 and ZIF–67 have fascinated researchers from numerous fields for computer simulation and experimental data in publications. Gas separation by adsorption and diffusion for small gases in ZIF–8 and ZIF–67 pores have been severally provided information. The aim of the present report is to study the interaction configurations and the permeability behaviors of gases molecules in ZIFs pores.

In previous work, hydrogen adsorptions in difference types of ZIFs such as ZIF–7 [12], ZIF–8 [10] and ZIF–11 [10] were extensively studied. Hydrogen permeations through various porous membranes of ZIF–8 [13], ZIF–7 [51], ZIF–90 [13] and hydrogen separation using ZIF–8 were investigated. Adsorption of CO_2, N_2 and CH_4 in ZIF–8, ZIF–78 and ZIF–79 was studied by different theoretical approaches for gas storage applications [11]. Studies for kinetic transformation on ZIF–8 and ZIF–67 [52] were made. Other types of ZIFs were synthesized and studied for CO_2 capture [8].

In 2015, Verploegh et al. [53] examined accurate and effective predictions of hydrocarbon (methane, ethane, ethylene, propane, propylene, n–butane, and 1–butene) diffusivities in zeolitic imidazolate frameworks (ZIFs) by the Wicke–Kallen bach (WK) technique and dynamically corrected transition state theory (dcTST). ZIFs are attractive, due to the small pore size of materials such as ZIF-8 and the extensive range of diffusion time scales of hydrocarbon molecules in ZIFs. They have computationally measured different molecules (kinetic diameters of 2.66−5.10 Å) in ZIF−8 through dcTST. The dcTST method was also used to study the effect of hydrocarbon loadings. Comparison of the computed diffusivities to extant experimental results shows surprising approval inside an order of magnitude for all the molecules.

In 2016, Wang et al [54] studied the separation performances of propylene/ propane mixtures in ZIF–67 by zinc–substituted nanocrystals and polycrystalline membranes using a counter diffusion–based in situ method. The result showed that the substituted amount of zinc ion increased the separation accomplishments for propylene/propane mixtures in ZIF–67 polycrystalline membranes and improved hydrothermal stability of membranes and crystals. This metal–substitution strategy

was considered to permit excellent–tuning of the efficient pore aperture for other MOF membranes and was achieved for efficiently separating other valuable and challenging gas–pairs, such as ethylene/ethane.

Many experimental results have been investigated to understand the separation, adsorption and diffusion of small gases in ZIF–8 and ZIF–67 pores. Experimental data give a straightforward and powerful way to obtain knowledge. For theoretical calculation methods studied to know the interaction behaviors of gas molecules on ZIF–8 and ZIF–67 pores in invisible mechanisms and results sketched from computer simulations product important guidelines for development of new ZIFs.

The main objective of this work is to investigate the diffusion and adsorption of gas molecules in ZIF–8 and ZIF–67 pores.

1.7 Scope of dissertation

The aim of this research is to investigate geometries, interaction and physical properties of the adsorption, separation, and diffusion behavior of propylene/propane mixtures in ZIF–8 and ZIF–67 pores.

The calculation of nanoporous materials to be employed for investigating adsorption, separation and diffusion behavior of propylene/propane mixtures studies can be carried out using DFTB periodic boundary conditions and the MD simulations method. The separation of propylene/propane using the ZIF–8 membranes, i.e. computed in terms of diffusivities, activation energies and adsorption properties of propane and propylene [33] and the adsorption and diffusion abilities, in terms of MSD, the self–diffusion coefficient, RDF and interaction energies, will be analyzed and reported.

CHAPTER II
THEORETICAL BACKGROUND

Quantum mechanical (QM) method is the fundamental knowledge and tools for physicists and chemists to solve scientific problems as numerical experiments can be carried out without synthesis. QM method is classified into ab initio, DFT and semi–empirical calculations. The aims of this technique are to copy and amplify real experiments. On the other hand, computational simulation can be applied as a beneficial predictive tool [55], which is used to describe and predict chemical and physical properties of chemical systems in porous materials.

Density functional tight binding (DFTB), was employed to calculate structures, interaction and properties of molecules. In this work.

2.1 *Ab Initio* Method

Ab initio calculation method is a computational chemistry method based on quantum mechanics. This method in principle can lead to a rational approximation to the solution of the Schrödinger equation as shown in equation (2.1).

$$\hat{H}\Psi = E\Psi \tag{2.1}$$

where $\hat{H}$ is Hamiltonian operator, Ψ is electronic wavefunction and E is the energy of an electron on orbital in independent particle model. Whereas there is no solution for many–electron systems and Hartree–Fock (HF) method is the starting point of *ab initio* method.

2.1.1 Hartree–Fock Method

The Hartree–Fock method is the basis of molecular theory. The simplest way to represent Ψ for many–electron systems is combination of all atomic orbitals in the system as linear combination of atomic orbitals (LCAO). The probable approximate wavefunction for a polyelectronic as product of one–electron wavefunctions is written and called Hartree product

$$\Psi_0 = \psi_0(1)\psi_0(2)\psi_0(3)...\psi_0(n) \tag{2.2}$$

Here Ψ_0 is function which depends on the coordinates of all electrons in the atom, is a $\psi_0(1)$ function of the first electron, $\psi(2)$ is a function of the second electron, etc., the one–electron, etc. are called atomic orbitals. $\psi_0(n)$ are the initial estimate which can be described for basis set. Owing to the HF nonlinear approximation, the mathematical method to solve equation of HF is called self–consistent–field–procedure (SCF). The major steps in initial function, ψ_0, is solved in Schrödinger equation. The first cycle calculation presents more correct set of orbitals.

The SCF procedure is moved for *k* cycles until self–consistency is completed. Therefore, the configuration state functions and spin–orbitals can be created by HF equation. Although these HF equations disregards electron correlation in the system. The electrons of the system can shift independently in an average field potential, which it is hard to practice the exact calculations with large basis sets containing many atoms and electrons. Consequently, DFT has become a necessary part for chemical system simulation.

2.2 Density functional theory (DFT) method [56]

DFT has become widely the popular method for calculating properties of many–electron system. This methods are founded by the Hohenberg–Kohn (HK) theorems [57]. The HK theorems constructed the electronic density as variable to calculate electronic–structure and the energy of a molecule is come from the electron density replaced in a wave function. HK–DFT shows that electron density function, $F(p_0)$, can define the ground state properties functional, $f(x)$, e.g. energy, E_0 of a many–electron system.

$$E_0 = F[\rho_0] = E[\rho_0] \tag{2.3}$$

The total electronic energy of molecule to obtain from a trial electron density, ρ_t, is the energy of the electrons in motion under the nuclear potential called external potential, $\upsilon(r)$. The energy functional of exact ground state electron density, E_v, was stated by the second HK–DFT.

$$E_v[\rho_t] \geq E[\rho_0] \tag{2.4}$$

where ρ_0 is exact ground state energy according to exact electronic density.

2.2.1 The Kohn–Sham Equations and the Kohn–Sham Energy

The Kohn and Sham (KS) DFT is the sum of the exchange and correlation energies of a uniform electron molecule. The KS–DFT presented an efficient one–electron system in the ground–state electronic energy which is obtained from a sum term of the kinetic energy, the potential energy, the Coulomb interaction energy and the exchange–correlation energy. Then, choose the initial guess of the electron density in the KS–DFT equations calculate the KS orbitals which are improved by a process

that like HF or SCF method. Finally, KS orbitals can be used to calculate an electron density which is used to calculate accurate total energy of system.

2.2.1.1 The KS Equations

The KS equations have theorem obtained from using the variation principle, which the second HK theorem convinces applies to DFT. We use the fact that the electron density of the reference system, which is the same as that of our real system, is given by

$$\rho_0 = \rho_r = \sum_{i=1}^{2n} \left|\psi_i^{KS}(1)\right|^2 \tag{2.5}$$

where the $\psi_{\mathrm{i}}^{\mathrm{KS}}$ are the KS spatial orbital. Replacing the above definition for the orbitals to the energy and fluctuating E_0 with consideration to the point to the limitation that these remain orthonormal lead to the KS equations, algorithm is like to that used in deriving the HF equations,

$$\left[-\frac{1}{2}\nabla_{\mathrm{i}}^2 - \sum_{nucleiA}\frac{Z_{\mathrm{A}}}{r_{\mathrm{iA}}} + \int\frac{\rho(r_2)}{r_{12}}dr_2 + v_{\mathrm{xc}}(1)\right]\psi_{\mathrm{i}}^{\mathrm{KS}}(1) = \varepsilon_{\mathrm{i}}^{\mathrm{KS}}\psi_{\mathrm{i}}^{\mathrm{KS}}(1) \tag{2.6}$$

where ε_i^{KS} are the KS energy levels and $v_{\mathrm{xc}}(1)$ is the exchange–correlation potential, arbitrarily determined here for electron number (1), because the KS equations have a fix of one electron equations with where subscript *i* operate over all the 2*n* electron in the system from 1 to *n*,. The exchange–correlation energy is determined as the functional derivative from ρ(r)

$$v_{\mathrm{xc}}(\mathrm{r}) = \frac{\delta E_{\mathrm{xc}}[\rho(\mathrm{r})]}{\delta\rho(\mathrm{r})} \tag{2.7}$$

We require the derivative v_{xc} for the KS equations, and the exchange–correlation function itself for the energy equation. The following KS equations can be written as

$$\hat{h}^{KS}(1)\psi_i^{KS}(1) = \varepsilon_i^{KS}\psi_i^{KS}(1) \tag{2.8}$$

The KS operator $\hat{h}^{KS}$ is determined by equation (2.6). The difference between DFT method is the selection of the functional from of the exchange–correlation energy. Functional of DFT forms are often created to obtain a confident restricting behavior, and fitting parameters to understand correct data. Which functional is the better will have to be solved by comparing the efficiency with experiments or high–level wave mechanics calculations.

2.3 Density functional tight–binding (DFTB) method [58]

Density functional tight–binding (DFTB) method, one of quantum mechanics method based on DFT was used to calculate molecular and material properties, which has an efficient and fast quantum mechanical simulation method. DFTB can be derived from a Taylor expansion of the KS–DFT density functional

$$\rho(r) = \rho^0(r) + \delta\rho(r) \tag{2.9}$$

The exchange–correlation energy functional is described in a Taylor series and the total energy can be written as

$$E^{DFTB3}[\rho+\delta\rho] = E^0[\rho_0] + E^1[\rho_0,\delta_\rho] + E^2\left[\rho_0,(\delta_\rho)^2\right] + E^3\left[\rho_0,(\delta_\rho)^3\right] \tag{2.10}$$

2.3.1 DFTB1

DFTB1 or non–self–consistent DFTB (non–SCC) DFTB is involved only the two terms of equation (2.10), $E^0[\rho_0]$ and $E^1[\rho_0, \delta_\rho]$. DFTB1 is based on linear combination of atomic orbital (LCAO) of the KS orbitals.

$$\varphi_i = \sum_\mu c_{\mu i} \phi_\mu \tag{2.11}$$

The atomic orbitals (AOs) are received from DFT calculations of the corresponding atoms.

$$\left|\phi_\mu\right\rangle = \left|\phi_\mu\right\rangle - \sum_{b\neq a}\sum_\kappa \left|\phi_\kappa^b\right\rangle\left\langle\phi_\kappa^b\middle|\phi_\mu\right\rangle,\ \mu\varepsilon\{a\} \tag{2.12}$$

where $\left|\phi_\mu\right\rangle$ is the valences AO μ at atom a and $\left|\phi_\kappa^b\right\rangle$ is a core orbital at atom b, as obtained from the corresponding atomic calculations.

The atomic KS equations are usually solved applying an additional potential to the atomic KS equations.

$$\left[-\frac{1}{2}\Delta^2 + v^{\text{eff}}\left[\rho^{\text{atom}}\right] + \left(\frac{r}{r_0}\right)^2\right]\phi_\mu = \varepsilon_\mu \phi_\mu \tag{2.13}$$

Then, with AO basis and initial density determined, the KS equation can be solved leading to the energy.

$$E^1 = \sum_i n_i \varepsilon_I \tag{2.14}$$

where n_i is an occupation number of KS orbital i.

This is the electronic energy of the DFTB method. To find the total energy, the E_0 is to be approximated. This term in DFTB is approximated by a sum of pair potentials called repulsive energy term.

$$E_0[\rho_0] \approx E_{\text{rep}} = \frac{1}{2}\sum_{\text{ab}} v_{\text{ab}}^{\text{rep}} \tag{2.15}$$

The total energy for DFTB1 is defined as

$$E^{\text{DFTB1}} = \sum_i n_i \varepsilon_i + \frac{1}{2}\sum_{ab} v_{\text{ab}}^{\text{rep}} \tag{2.16}$$

2.3.2 DFTB2

DFTB2 approximates E^2 term in equation (2.10) further. The density fluctuations are written as a superposition of atomic contributions.

$$\Delta\rho = \sum_a \delta\rho_a \tag{2.17}$$

By assessed assuming an exponentially decaying charge density

$$\Delta\rho \approx \Delta q_a \frac{\tau_a^3}{8\pi} e^{-\tau_a |r - R_0|} \tag{2.18}$$

E^2 in (2.10) is defined as

$$E^2(\tau_a, \tau_b, R_{ab}) = \frac{1}{2}\sum_{ab} \Delta q_a \Delta q_b \gamma_{ab}(\tau_q, \tau_b, R_{ab}) \tag{2.19}$$

The Hartree term therefore explains the interaction of the charge density fluctuations $\delta\rho a$ and $\delta\rho b$, which decreases to Coulomb interaction of partial charges Δqa and Δqb for large distances, i.e. γab approaches $1/Rab$ for huge distances.

2.3.3 DFTB3

For E^3, the same approximations are started as for E^2. The third–order terms explain the change of the chemical hardness of an atom with its charge state, a new parameter is introduced, the chemical hardness derivative. A function Γ_{ab} results as derivative of the γ–function with point to charge by introducing the Hubbard derivative parameter.

With all these approximations, the SCC–DFTB total energy in the third order is given by

$$E^{DFTB3} = \sum_{iab}\sum_{\mu\in a}\sum_{\nu\in b} n_i c_{\mu i} c_{\nu i} H^0_{\mu\nu} + \frac{1}{2}\sum_{ab}\Delta q_a \Delta q_b \gamma^h_{ab} + \frac{1}{3}\sum_{ab} q_a^2 \Delta q_b \Gamma_{ab} + \frac{1}{2}\sum_{ab} V^{rep}_{ab} \quad (2.20)$$

2.4 Molecular dynamics (MD) simulation

Molecular dynamics (MD) simulations compute the time dependent behavior of a molecular system that can be used effectively to study in physical chemistry. The basic idea here is predicted accurately motion, which describes how the behavior of a physical system such as positions, velocities and conformational changes of molecule with time. Since the time evolution of chemical and physical properties and many phenomena such as diffusions, chemical reactions are described by MD simulation. In general, motion was calculated from integrating Newton's equations. The integration ought to be done numerically using one of some well–known numerical integrators and the potential energy function.

2.4.1 Classical mechanics

MD simulation method is based on Newton's second law or another equation of motion for suitable boundary conditions of the geometry in system. Knowledge of the force on each atom and of conformational energy is required, it is probable to define the acceleration of molecule in the system. Integration of Newton's second law of equations then yields a trajectory which explains the accelerations, velocities and positions of atoms as they fluctuate with time. The average values from this trajectory of properties can be defined from this trajectory. The velocities and positions of each atom in system can be predicted at any time in the future or the past [59-60].

Newton's equation of motion is given by equation (2.21).

$$F_i = m_i a_i \tag{2.21}$$

where F_i is the total force of atom i, m_i is the mass of atom i and a_i is the acceleration of atom i. After that force can also be shown as the gradient of the potential energy by equation (2.22).

$$F_i = -\nabla_i U \tag{2.22}$$

Then, integrating these two equations yields from (2.21) and (2.22) are giving in equation (2.23).

$$F = -\frac{dU}{dr_i} = m_i \frac{d^2 r_i}{dt^2} \tag{2.23}$$

where U is the potential or conformational energy of the system. Therefore, Newton's equations of motion associated with the potential energy for changing the position as a function of time.

The average positions of the lattice atoms obtain from experimental structures such as the X–ray crystal structure determined by NMR spectroscopy. These can be used as initial position of the lattice atoms while the initial positions of the guests are chosen randomly.

The initial of velocities are defined from a random distribution with the magnitudes conforming to the needed temperature, which gives the possibility density (W) that an atom i has *a* velocity v_x in the x direction at a temperature (T) shown in equation (2.24)

$$W\left(v_{ix}\right)=\left(\frac{m_{\mathrm{i}}}{2\pi k_{\mathrm{B}}T}\right)^{1/2} exp\left(-\frac{1}{2}\frac{m_{\mathrm{i}}}{k_{\mathrm{B}}}\frac{v_{ix}^{2}}{T}\right) \tag{2.24}$$

The velocities are corrected to fulfill.

$$P=\sum_{\mathrm{i}=1}^{\mathrm{N}} m_{\mathrm{i}} v_{\mathrm{i}0}=0 \tag{2.25}$$

The temperature is estimated from the velocities using equation (2.26) when N is the number of atoms in the system using the equipartition theorem of statistical mechanics. k_B is Boltzmann constant.

$$T=\frac{1}{\left(3Nk_{\mathrm{b}}\right)}\sum_{i=1}^{\mathrm{N}}\frac{\left|P_{\mathrm{i}}v_{\mathrm{i}}\right|}{m_{\mathrm{i}}} \tag{2.26}$$

While the MD simulation the sites and velocities are stored. The trajectory can be used to estimate configurational properties (accelerations, positions and velocities)

and dynamic quantities like to time correlation functions and transport coefficients of all N atoms from the trajectory [60].

2.4.2 Integration algorithms

Function of potential energy is atomic positions (3N) of all the atoms in the system. Due to the complexed nature of this function, there is no analytical solution to the equations of motion, they must be solved numerically. Therefore, the solution of equations of motion use a finite difference approach that is performed by the use of an integration algorithm. Many numerical algorithms are developed for the integration processes in molecular dynamics for integrating the equations of motion such as Toxvaerd, Verlet, Leapfrog and Gear algorithm. The importance in choosing which algorithm to apply. The criteria should be dealt with computational performance, long time step for integration and conserved energy and momentum. The Velocity–Verlet algorithm has been chosen which is the most common one.

This algorithm defines accelerations, velocities, positions and combines two Taylor expansions, as follows. The Taylor series for position from time t forward to $t + \Delta t$ is:

$$x_i(t+\Delta t) = x_i(t) + \frac{dx_i(t)}{dt}\Delta t + \frac{1}{2}\frac{d^2x_i(t)}{dt^2}\Delta t^2 + \frac{1}{3!}\frac{d^3x_i(t)}{dt^3}\Delta t^3 + O\left(t^4\right) \qquad (2.27)$$

The Taylor series from t backward to $t–\Delta t$ is:

$$x_i(t-\Delta t) = x_i(t) - \frac{dx_i(t)}{dt}\Delta t + \frac{1}{2}\frac{d^2x_i(t)}{dt^2}\Delta t^2 - \frac{1}{3!}\frac{d^3x_i(t)}{dt^3}\Delta t^3 + O\left(t^4\right) \qquad (2.28)$$

Adding these two expansions eliminates all odd–order terms, leaving

$$x_i(t+\Delta t) = 2x_i(t) - x_i(t-\Delta t) + \frac{d^2x_i(t)}{dt^2}\Delta t^2 + O\left(\Delta t^4\right) \qquad (2.29)$$

The acceleration in (2.29) is obtained from the intermolecular forces. To approximate velocities, practitioners have designed different schemes, one being an estimate for the velocity at the half–step:

$$v_i\left(t+\frac{1}{2}\Delta t\right)\approx\frac{x_i\left(t+\Delta t\right)-x_i\left(t\right)}{\Delta t} \tag{2.30}$$

Verlet himself is used the first–order central difference estimator.

$$v_i\left(t\right)\approx\frac{x_i\left(t+\Delta t\right)-x_i\left(t-\Delta t\right)}{2\Delta t} \tag{2.31}$$

Verlet's algorithm is a two–step method because it approximates x_i $(t + \Delta t)$ from the present position x_i (t) and the former position x_i $(t – \Delta t)$. Consequently, it is not self–starting initial positions (x_0) and velocities (v_0) are not enough to start a calculation, and something specific must be done for example hypothesis about $x(–\Delta t)$ can be made. The Verlet algorithm is normal and has very good stability for reasonably large time steps. In its initial form molecular velocities do not resemble, in struggle with the viewpoint that the phase–space trajectory depends equally on velocities and positions. The current formulations [43, 44] of the method often overcome this asymmetric view [61-62].

2.4.3 Canonical (NVT) ensemble

The canonical ensemble is a statistical ensemble that is specified via the system, number of particles N, volume V and temperature T. These systems describe a system in contact with a heat bath. Energy of endothermic and exothermic processes can be exchanged with the bath that has the wished temperature [63].

2.4.3.1 Andersen thermostat

The Andersen thermostat is a scheme in molecular dynamics simulation for keeping constant temperature conditions. It is couple the system to a heat bath that imposes the desired temperature. The coupling to a heat bath is substituted by stochastic conflict that perform sometimes on randomly selected particles [64].

2.4.3.2 Berendsen thermostat

In Berendsen thermostat, another way to control the temperature is weakly coupled to an external heat bath. This thermostat suppresses fluctuations of the kinetic energy of the system and consequently cannot produce trajectories correspond to the canonical ensemble. The temperature of the system is corrected such that the deviation exponentially decays with some time constant.

2.4.4 Gas diffusion

Gas diffusion is the transport process of particles moving, which is the movement of particles or molecules from an area of higher concentration to an area of lower concentration and self–diffusion, which is a mixing migration by irregular thermal motion.

2.4.4.1 The mean-square displacement (MSD)

The mean–square displacement (MSD) [65] is one of the most significant dynamical quantities that can be calculated from the time evolution of a simulated system defined by,

$$MSD = \frac{1}{N}\left\langle \sum_{i=1}^{N}\left[r_{\mathrm{i}}^{\mathrm{c}}(t) - r_{\mathrm{i}}^{\mathrm{c}}(0)\right]^2 \right\rangle = \Delta\left|r(t)\right|^2 \tag{2.32}$$

where $r_i^c(t)$ is the location of the center of mass of particle i at time t.

2.4.4.2 The self–diffusion coefficient

This type of diffusion can be noticed by marking some of the molecules and following the motion of marked and unmarked molecules. The self–diffusion coefficient [65] can be calculated from the long–time limit of MSD using Einstein relation. It is a direct measurement of MSD of guest molecules under equilibrium conditions.

$$D_i = \frac{1}{6}\lim_{t\to\infty}\frac{d}{dt}\left\langle \left[r_{\mathrm{i}}^{\mathrm{c}}(t) - r_{\mathrm{i}}^{\mathrm{c}}(0)\right]^2 \right\rangle \tag{2.33}$$

2.4.4.3 The radial distribution function (RDF)

The radial distribution function (RDF) represented by $g(r)$. This system, particles explains how density varies as a function of distance from a reference particle. For a system of N atoms in a volume V (with number density ρ), RDF is defined by the expression.

$$\rho g(r) = \frac{1}{N} < \sum_{i=1}^{N}\sum_{j\neq i}^{N}\delta\left(r - r_{\mathrm{ij}}\right) > \tag{2.34}$$

where the bracket indicates time average and r_{ij} is the distance between atoms *i* and *j*. If we explicitly consider the time average over the total of M time steps, t_k, in the MD, we have

$$g(r) = \frac{\sum_{K=1}^{M} N_k(r, \Delta r)}{M\left(\frac{1}{2}N\right)\rho V(r, \Delta r)} \tag{2.35}$$

where $N(r,\Delta r)$ and $V(r,\Delta r)$ are the number of local atoms and volume between the spherical shells of radius r and $(r + \Delta r)$ with the shell centered on another atom.

2.4.5 Gas adsorption

The adsorption energy (ΔE_{ads}) for gas molecules adsorbed on the surface has been computed by the equation

$$\Delta E_{ads} = E_{gas/surface} - (E_{gas} + E_{surface}) \tag{2.36}$$

where $E_{gas/surface}$ is the total energy of gas adsorbed on the surface, $E_{surface}$ is the total energy of isolated surface and E_{gas} is total energy of free gas molecule.

CHAPTER III
DETAILS OF THE CALCULATIONS

3.1 Computational method

The ZIF–8 and ZIF–67 pores, based on the X–ray diffraction structures [66-67], have a cubic space group $I\bar{4}3m$. The ZIF–8 unit–cell dimension is a=16.705 Å, V=4860.0 $Å^3$, in the case of the ZIF–67 this unit cell dimension is a=16.959 Å, V= 4833.4 $Å^3$. The geometry of the ZIF–8 and ZIF–67 pores were geometrically optimized using density functional tight binding (DFTB) periodic calculations. The geometry of ZIF–8 and ZIF–67 (Figure 1) were geometrically optimized using self–consistent charge density functional tight–binding (SCC–DFTB) periodic calculations. All SCC–DFTB calculations were performed with the code of DFTB+ version 1.3 [68]. Parameter sets "mio–0–1" for H, C, N atoms [69] "znorg–0–1" for Zn atom [70] and "trans3d–0–1" for Co atom were employed in SCC–DFTB calculations. Solid–state cubic ZIF–8 and ZIF–67 properties were calculated using PBC and converged $(1 \times 1 \times 1)$ MP k–points. In all SCC–DFTB calculations, the atomic positions were relaxed until the forces in the system became smaller than 1.9×10^{-5} eV/Å with SCC tolerance being smaller than 1.0×10^{-5} eV/Å. The periodic structures of the ZIF–8 and ZIF–67 pores based on ($Zn_{12}N_{48}C_{96}H_{120}$) and ($Co_{12}N_{48}C_{96}H_{120}$), respectively, are defined as supercell size. The ZIF–8 and ZIF–67 pores are composed of Zn and Co ions, respectively and linked by 2–methylimidazole ligands, forming the sodalite (SOD) zeolite topology (Figure 6).

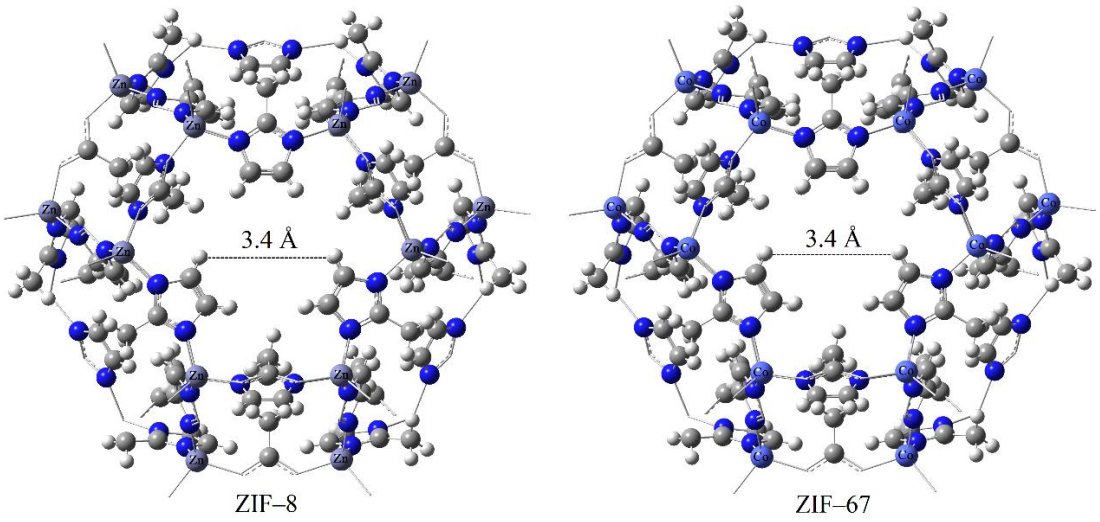

Figure 6 The DFTB optimized structures of the ZIF–8 and ZIF–67 pores and approximated pore apertures (six–membered ring window), based on ($Zn_{12}N_{48}C_{96}H_{120}$) and ($Co_{12}N_{48}C_{96}H_{120}$) periodic formulas, respectively.

All quantum–mechanical computations were carried out using the CRYSTAL14 software packages [71] implementing a periodic linear combination of atomic orbitals (LCAO) approach with atom–centered Gaussian type basis functions. Density functional theory (DFT), the B3LYP hybrid functional including Becke's three–parameter exchange [72] and Lee–Yang–Parr correlation [73] as a hybrid functional have been adopted. Basis sets used for atoms of the ZIF–8, 6–31d1G [74], 6–311G(d) [75], 86–411d31G [76], 3–1p1G [74] were used for C, N, Zn and H atoms, respectively. The basis sets of C and H atoms in propane and propylene molecules, Gatti basis sets [74] were also employed. A Monkhorst−Pack shrinking factor of 1×1×1 *k*–point was used to sample the Brillouin zone. The tolerances for geometry optimization convergence have been set to the default values and the default truncation thresholds of 10^{-6}, 10^{-6}, 10^{-6}, 10^{-6} and 10^{-12} eV/Å for the coulomb–exchange screening tolerances. Fock/Kohn–Sham matrices mixing, default value of 30 was set.

3.2 MD simulations details

The MD simulations were performed using the code of DFTB+ version 1.3 [68] to calculate structural and properties based on Newton's equation of motion. In this work, we inserted guest molecules in ZIF–8 and simulated in the NVT ensemble using the Berendsen thermostat [77] method. The MD simulations for the host–guest systems of 4, 8, 12 and 16 molecules of propane, propylene and propane/propylene mixtures in ZIF–8 pore were investigated at 298 K.

3.3 Adsorption energies of propylene and propane molecules in the ZIF–8 and ZIF–67

Adsorption energy (ΔE_{ads}) of propylene (PPE)/propane (PPA) guest molecule (G) in ZIF–8 and ZIF–67 host molecules are defined by

$$\Delta E_{ads} = E_{G/ZIF\text{-}8/67} - (E_G + E_{ZIF-8/67}) \quad (3.1)$$

where $E_{G/ZIF-8/67}$, $E_{ZIF-8/67}$, and E_G are the total energies of guest molecule (propylene/ propane) in the host (ZIF–8/ZIF–67), ZIF–8/ZIF–67 host, and propylene/propane guest molecule, respectively.

3.4 Transition–state structure of gases moving through hexagonal aperture of ZIF–8 and some related theories

Transition–state structures of adsorbate gas during diffusion through the hexagonal aperture (HA) were obtained using stationary transition–state optimization approach. The transition state theory (TST) in its classical form used for discussing and correlating on guest diffusion in MOF ZIF–8 was mentioned[78]. The transport behavior of ethylene and ethane components as a function of temperature can be elucidated through analysis of the temperature dependency of both diffusivity and solubility through the Arrhenius equation and van't Hoff equation[79], as shown in Eq. (3.2) and (3.3), respectively.

$$D_0 = D_0 e^{-E_{\alpha/RT}} \tag{3.2}$$

where D_c is corrected diffusion coefficient. D_0 is pre–exponential factor (diffusion rate) which is a function of distance between two neighboring gates (λ), and E_α is the activation energy of diffusion. *R* and *T* are the universal gas constant and the absolute temperature, respectively.

$$D_0 = \frac{1}{2}\upsilon_0 \lambda \tag{3.3}$$

$$\rho = e^{-\Delta E/RT} \tag{3.4}$$

where ν_0 is the probability of guest passing through the aperture. Permeability (*P*) of a penetrant through a membrane material, its temperature dependency follows the Arrhenius equation expressed in term of *P*, as shown in Eq. (3.5).

$$P = P_0 e^{-E_p/RT} \tag{3.5}$$

where P_0 is the pre–exponential factor, E_p is the apparent activation energy for permeation of a penetrant through a given material.

3.5 Adsorption–based energy barrier

The hopping rate of guest in the ZIF–8 material can be computed through using transition state theory (TST) [79] and Arrhenius equation, a formula for the temperature dependence of reaction rate can be stated as Eq. (3.6).

$$k = k_0 e^{-\Delta E/RT} \tag{3.6}$$

where k is rate constant, k_0 is pre–exponential factor, and ΔE is the energy barrier. Values of energy barrier were obtained through using two calculation strategies. One employed the Boltzmann–weighted free energy equation [80], as shown below:

$$E_{\mathrm{B}} = -k_{\mathrm{B}}T\ln(\rho) \qquad (3.7)$$

where E_{B} and ρ are the Boltzmann free energy profile and sorbate probability respectively.

3.6 Separation factor for two gases competition

Separation factor (α), used as guide both experimental testing and practical applications, is defined for the guest's separation by MOFs as shown in eq. (3.8) [79].

$$\alpha = \frac{e^{-E_{\mathrm{B}}^{1}/RT}}{e^{-E_{\mathrm{B}}^{2}/RT}} = e^{\Delta E_{\mathrm{B}}/RT} \qquad (3.8)$$

where E_B^1 and E_B^2 are energy barriers (activation energies) of guest molecule of number 1 and 2, respectively. ΔE_{B} is a difference of energy barriers $(E_{\mathrm{B}}^2 - E_{\mathrm{B}}^1)$.

CHATER IV
RESULTS AND DISCUSSION

This research is aimed to investigate geometries, the adsorption, separation, and diffusion behavior of propylene/propane mixtures in ZIF–8 and ZIF–67 pores. The calculation of nanoporous materials to be employed for investigating adsorption, separation, and diffusion behavior of propylene/propane mixtures studies can be carried out using DFTB periodic boundary conditions and the MD simulations. The adsorption, separation, and diffusion abilities, in terms of MSD, the self–diffusion coefficient and interaction energies, will be analyzed and reported. The details of results and discussion were shown below.

4.1 Geometry optimization of ZIF–8 and ZIF–67

The optimized structures of ZIF–8 and ZIF–67 unit–cell obtained by the SCC–DFTB method, and the unit cell parameter a = 16.705 Å and 16.959 Å, respectively at 298.15 K, were obtained. Tetragonal and hexagonal apertures of the SCC− DFTB− optimized structure of ZIF−8 and ZIF–67 unit-cell, are shown in Figure 7. Nevertheless, the gate size, size of hexagonal aperture for the optimized ZIF−8 structure (3.27 Å), computed using a model introduced by Zheng et al. (2016) being smaller than the X−ray structure (Novaković et al. 2015) (3.53 Å), in the case of the ZIF–67's aperture (3.11) computed using a model introduced by Eric et al. (2013) which is smaller than ZIF-8's, were found. This difference of approximately 0.2 Å, which agrees with experiments,[49] persists at 298 K.

ZIF–8 and ZIF–67 are sodalite (SOD) topology and sub–class of MOFs consisting of zinc ions and cobalt ions, respectively and 2-methyl imidazolate linkers and crystallizes in a cubic lattice with I43m space group (Yao and Wang 2014). It contains cavities with a diameter of 11.6 Å connected with tetragonal aperture and flexible hexagonal aperture with diameters of ~3.3 Å and ~2.2 Å, respectively (Huang et al. 2006).

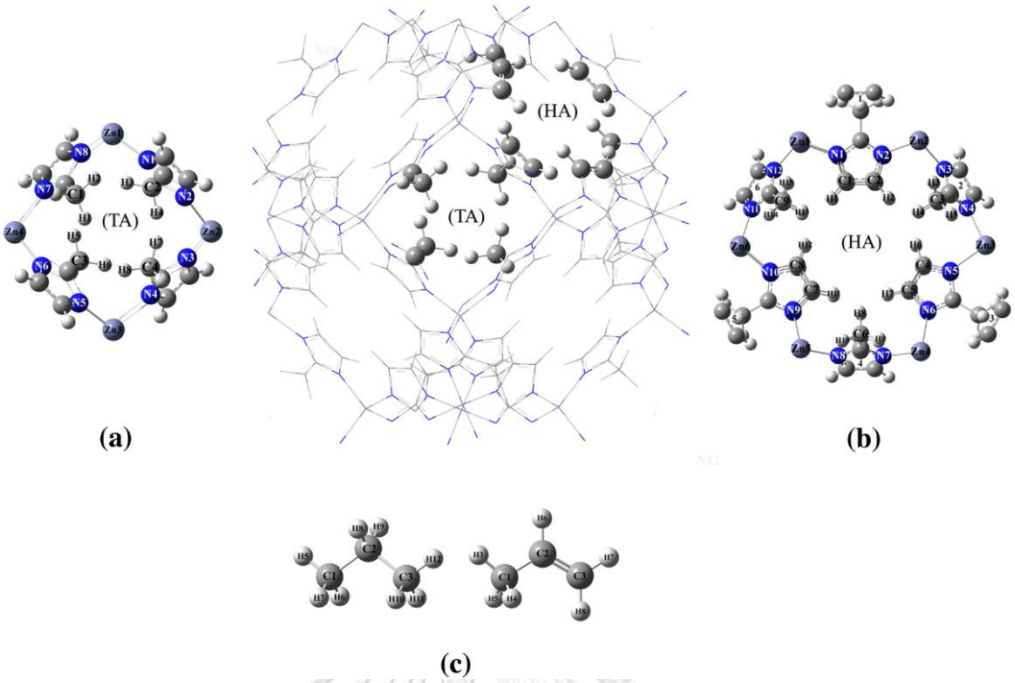

Figure 7 The SCC−DFTB optimized structure of ZIF−8 and ZIF–67 unit−cell depicted by tube model, shown its **a** tetragonal aperture (TA), **b** hexagonal aperture (HA) and **c** propane (left) and propylene (right) molecules, shown by ball–stick model.

4.1.1 Interaction energy of propane on windows of the ZIF−8 pore

The SCC−DFTB−optimized structures of propane interacting with atoms of the ZIF−8 pore are shown in Figure 7. Six configurations of propane adsorbed on wall of the ZIF−8 were found. All the configurations named as PPA/ZIF−8_H, PPA/ZIF−8_T, PPA/ZIF−8_H/T_1, PPA/ZIF−8_h−H, PPA/ZIF−8_H/T_2 and PPA/ZIF−8_h−T are defined. The first (PPA/ZIF−8_H) and second (PPA/ZIF−8_T) configurations are structures of which propane is located near the hexagonal aperture (H) and tetragonal aperture (T), respectively. The third (PPA/ZIF−8_H/T_1) is the structure of which propane is located in between the hexagonal and tetragonal apertures. PPA/ZIF−8_h−H is the structure of which propane is located at the center of the hexagonal aperture. PPA/ZIF-8_H/T_2 is quite similar to the PPA/ZIF−8_H/T_1. PPA/ZIF−8_h−T is the structure of which propane is located at the center of the tetragonal aperture. Adsorption energies (ΔE_{ads}) of propane on the

ZIF−8 cage are shown in Table 4.1. Adsorption strengths are in order: PPA/ZIF−8_H/T_1 (ΔE_{ads} = − 1.38 kcal/mol) > PPA/ZIF−8_h−H (ΔE_{ads} = − 1.08 kcal/mol) > PPA/ZIF−8_H (ΔE_{ads} = − 0.95 kcal/mol) > PPA/ ZIF−8_ H/T_2 (ΔE_{ads} = − 0.90 kcal/mol) > PPA/ZIF−8_h−T (ΔE_{ads} = − 0.66 kcal/mol) > PPA/ZIF−8_T (ΔE_{ads} = − 0.39 kcal/mol).

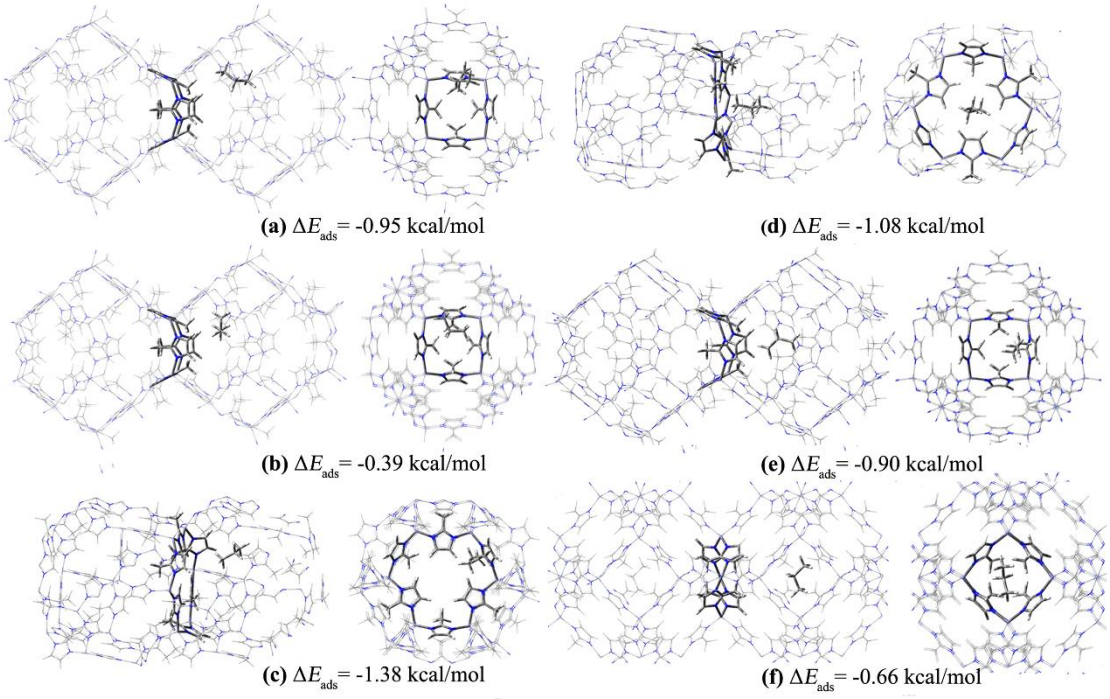

Figure 8 Adsorption structures of propane in the ZIF−8 pore, which the propane molecule is located close to the tetragonal aperture as configuration **a** PPA/ZIF-8_H, **b** PPA/ZIF−8_T, **c** PPA/ZIF−8_H/T_1, **d** PPA/ZIF−8_h−H, **e** PPA/ZIF−8_H/T_2 and **f** PPA/ZIF−8_h−T. “H” and “T” stand for hexagonal and tetragonal apertures, respectively, and h means at hollow position. Atoms in ZIF apertures and propane molecule, shown by tube model are the main adsorption interaction. The left and right graphics are side and top views, respectively. The adsorption energies (ΔE_{ads}), in kcal/mol are shown.

Table 1 Total energies of the SCC−DFTB−optimized structure of propane and propylene adsorbed on wall of the ZIF−8 pore and their components, and its corresponding adsorption energies.

Compound	E_{total}, au	ΔE_{ads}, kcal/mol
ZIF–8	–379.2730472	–
Propane	–8.178396288	–
Propene	–7.388266617	–
Propane/ZIF–8:		
2a (PPA/ZIF–8_H)	–387.4529502	–0.95
2b (PPA/ZIF–8_T)	–387.4520560	–0.39
2c (PPA/ZIF–8_H/T_1)	–387.4536361	–1.38
2d (PPA/ZIF–8_h–H)	–387.4531617	–1.08
2e (PPA/ZIF–8_H/T_2)	–387.4528811	–0.90
2f (PPA/ZIF–8_h–T)	–387.4524916	–0.66
Propylene/ZIF–8:		
3a (PPE/ZIF–8_H_1)	–386.6626219	–0.82
3b (PPE/ZIF–8_h–H_1)	–386.6626177	–0.82
3c (PPE/ZIF–8_H/T_1)	–386.6621387	–0.52
3d (PPE/ZIF–8_H/T_2)	–386.6618589	–0.34
3e (PPE/ZIF–8_T_1)	–386.6632995	–1.25
3f (PPE/ZIF–8_T_2)	–386.6630932	–1.12
3g (PPE/ZIF–8_h–H_2(CH_2))	–386.6632341	–1.20
3h (PPE/ZIF–8_H_2)	–386.6629239	–1.01
3i (PPE/ZIF–8_h–H_3(CH_3))	–386.6632785	–0.83
3j (PPE/ZIF–8_h–H_4(CH_2))	–386.6625597	–0.78
3k (PPE/ZIF–8_center)	–386.6623603	–0.66

The shortest bond−distances between propane's atoms and atoms of the ZIF−8 of all the (six) adsorption configurations are shown in Table 1 of which all locations of propane molecule in the ZIF−8 are specified. The shortest bond-distances between hydrogen atoms (ether methyl or ethylene group) of propane and hydrogen atoms of either methyl or ethylene group of imidazolate unit of the ZIF−8 are within the range of 2.14–2.66 Å.

Table 2 The shortest bond−distances between specific atoms of propane and the ZIF−8.

Configuration/bonds[a]	Bond distances (Å)
Propane/ZIF–8	
2a (PPA/ZIF–8_H)	
H1(H)···H6(G)	2.26
C2(H)···H6(G)	3.31
2b (PPA/ZIF–8_T)	
H1(H)···H5(G)	2.34
C2(H)···H5(G)	3.18
2c (PPA/ZIF–8_H/T_1)	
H1(H)···H6(G)	2.66
H2(H)···H5(G)	2.63
H3(H)···H2(G)	2.14
2d (PPA/ZIF–8_h–H)	
H1(H)···H6(G)	2.19
H2(H)···H5(G)	2.44
H3(H)···H7(G)	2.30
2e (PPA/ZIF–8_H/T_2)	
H1(H)···H6(G)	2.19
H2(H)···H5(G)	2.44
H3(H)···H7(G)	2.30
2f (PPA/ZIF–8_h–T)	
H1(H)···H6(G)	5.43
H2(H)···H5(G)	6.34
H3(H)···H7(G)	6.20

[a]A(G)···B(H) represents atom A of guest (G) bonding to atom B of host (H) and labels for all atoms are defined in Figure 8.

[b]The most stable configuration.

4.1.2 Interaction energy of propylene on windows of the ZIF-8 pore

The SCC−DFTB−optimized structures of propylene interacting with atoms of the ZIF−8 pore are shown in Figure 9. Eleven configurations of propylene adsorbed on wall of the ZIF−8 were found. All the configurations named as PPE/ZIF−8_H_1, PPE/ZIF−8_h−H,PPE/ZIF−8_H/T_1, PPE/ZIF-8_H/T_2, PPE/ ZIF−8_T_1, PPE/ ZIF−8_T_2, PPE/ZIF−8_h−H(CH_2), PPE/ZIF−8_H_2, PPE/ ZIF−8_h−H_2(CH3, PPE/ZIF−8_h−H_3(CH_2) and PPE/ZIF−8_center are defined. These configurations can be categorized into four groups as follows. The first group is collected of PPE/ZIF−8_H_1, PPE/ZIF−8_H_2, PPE/ZIF−8_h−H_1, PPE/ ZIF−8_h−H_2(CH_2), PPE/ZIF−8_h−H_3(CH_3) and PPE/ZIF−8_h−H_4(CH_2) of which propylene is located close to the hexagonal apertures. The second group is composed of PPE/ZIF−8_T_1 and PPE/ZIF−8_T_2 of which propylene is located close to the tetragonal aperture. The PPE/ZIF−8_H/T_1 and PPE/ZIF−8_H/T_2, the third group, are configurations of which propylene is located in between hexagonal and tetragonal apertures. The last group, PPE/ZIF−8_center is the configuration of which propylene is located at center of the cage. Adsorption strengths are in order: PPE/ZIF−8_T_1 ($\Delta \boldsymbol{E}_{ads}$= − 1.25 kcal/mol) > PPE/ZIF−8_h−H_2(CH_2) (ΔE_{ads}= − 1.20 kcal/mol) > PPE/ZIF−8_T_2 (ΔE_{ads} = − 1.12 kcal/mol) > PPE/ZIF−8_H_2 (ΔE_{ads}=− 1.01 kcal/mol) > PPE/ZIF−8_h−H_3(CH_3) (ΔE_{ads} = − 0.83 kcal/mol) > PPE/ZIF−8_H_1 (ΔE_{ads} = − 0.82kcal/mol) ~ PPE/ZIF−8_h−H_1 (ΔE_{ads}=− 0.82 kcal/mol) > PPE/ ZIF−8_ h−H_4(CH_2) (ΔE_{ads} = − 0.78 kcal/mol) > PPE/ ZIF−8_ center (ΔE_{ads} = − 0.66 kcal/mol) > PPE/ZIF−8_H/T_1 (ΔE_{ads} = − 0.52 kcal/mol) > PPE/ZIF−8_H/T_2 (ΔE_{ads} = − 0.34 kcal/mol).

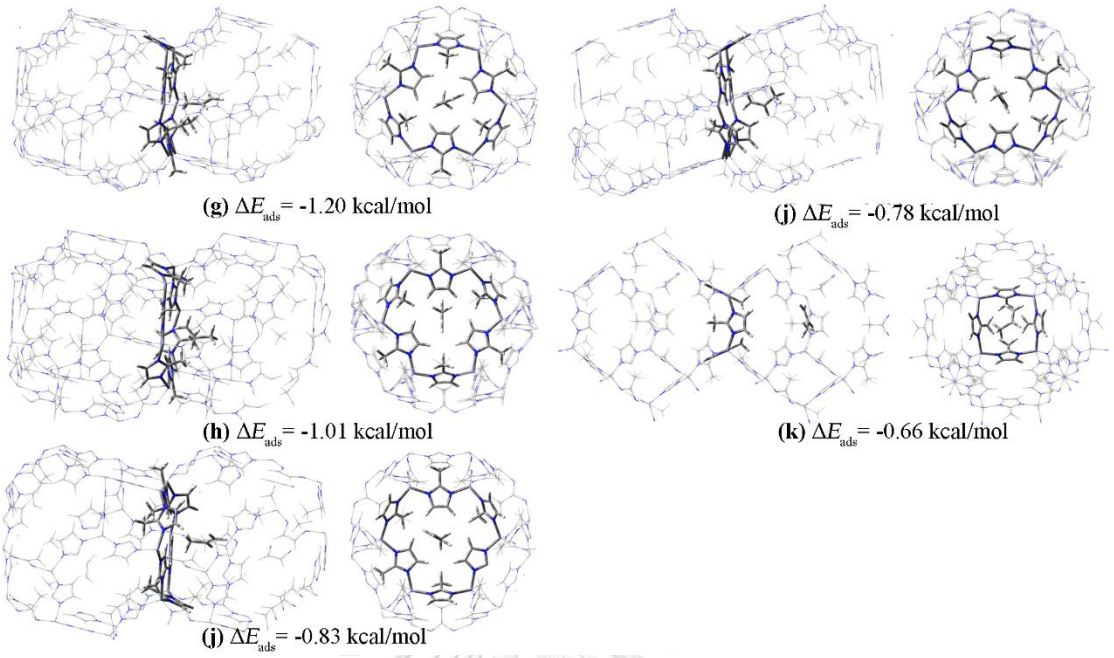

Figure 9 Adsorption structures of propene in the ZIF−8 pore, which the propene molecule located close to the tetragonal aperture as configuration **a** PPE/ZIF−8_H_1, **b** PPE/ZIF−8_h−H, **c** PPE/ZIF−8_H/T_1, **d** PPE/ZIF−8_H/T_2, **e** PPE/ZIF−8_T_1, **f** PPE/ZIF−8_T_2, close to the hexagonal aperture as **g** PPE/ZIF−8_h−H(CH_2), **h** PPE/ZIF−8_H_2, **i** PPE/ZIF−8_h−H_2(CH_3), **j** PPE/ZIF−8_h−H_3(CH_2) and close to the center as **k** PPE/ZIF−8_center. Atoms of apertures and the propane molecule, shown by tube are the main adsorption interaction. The left and right graphics are side and top views, respectively. The adsorption energies (ΔE_{ads}), in kcal/mol are shown.

Table 3 The shortest bond−distances between specific atoms of propylene and the ZIF−8.

Configuration/bonds[a]	Bond distances (Å)
Propylene/ZIF–8	
3a (PPE/ZIF–8_H_1)	
H1(H)···H7(G)	2.32
C2(H)···H7(G)	3.20
3b (PPE/ZIF–8_h–H_1)	
H1(H)···H9(G)	2.44
C1(H)···H9(G)	2.62
3c (PPE/ZIF–8_H/T_1)	
H1(H)···H8(G)	2.73
C2(H)···H8(G)	3.34
3d (PPE/ZIF–8_H/T_2)	
H1(H)···H5(G)	2.76
C2(H)···H5(G)	3.25
3e (PPE/ZIF–8_T_1)	
H1(H)···H4(G)	2.43
H2(H)···H4(G)	3.14
3f (PPE/ZIF–8_T_2)	
H1(H)···H8(G)	2.22
H2(H)···H8(G)	1.56
3g (PPE/ZIF–8_h–H_2(CH_2))	
H1(H)···H6(G)	2.47
H1(H)···H6(G)	2.45
H2(H)···H7(G)	2.52
3h (PPE/ZIF–8_H_2)	
H1(H)···H9(G)	2.90
H2(H)···H9(G)	3.00
H3(H)···H10(G)	2.27
3i (PPE/ZIF–8_h–H_3(CH_3))	
H4(H)···H6(G)	2.47
H1(H)···H6(G)	2.47
H2(H)···H7(G)	2.52
3j (PPE/ZIF–8_h–H_4(CH_2))	
H4(H)···H10(G)	2.37
H1(H)···H10(G)	2.80
H2(H)···H9(G)	2.66
3k (PPE/ZIF–8_center)	
H1(H)···H5(G)	6.22
H2(H)···H6(G)	6.42
H3(H)···H6(G)	5.17

[a]A(G)···B(H) represents atom A of guest (G) bonding to atom B of host (H) and labels for all atoms are defined in Figure 7.

[b]The most stable configuration.

The shortest bond−distances between propylene's atoms and atoms of the ZIF−8 of all the (eleven) adsorption configurations are shown in Table 3 of which all locations of propylene molecule in the ZIF−8 are specified. The shortest bond−distances between hydrogen atoms (ether methyl or ethylene group) of propylene and hydrogen atoms of either methyl or ethylene group of imidazolate unit of the ZIF−8 are within the wide range of 1.56–3.25 Å, except the adsorption at center of the pore.

4.1.3 Effect of adsorption configurations on separation of propane and propylene mixture in ZIF−8

The most stable adsorption−structures of propane and propylene in the ZIF−8 are illustrated in Figure 10. It shows that propane points its methyl hydrogen atoms towards ethylene and methyl hydrogen atoms of imidazolate unit belonging to the hexagonal aperture of the ZIF−8 of which bond distances are 2.66, 2.63 and 2.14 Å, respectively. For propylene adsorption, propylene points its methyl hydrogen atoms towards hydrogen atoms of two methyl groups of imidazolate unit belonging to the tetragonal aperture of the ZIF−8 of which bond distances are 2.43 and 3.14 Å, respectively. Based on the separation of propane/propylene mixture and partition theory, the adsorption configurations of propane or propylene in the ZIF−8 located close to the hexagonal aperture has more effect on its moving rate through the hexagonal aperture than further location. As consideration of adsorption configuration, PPE/ZIF−8_h−H_2(CH_2) for propylene adsorption of which adsorption is the strongest (ΔE_{ads} = − 1.20 kcal/mol), must be taken into consideration of moving rate through the hexagonal aperture. Bond−distance data shown in Tables 2 and 3 were used to confirm locations of propane and propylene molecules of related adsorption configurations.

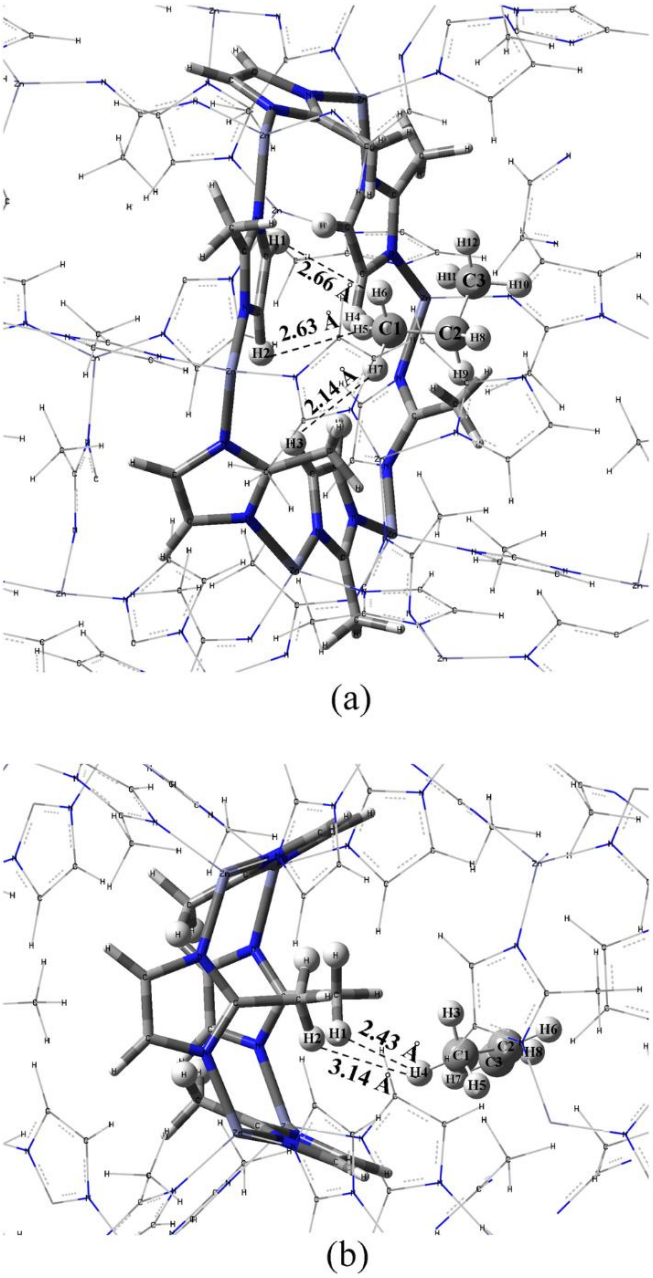

Figure 10 The most stable adsorption−structures of **a** propane and **b** propylene in ZIF−8 pore as configurations PPA/ZIF−8_H/T_1 and PPE/ZIF−8_T_1, respectively. Bond distances between nearest atoms of guest molecule (propane or propylene) and ZIF−8 pore are illustrated.

4.1.4 Interaction energy of propane on windows of the ZIF−67 pore

The SCC–DFTB–optimized structures of propane interacting with atoms of the ZIF–67 pore which are shown in Figure 11. Four configurations of propane adsorbed on wall of the ZIF–67 were found. All the configurations named as PPA/ZIF–67_H, PPA/ZIF–67_H/T, PPA/ZIF–67_h–H and PPA/ZIF–67_T are defined. The first configuration is structure of PPA/ZIF–67_H of which propane is located near the hexagonal aperture (H). The second (PPA/ZIF–67_H/T) is the structure of which propane is located in between the hexagonal and tetragonal apertures. The third (PPA/ZIF–67_h–H) is the structure of which propane's located at the center of the hexagonal aperture. PPA/ZIF–67_T is the structure of which propane is located near the tetragonal apertures (T). Adsorption energies (ΔE_{ads}) of propane on the ZIF–67 cage which are shown in Table 4. Adsorption strengths are in order: PPA/ZIF–67_h–T (ΔE_{ads} = − 1.24 kcal/mol) > PPA/ZIF–67_H/T (ΔE_{ads} = − 0.16 kcal/mol) > PPA/ZIF–67_H (ΔE_{ads} = − 0.15 kcal/mol) > PPA/ZIF–67_T (ΔE_{ads} = − 0.12 kcal/mol).

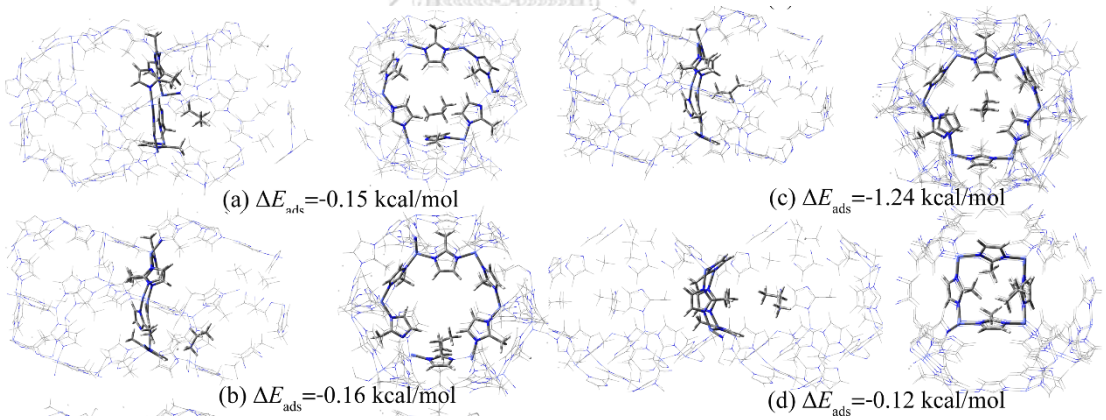

Figure 11 Adsorption structures of propane in the ZIF–67 pore, which the propane molecule is located close to the tetragonal aperture as configuration **a** PPA/ZIF–67_H, **b** PPA/ZIF–67_H/T, **c** PPA/ZIF–67_h–H and **d** PPA/ZIF–67_T. "H" and "T" stand for hexagonal and tetragonal apertures, respectively, and h means at hollow position. Atoms in ZIF apertures and propane molecule, shown by tube model are the main adsorption interaction. The left and right graphics are side and top views, respectively. The adsorption energies (ΔE_{ads}), in kcal/mol are shown.

Table 4 Total energies of the SCC–DFTB–optimized structure of propane and propene adsorbed on windows of the ZIF–67 pore and their components, and its corresponding adsorption energies.

Compound	E_{total}, au	ΔE_{ads}, kcal/mol
ZIF–67	–379.2730472	–
Propane	–8.178396288	–
Propene	–7.388266617	–
***Propane/ZIF–67*:**		
2a (PPA/ZIF–67_H)	–353.6547518	–0.15
2b (PPA/ZIF–67_H/T)	–353.6547606	–0.16
2c (PPA/ZIF–67_h–H)	–353.6554942	–1.24
2d (PPA/ZIF–67_T)	–353.6547094	–0.12
***Propylene/ZIF–67*:**		
3a (PPE/ZIF–67_h–H_1)	–352.8654959	–0.70
3b (PPE/ZIF–67_H/T_1)	–352.8661105	–1.08
3c (PPE/ZIF–67_h–H_2)	–352.8650729	–0.43
3d (PPE/ZIF–67_T)	–352.8648718	–0.30

Table 5 The shortest bond−distances between specific atoms of propane and the ZIF−8.

Configuration/bonds[a]	Bond distances (Å)
Propane/ZIF–67	
2a (PPA/ZIF–67_H)	
H1(H)···H6(G)	2.53
C2(H)···H6(G)	3.04
2b (PPA/ZIF–67_H/T)	
H1(H)···H3(G)	2.42
H2(H)···H6(G)	2.60
H3(H)···H7(G)	2.95
2c (PPA/ZIF–67_h–T)	
H1(H)···H6(G)	2.43
H2(H)···H5(G)	2.30
H3(H)···H7(G)	2.42
2d (PPA/ZIF–67_T)	
H1(H)···H6(G)	2.75
H2(H)···H5(G)	3.11
H3(H)···H7(G)	2.94

[a]A(G)···B(H) represents atom A of guest (G) bonding to atom B of host (H) and labels for all atoms are defined in Figure 5.

[b]The most stable configuration.

The shortest bond−distances between propane's atoms and atoms of the ZIF−67 of all the (four) adsorption configurations are shown in Table 4 of which all locations of propane molecule in the ZIF−67 are specified. The shortest bond−distances between hydrogen atoms (ether methyl or ethylene group) of propane and hydrogen atoms of either methyl or ethylene group of imidazolate unit of the ZIF−67 are within the range of 2.30–3.11 Å.

4.1.5 Interaction energy of propylene on windows of the ZIF–67 pore

The SCC–DFTB–optimized structures of propylene interacting with atoms of the ZIF–67 pore which are shown in Figure 6. Four configurations of propylene adsorbed on wall of the ZIF–67 were found. All the configurations named as PPE/ZIF–67_h–H_1, ZIF–67_H/T_1, PPE/ZIF–67_h–H_2 and PPE/ZIF–67_T are defined. These configurations can be categorized into four structures as follows. The first (PPE/ZIF–67_h–H_1) and second (PPE/ZIF–67_h–H_2) configurations are structures of which propylene are located at the center of the hexagonal aperture. The third (ZIF–67_H/T_1) is the structure of which propylene is located in between the hexagonal and tetragonal aperture. The last configuration, PPE/ZIF–67_T is the structure of which propylene is located at center of the cage. Adsorption strengths are in order: ZIF–67_H/T_1 (ΔE_{ads} = −1.08 kcal/mol) > PPE/ZIF–67_h–H_1 (ΔE_{ads} = −0.70 kcal/mol) > PPE/ZIF–67_h–H_2 (ΔE_{ads} = −0.43 kcal/mol) > (ΔE_{ads} = −0.30 kcal/mol).

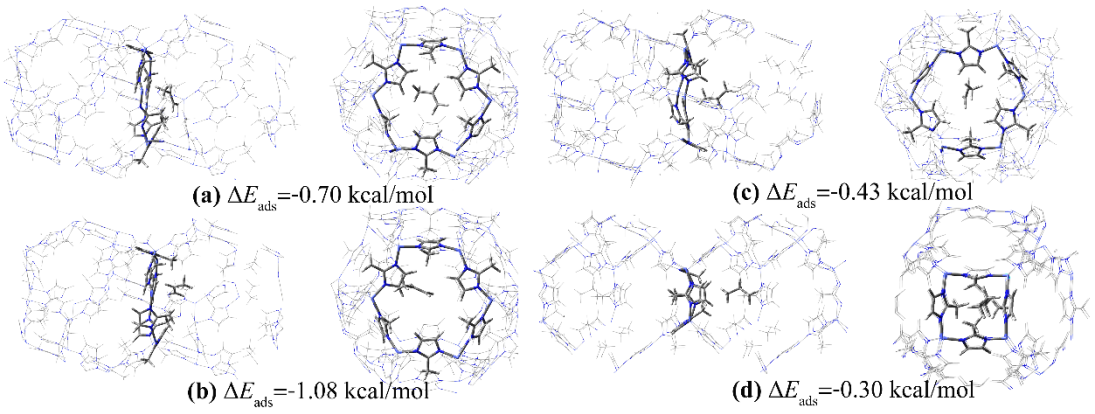

Figure 12 Adsorption structures of propylene in the ZIF–67 pore, which the propylene molecule located close to the tetragonal aperture as configuration **a** PPE/ZIF–67_h–H_1, **b** ZIF–67_H/T_1, **c** PPE/ZIF–67_h–H_2 and **d** PPE/ZIF–67_T. Atoms of apertures and the propylene molecule, shown by tube are the main adsorption interaction. The left and right graphics are side and top views, respectively. The adsorption energies (ΔE_{ads}), in kcal/mol are shown.

Table 6 The shortest bond−distances between specific atoms of propylene and the ZIF−67.

Configuration/bonds[a]	Bond distances (Å)
Propylene/ZIF–67	
3a (PPE/ZIF–67_h–T_1)	
H1(H)···H6(G)	2.70
C2(H)···H6(G)	2.75
3b (PPE/ZIF–67_H/T_1)	
H1(H)···H5(G)	2.20
C2(H)···H5(G)	3.30
3c (PPE/ZIF–67_h–T_2)	
H1(H)···H6(G)	1.77
H2(H)···H5(G)	2.85
H3(H)···H7(G)	2.30
3d (PPA/ZIF–67_T)	
H1(H)···H6(G)	2.54
H2(H)···H5(G)	2.52
H3(H)···H7(G)	2.85

[a]A(G)···B(H) represents atom A of guest (G) bonding to atom B of host (H) and labels for all atoms are defined in Figure 6.

[b]The most stable configuration.

The shortest bond–distances between propylene's atoms and atoms of the ZIF–67 of all the (four) adsorption configurations are shown in Table 6 of which all locations of propylene molecule in the ZIF–67 are specified. The shortest bond–distances between hydrogen atoms (ether methyl or ethylene group) of propylene and hydrogen atoms of either methyl or ethylene group of imidazolate unit of the ZIF–67 are within the wide range of 1.77–3.30 Å, except the adsorption at center of the pore.

4.1.6 Effect of adsorption configurations on separation of propane and propylene mixture in ZIF–67

The most stable adsorption–structures of propane and propylene in the ZIF–67 are illustrated in Figure 13. It shows that propane points its methyl hydrogen atoms towards ethylene and methyl hydrogen atoms of imidazolate unit belonging to the hexagonal aperture of the ZIF−67 of which bond distances are 2.43, 2.42 and 2.30 Å, respectively. For propylene adsorption, propylene points its methyl hydrogen atoms towards hydrogen atoms of two methyl groups of imidazolate unit belonging to the tetragonal aperture of the ZIF−67 of which bond distances are 2.42, 2.60 and 3.14 Å, respectively. Based on the separation of propane/propylene mixture and partition theory, the adsorption configurations of propane or propylene in the ZIF−67 located close to the hexagonal aperture has more effect on its moving rate through the hexagonal aperture than further location. As consideration of adsorption configuration, PPE/ZIF–67_H/T_1(CH_2) for propylene adsorption of which adsorption is the strongest (ΔE_{ads} = − 1.20 kcal/mol), must be taken into consideration of moving rate through the hexagonal aperture. Bond distance data shown in Tables 5 and 6 were used to confirm locations of propane and propylene molecules of related adsorption configurations.

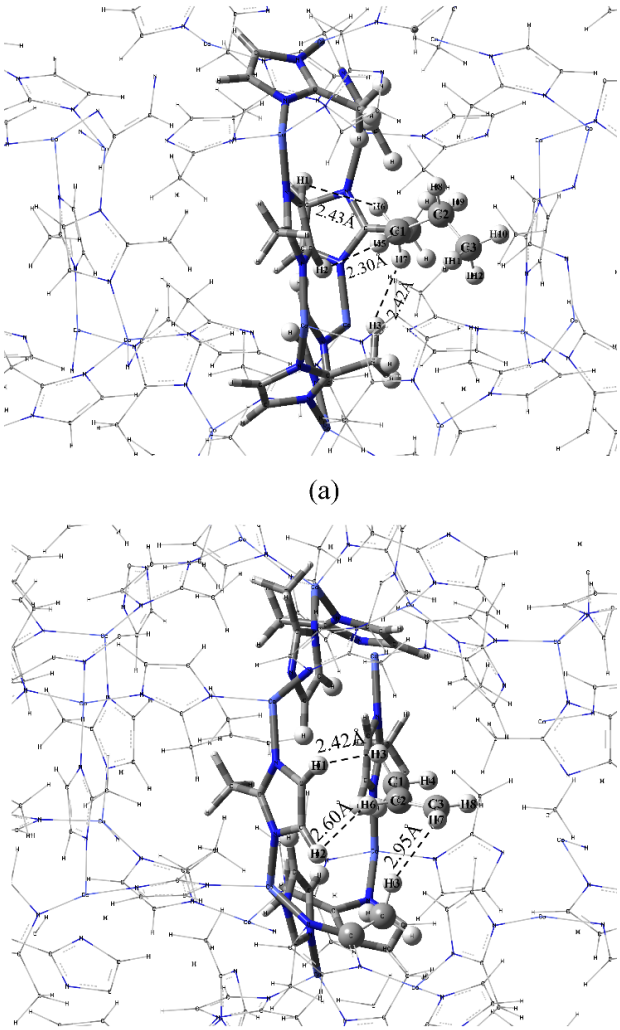

Figure 13 The most stable adsorption–structures of **a** propane and **b** propylene in ZIF–67 pore as configurations PPA/ZIF–67_h–H and PPE/ZIF–67_H/T_1, respectively. Bond distances between nearest atoms of guest molecule (propane or propylene) and ZIF–67 pore are illustrated.

From the adsorption studies it is known that propylene rapidly diffuse through the hexagonal aperture of both ZIF–8 and ZIF–67, so this high energetic motion likely corresponds to the diffusion, while the adsorption capacity of propane and propylene in ZIF–8 is obviously stronger than that of ZIF–67 due to the power of the pore structure and the way the chemical nature of the linker affected the adsorption were investigated.

Moreover, this research also demonstrates that adsorption behavior is determined by the containing arrangement of the guest inside the host, which in turn defines how the adsorbed gas molecules distribute inside the cavities and control the gas induced opening of both ZIF–8 and ZIF–67structures.

4.2 Adsorption configurations of propane and propylene in ZIF–8

Total energies, adsorption energies of propane and propylene gases in the ZIF–8, their energy barrier and separation factor for their mixture are shown in Table 7. It shows that the adsorption energy of propane (ΔE_{ads} = –1.8 kcal/mol) is clearly stronger than of propylene (ΔE_{ads} = –0.51 kcal/mol). This means that propylene molecule can easily desorb as compared with the propane molecule. The configuration structures of propane and propylene adsorbed in the ZIF–8 are shown in Figures 14 and 15, respectively. Based on transportation of propylene and propane gases passing through the hexagonal aperture, their transition–state structures of which configurations are within the hexagonal aperture. The optimized transition–state structure of propane molecule adsorbed on the ZIF–8 (TS–PPA) located in between its hexagonal aperture is shown in Figure 16.

Table 7 Total (E_{Total}), adsorption (ΔE_{ads}) energies of propane and propylene molecules in the ZIF–8, their energy barrier (E_B), and separation factor (α) of propylene from the propylene/propane.

Compounds	E_{Total}, au	ΔE_{ads}, kcal/mol	E_B, kcal/mol	α
Propane (PPA) gas system:				
PPA	–119.0586798214	–	–	–
PPA/ZIF–8	–	–1.85	–	–
	27708.0404355700			
TS–PPA/ZIF–8[a]	–	–	6.96[b]	–
	27825.7624232480			
			7.8[c],9.2[c],7.48[d]	–
Propylene (PPE) gas system:				
PPE	–117.8265789848	–	–	–
PPE/ZIF–8	–	–0.51	–	–
	27824.5392816150			
TSI–PPE/ZIF–8[e]	–27824.53467660	–	2.89[f]	–
TSII–PPE/ZIF–8[g]	–27824.53394626	–	3.35[f]	–
Separation factor:				
PPE/PPA system[e]	–	–	–	985
PPE/PPA system[g]	–	–	–	453
PPE/PPA[h]				~50[h]

[a] The transition–state structure within hexagonal aperture.

[b] Based on the most stable structure, PPA/ZIF–8.

[c] Taken from ref. [79].

[d] Taken from ref. [81].

[e] The transition–state structure (TSI–PPE) by pointing methyl group of propylene through the inside hexagonal aperture.

[f] Based on the most stable structure, PPE/ZIF–8.

[g] The transition–state structure (TSII–PPE) by pointing methylene group of propylene through the outside hexagonal aperture.

[h] Taken from ref. [28].

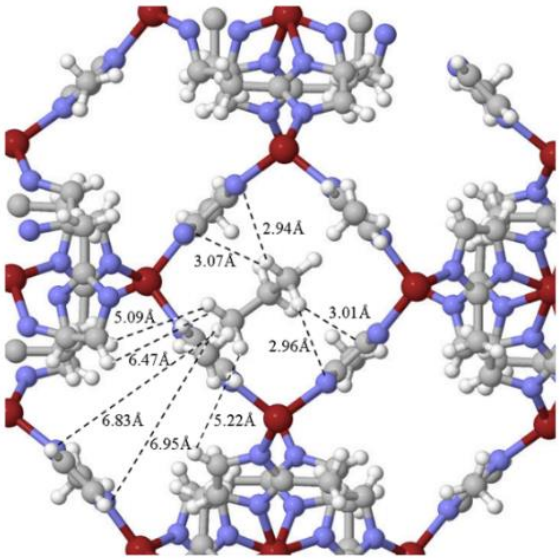

(a)

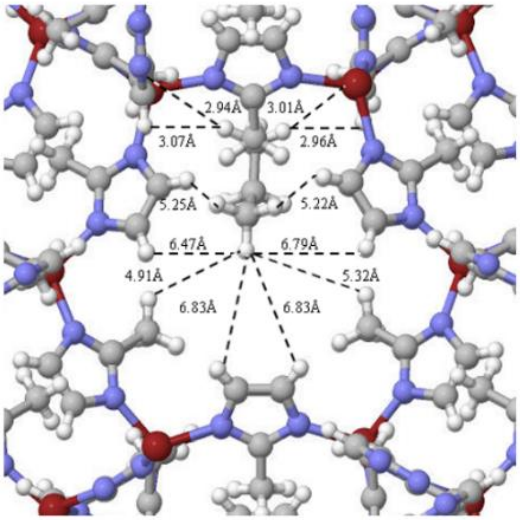

(b)

Figure 14 The optimized structure of the most stable configuration of propane molecule adsorbed on the ZIF–8 cage, (a) through–tetragonal view and (b) through–hexagonal view. All bond distances are in Å.

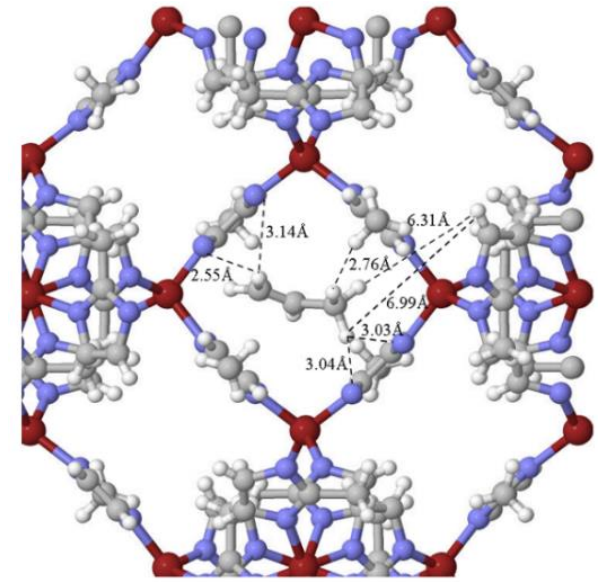

(a)

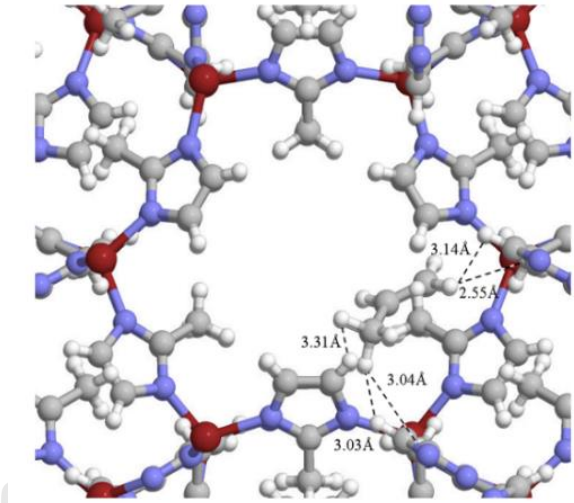

(b)

Figure 15 The optimized structure of the most stable configuration of propylene molecule adsorbed on the ZIF–8 cage, (a) through–tetragonal view and (b) through–hexagonal view. All bond distances are in Å.

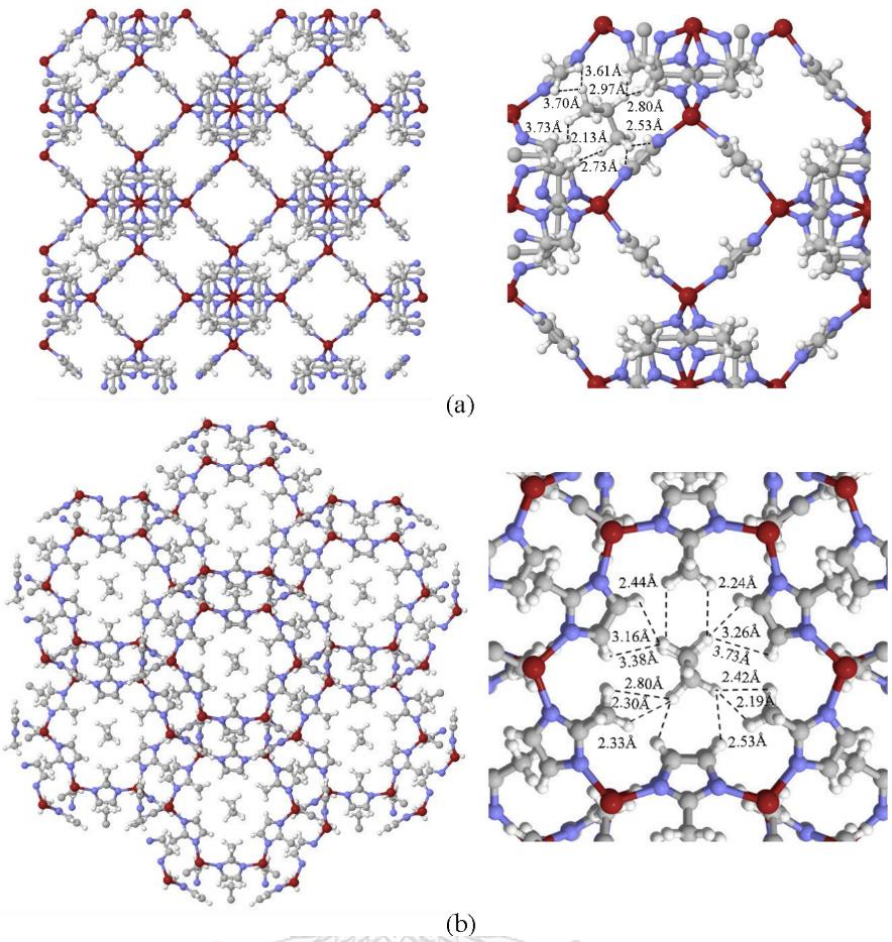

Figure 16 The optimized transition–state structure of propane molecule adsorbed on the ZIF–8 (TS_PPA) located in between its hexagonal aperture, (a) looking through tetragonal aperture and (b) through hexagonal aperture. The right views are zoomed images of the left views. All bond distances are in Å.

The transition–state structures (type I) and (type II) of propylene molecule adsorbed on the ZIF–8 located in between its hexagonal aperture, called as TSI–PPE and TSII–PPE are shown in Figure 17 and 18, respectively. The energy barriers for propane (E_B^1 = 6.96 kcal/mol) and for propylene ($E_B^{2(I)}$ = 2.89 and $E_B^{2(II)}$ = 3.35 kcal/mol) are obtained. Based on interaction of guest/host system, the potential profile for propylene and propane transportation from pore to pore via the hexagonal aperture is shown in Figure 17. Based on diffusion rate, the energy barrier of propane (E_B^D = 7.48 kcal/mol) in ZIF–8 was found [36].

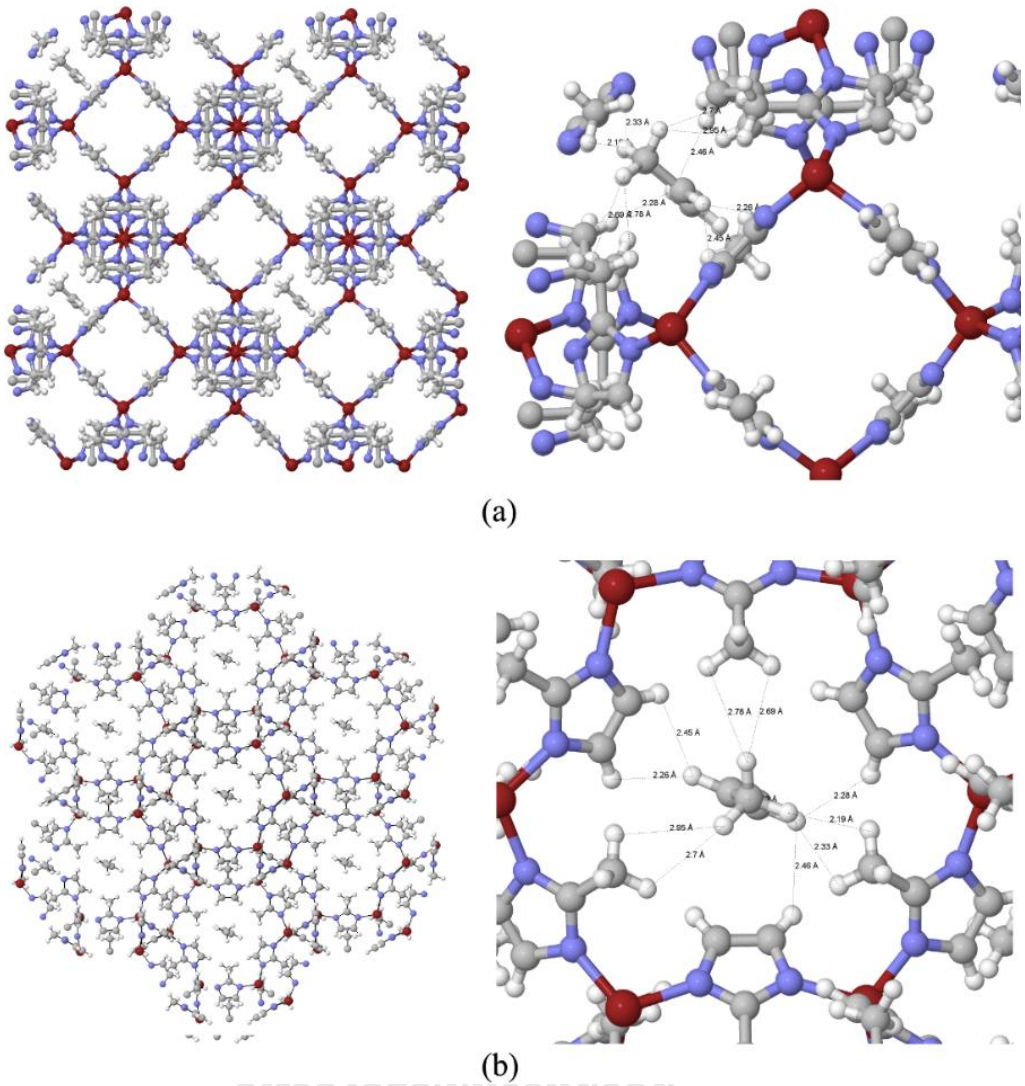

Figure 17 The optimized transition–state structure (type I) of propylene molecule adsorbed on the ZIF–8 (TS–I_PPE) located in between its hexagonal aperture, (a) looking through tetragonal aperture and (b) through hexagonal aperture. The right views are zoomed images of the left views. All bond distances are in Å.

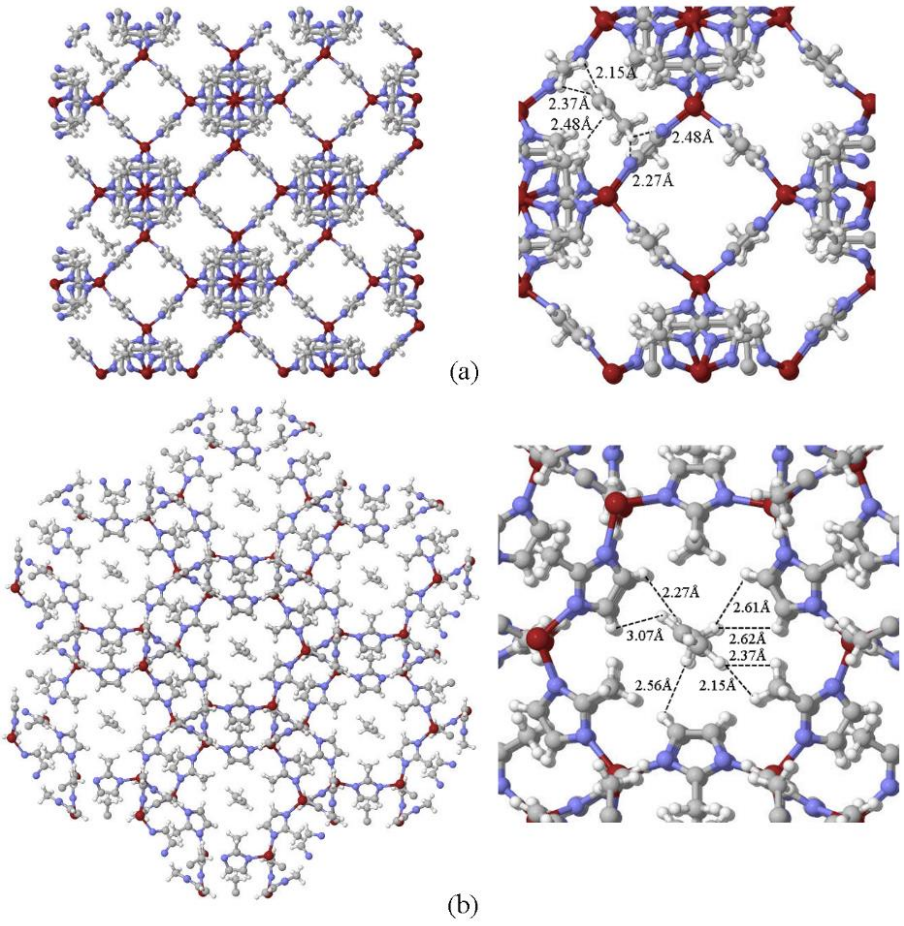

Figure 18 The optimized transition–state structure (type II) of propylene molecule adsorbed on the ZIF–8 (TS–II_PPE) located in between its hexagonal aperture, (a) looking through tetragonal aperture and (b) through hexagonal aperture. The right views are zoomed images of the left views. All bond distances are in Å.

4.3 Estimation of the separation factor from activation energy

Based on the permeance of propylene and propane depending on both the heat of adsorption and the activation energy for their diffusion, $P = P_0 e^{(\Delta H_{ads} - E_p / RT)}$,the heats of adsorption of propylene and propane on ZIF–8 are 7.2 kcal/mol (30 kJ/mol) and 8.1 kcal/mol (34 kJ/mol), respectively, while the diffusional activation energies for propylene and propane are 2.3 kcal/mol (9.7 kJ/mol) and 17.7 kcal/mol (74.1 kJ/mol), respectively [82]. All activation energies are listed in Table 8. Based on definitions,

types of activation energies i.e. diffusion and permeance, are composed of single values except the activation energy of adsorption (referred to transition state) comprising two different values (2.89 and 3.35 kcal/mol) for propylene adsorption. Table 8 shows that adsorption energies dues to the propylene gas are smaller than that of propane gas. These results agree with solubilities of the propylene gas are smaller than the propane gas. The energetic profile for transportation of (a) propane (PPA) molecule via transition–state structure, TS–PPA, (b) propylene (PPE) molecule via transition–state structure, TSI–PPE by pointing its methyl group through the hexagonal aperture from inside to outside cage and (c) PPE molecule via transition–state structure, TSII–PPE by pointing its methyl group through the hexagonal aperture from inside to outside cage, which are shown in Figure 19.

Due to the Eq. 4.7, the separation factor (α) of propylene/propane of 989 was obtained. This α value is much higher than that propylene/propane separated by ZIF–8 of which separation factor of ~50 was reported [28].

Table 8 The activation energies based on various properties (adsorption, diffusion and permeance) of propane and propylene molecules in the ZIF–8 cage.

Activation energies [a]/Properties	Propylene		Propane
	Configuration I	Configuration II	
Adsorption	2.89	3.35	6.96
Diffusion	2.3 [b]		7.48 [c]
Permeance	7.2 [b]		17.7 [b] 8.1 [b]

[a] In kcal/mol, based on

[b] Taken from ref. [82].

[c] Taken from ref. [81].

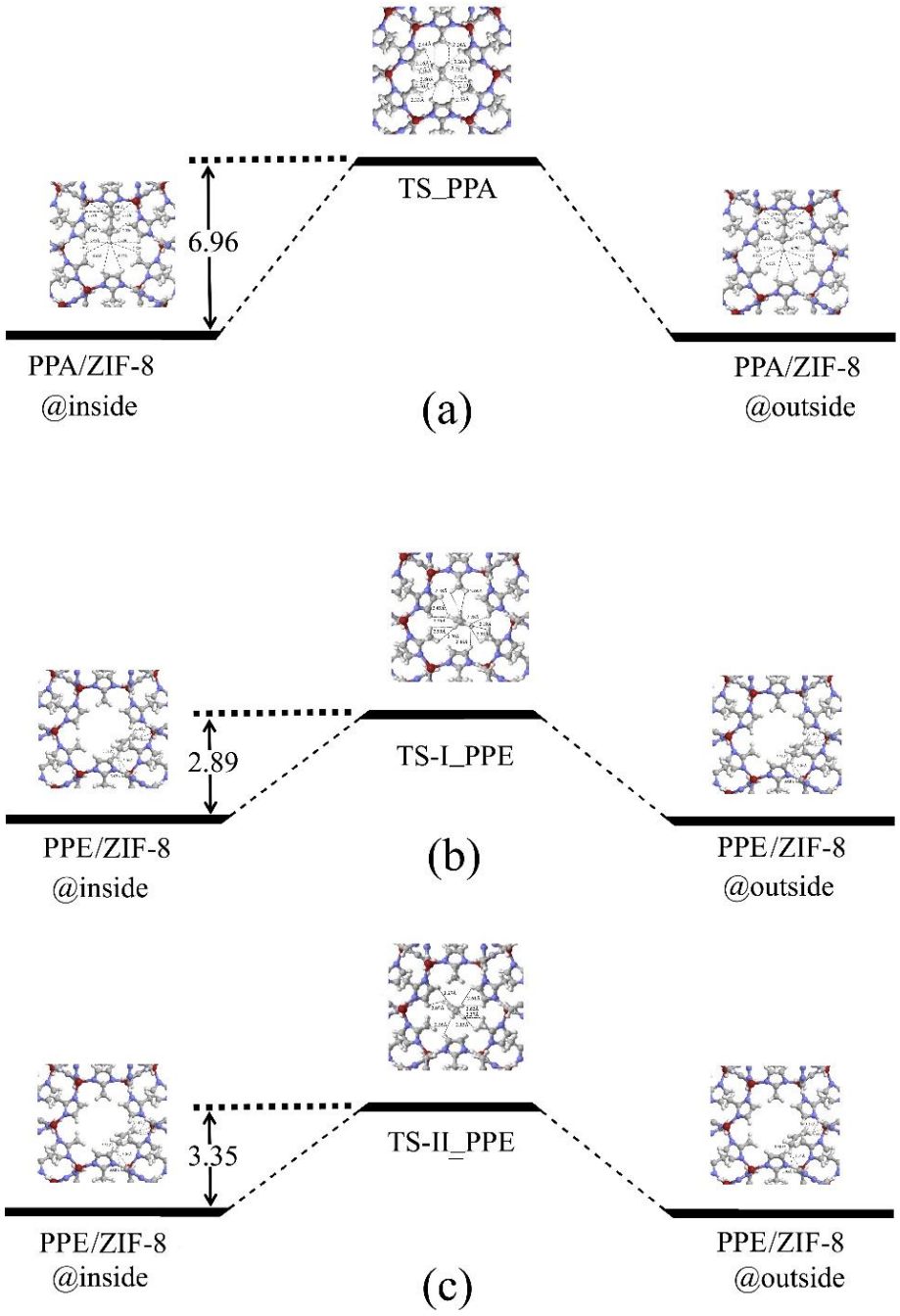

Figure 19 The energetic profile for transportation of (a) propane (PPA) molecule via transition–state structure, TS_PPA, (b) propylene (PPE) molecule via transition–state structure, TS–I_PPE by pointing its methyl group through the hexagonal aperture from inside to outside cage and (c) PPE molecule via transition–state structure, TS–II_PPE by pointing its methyl group through the hexagonal aperture from inside to outside cage. The activation energies are in kcal/mol.

The results showed that isotropic rotation of propylene inside the cavity is more hindered than the rotation of propane. Activation barrier for motion in case of propane is 6.96 kcal/mol which is higher than the barrier of propylene ($E_B^{2(I)}$ = 2.89 and $E_B^{2(II)}$ = 3.35 kcal/mol). It resembles that slightly larger size of propane molecule decelerates the rotation weaker than the interaction of double bond of propylene with the framework. Therefore, it is harder for propane to rotate inside the cavity while the transport between pores occurs faster than for the propylene. From high activation energy for the rotation inside the cavity of propane compared to propylene indicates stronger interaction of this adsorbate with the walls of the cavity.

4.4 MD simulations and dynamical quantities of propane and propylene in ZIF–8 pore

The particle positions were stored every 10 steps from the last 500,000 steps and the mean square displacement (MSD) was investigated at the host–guest systems of 4, 8, 12 and 16 molecules of propane, propylene and propane/propylene mixtures in ZIF–8 pores. The self–diffusion coefficients (D_s) were calculated from the MSD using Einstein's equation. The MD simulations based on the SCC–DFTB method with the Berendsen thermostat for the host–guest systems of 4, 8, 12 and 16 molecules of propane, propylene and propane/propylene mixtures in ZIF–8 pores were observed as shown in Figure 20, 21 and 22, respectively. The D_s of propane, propylene and propane/propylene mixtures in ZIF–8 pores at different systems in NVT ensemble are shown in Table 9. The highest values of D_s are 6.68×10^{-10} m^2s^{-1} of 16 molecules of propane systems, 3.49×10^{-10} m^2s^{-1} of 12 molecules of propylene systems and 1.69×10^{-10} m^2s^{-1} of 12 molecules of propane/propylene mixtures systems. This observation is similar to Anastasios et.al.[83], which reported the decreasing diffusion of guest molecules with increase of the loading high density. This behavior is one of the most usual forms of inserting dependency observed in porous materials, arisen from a natural consequence of steric hindrance between diffusing molecules. Due to our simulations only probed low and medium pore inserting related to the saturation capacity, the effect of system on D_s is weak.

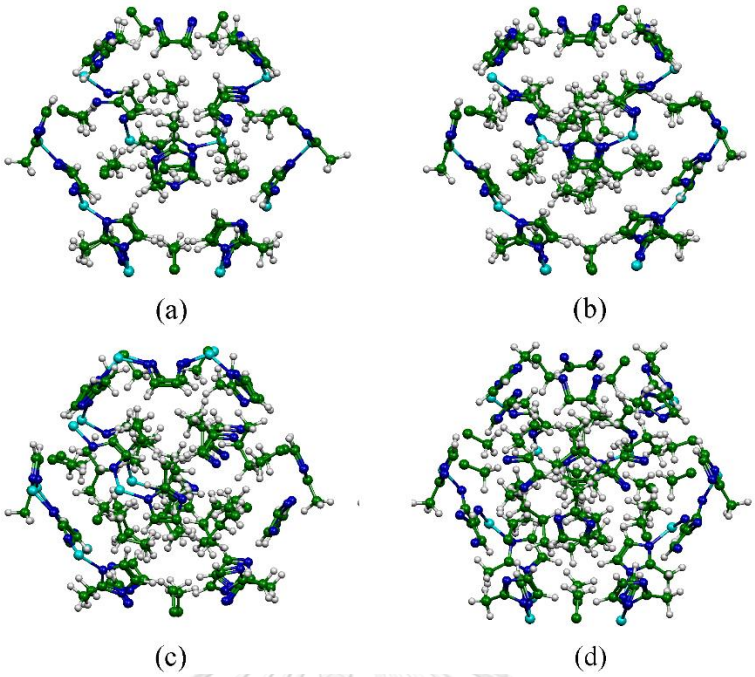

Figure 20 The MD simulations based on the SCC–DFTB method with the Berendsen thermostat for the host–guest systems of 4, 8, 12 and 16 molecules of propane in ZIF–8 pore.

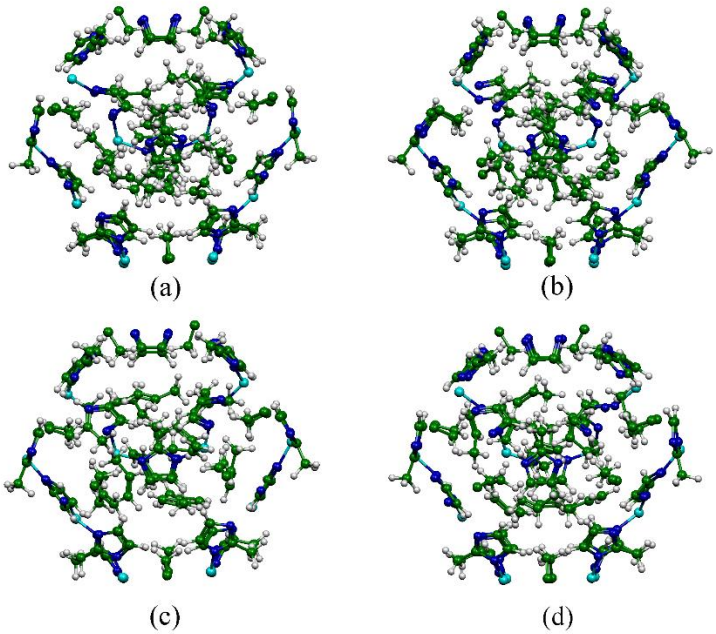

Figure 21 The MD simulations based on the SCC–DFTB method with the Berendsen thermostat for the host–guest systems of 4, 8, 12 and 16 molecules of propylene in ZIF–8 pore.

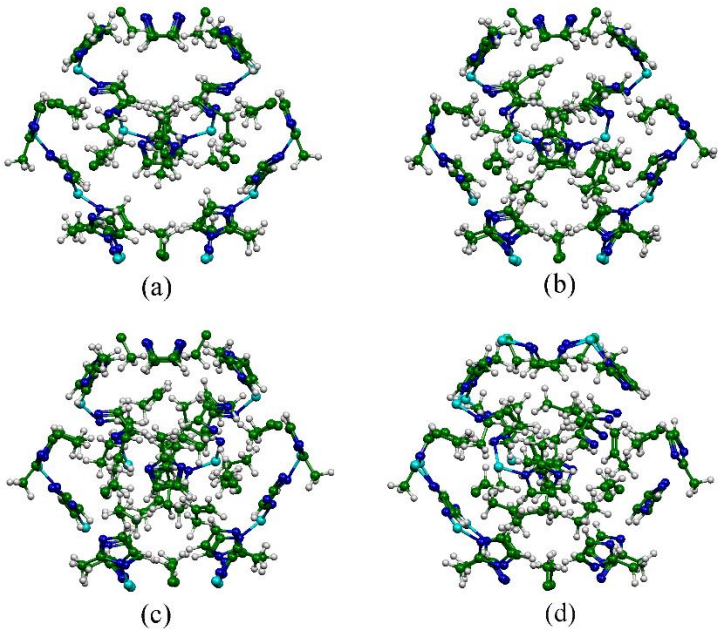

Figure 22 The MD simulations based on the SCC–DFTB method with the Berendsen thermostat for the host–guest systems of 4, 8, 12 and 16 molecules of propane/propylene mixtures in ZIF–8 pore.

Table 9 Diffusion constants D_s ,for the host–guest systems of 4, 8, 12 and 16 molecules of propane, propylene and propane/propylene mixtures in ZIF–8 pore at 298.15 K.

Systems	D_s, m^2s^{-1}
propane/ZIF–8	
4Propane	2.10×10^{-10}
8Propane	1.19×10^{-10}
12Propane	1.34×10^{-10}
16Propane	6.68×10^{-10}
propylene/ZIF–8	
4Propylene	8.29×10^{-9}
8Propylene	6.60×10^{-9}
12Propylene	3.49×10^{-9}
16Propylene	5.21×10^{-9}
propane/propylene mixtures/ZIF–8	
2Propane_2Propylene_Propane	4.80×10^{-10}
2Propane_2Propylene_Propylene	1.68×10^{-9}
4Propane_4Propylene_Propane	9.82×10^{-10}
4Propane_4Propylene_Propylene	1.41×10^{-9}
6Propane_6Propylene_Propane	1.69×10^{-10}
6Propane_6Propylene_Propylene	4.61×10^{-9}
8Propane_8Propylene_Propane	7.56×10^{-10}
8Propane_8Propylene_Propylene	1.78×10^{-9}

This study exhibited that propane can better adsorb than propylene in ZIF–8 and ZIF–67 pores material. From adsorption energies, it could be seen that the number of adsorbed propane is higher than propylene in ZIF–8 and ZIF–67 pores. Therefore, ZIF–8 and ZIF–67 pores can be used for propane/propylene mixtures separation. The past of MD simulations, this research aims to investigate the impact of structural changes on the dynamics of propane/propylene molecules in the ZIF–8. The results showed that propylene can diffuse faster than propane in ZIF–8 material due to the self–diffusion coefficient values of propylene is higher than propane at the same systems. Moreover, we can know the close containing of propane/propylene molecules which indicates propane/propylene molecules can diffuse at high loadings less than at lower loadings because of correlate hindrance. This data agreed with the

diffusion coefficient. Consequently, ZIF–8 adsorbs both propane and propylene in the different sites and the gases can pass through ZIF–8 framework with the different velocities. Hence, we expected that ZIF–8 and ZIF–67 pores materials probably used as separation of propane and propylene.

CHAPTER V
CONCLUSIONS

Adsorption of propane and propylene in the ZIF–8 and ZIF–67 pores, were studied using periodic SCC–DFTB method. Adsorption energies of the most stable configurations of propane and propylene molecules in ZIF–8 are −1.38 and −1.25 kcal/mol and ZIF–67 are −1.24 and − 1.08 kcal/mol, respectively. As trend of adsorption abilities of the ZIF–8 and ZIF–67 pores for adsorption of propane better than propylene, the ZIF–8 and ZIF–67 cages can differentiate diffusion fluxes of propane and propylene via hexagonal aperture. Therefore, lower diffusion flux of propane gas via hexagonal aperture of ZIF–8 and ZIF–67, compared with propylene gas, is expected.

The adsorption structures of propane and propylene molecules on the high–pressure synthesized ZIF–8 cage which was synthesized at 1.47 GPa, and their corresponding transition–state structures which represent molecular transportation of propane and propylene passing through the hexagonal aperture were obtained using the periodic DFT method. The adsorption energy of propane (ΔE_{ads} =–1.8 kcal/mol) was found to be stronger than that of propylene (ΔE_{ads} =–0.51 kcal/ mol). Two transition–state structures for propylene interacting with the hexagonal aperture were obtained. One configuration (TSI–PPE) is alignment of propylene by pointing its methyl group along the hexagonal aperture which the ethylene hydrogen atoms of imidazolate units point against the propylene. The other configuration (TSII–PPE), the propylene points its ethylene group against the hexagonal aperture. Two estimated separation–factors (~453 and ~985) of propylene/propane were found. The ZIF–8 cage can effectively separate the propylene/propane mixture. The results suggest that the ZIF–8 cage synthesized under high–pressure of 1.47 GPa could be an excellent material for separation of propylene/propane.

Diffusion of propane and propylene in the ZIF–8 were investigated using molecular simulations. The self–diffusivity of propane, propylene and propane/ propylene mixtures were within the ranges of 1.19–6.68 x 10^{-9} m^2/s, 3.49–8.29 x 10^{-10} m^2/s and 1.68 x 10^{-9} – 9.82 x 10^{-10} m^2/s, respectively. For low loadings the diffusivity

increases slightly with increasing loadings while at higher loadings it decreases as a consequence of steric hindrance of the guest molecules in ZIF–8 pore. Therefore, we expected that ZIF–8 and ZIF–67 pores materials probably used as separation of propane and propylene.

REFERENCES

1. Ahmadi, M.; Elmongy, H.; Madrakian, T.; Abdel-Rehim, M., Nanomaterials as Sorbents for Sample Preparation in Bioanalysis: A Review. *Anal Chim Acta* **2017**, *958*, 1-21.

2. Vallet-Regi, M.; Balas, F.; Arcos, D., Mesoporous Materials for Drug Delivery. *Angew Chem Int Ed Engl* **2007**, *46*, 7548-58.

3. Tan, K. B.; Vakili, M.; Horri, B. A.; Poh, P. E.; Abdullah, A. Z.; Salamatinia, B., Adsorption of Dyes by Nanomaterials: Recent Developments and Adsorption Mechanisms. *Separation and Purification Technology* **2015**, *150*, 229-242.

4. Eroglu, N.; Emekci, M.; Athanassiou, C. G., Applications of Natural Zeolites on Agriculture and Food Production. *J Sci Food Agric* **2017**, *97*, 3487-3499.

5. Bowen, T. C.; Noble, R. D.; Falconer, J. L., Fundamentals and Applications of Pervaporation through Zeolite Membranes. *Journal of Membrane Science* **2004**, *245*, 1-33.

6. Czaja, A. U.; Trukhan, N.; Muller, U., Industrial Applications of Metal-Organic Frameworks. *Chem Soc Rev* **2009**, *38*, 1284-1293.

7. Tang, J.; Salunkhe, R. R.; Liu, J.; Torad, N. L.; Imura, M.; Furukawa, S.; Yamauchi, Y., Thermal Conversion of Core-Shell Metal-Organic Frameworks: A New Method for Selectively Functionalized Nanoporous Hybrid Carbon. *J Am Chem Soc* **2015**, *137*, 1572-1580.

8. Banerjee, R.; Furukawa, H.; Britt, D.; Knobler, C.; O'Keeffe, M.; Yaghi, O. M., Control of Pore Size and Functionality in Isoreticular Zeolitic Imidazolate Frameworks and Their Carbon Dioxide Selective Capture Properties. *Journal of the American Chemical Society* **2009**, *131*, 3875-3877.

9. Yang, T.; Chung, T.-S., Room-Temperature Synthesis of ZIF-90 Nanocrystals and the Derived Nano-Composite Membranes for Hydrogen Separation. *Journal of Materials Chemistry A* **2013**, *1*, 6081.

10. Assfour, B.; Leoni, S.; Seifert, G., Hydrogen Adsorption Sites in Zeolite Imidazolate Frameworks Zif-8 and ZIF-11. *Journal of Physical Chemistry C* **2010**, *114*, 13381-13384.

11. Perez-Pellitero, J.; Amrouche, H.; Siperstein, F. R.; Pirngruber, G.; Nieto-Draghi, C.; Chaplais, G.; Simon-Masseron, A.; Bazer-Bachi, D.; Peralta, D.; Bats, N., Adsorption of CO_2, CH_4, and N_2 on Zeolitic Imidazolate Frameworks: Experiments and Simulations. *Chemistry* **2010**, *16*, 1560-1571.

12. Dixit, M.; Major, D. T.; Pal, S., Hydrogen Adsorption in ZIF-7: A DFT and *Ab-Initio* Molecular Dynamics Study. *Chemical Physics Letters* **2016**, *651*, 178-182.

13. Friebe, S.; Wang, N.; Diestel, L.; Liu, Y.; Schulz, A.; Mundstock, A.; Caro, J., Deuterium/Hydrogen Permeation through Different Molecular Sieve Membranes: ZIF, LDH, Zeolite. *Microporous and Mesoporous Materials* **2015**, *216*, 127-132.

14. Chen, L.; Yuan, S.; Qian, J.-F.; Fan, W.; He, M.-Y.; Chen, Q.; Zhang, Z.-H., Effective Adsorption Separation of N-Hexane/2-Methylpentane in Facilely Synthesized Zeolitic Imidazolate Frameworks ZIF-8 and ZIF-69. *Industrial & Engineering Chemistry Research* **2016**, *55*, 10751-10757.

15. Li, Y.; Zhou, K.; He, M.; Yao, J., Synthesis of Zif-8 and ZIF-67 Using Mixed-Base and Their Dye Adsorption. *Microporous and Mesoporous Materials* **2016**, *234*, 287-292.

16. Park, K. S.; Ni, Z.; Côté, A. P.; Choi, J. Y.; Huang, R.; Uribe-Romo, F. J.; Chae, H. K.; O'Keeffe, M.; Yaghi, O. M., Exceptional Chemical and Thermal Stability of Zeolitic Imidazolate Frameworks. *Proceedings of the National Academy of Sciences of the United States of America* **2006**, *103*, 10186-10191.

17. Huang, X. C.; Lin, Y. Y.; Zhang, J. P.; Chen, X. M., Ligand-Directed Strategy for Zeolite-Type Metal-Organic Frameworks: Zinc(II) Imidazolates with Unusual Zeolitic Topologies. *Angew Chem Int Ed Engl* **2006**, *45*, 1557-1559.

18. Liu, Y.; Kravtsov, V.; Larsen, R.; Eddaoudi, M., Molecular Building Blocks

Approach to the Assembly of Zeolite-Like Metal-Organic Frameworks (ZMOFs) with Extra-Large Cavities. *Chem Commun (Camb)* **2006**, 1488-14890.

19. Nugent, P., et al., Porous Materials with Optimal Adsorption Thermodynamics and Kinetics for CO_2 Separation. *Nature* **2013**, *495*, 80-84.

20. Liao, P.-Q.; Chen, H.; Zhou, D.-D.; Liu, S.-Y.; He, C.-T.; Rui, Z.; Ji, H.; Zhang, J.-P.; Chen, X.-M., Monodentate Hydroxide as a Super Strong yet Reversible Active Site for CO_2 Capture from High-Humidity Flue Gas. *Energy & Environmental Science* **2015**, *8*, 1011-1016.

21. Wu, H., et al., Metal-Organic Frameworks with Exceptionally High Methane Uptake: Where and How Is Methane Stored? *Chemistry* **2010**, *16*, 5205-5214.

22. Schlichte, K.; Kratzke, T.; Kaskel, S., Improved Synthesis, Thermal Stability and Catalytic Properties of the Metal-Organic Framework Compound $Cu_3(Btc)_2$. *Microporous and Mesoporous Materials* **2004**, *73*, 81-88.

23. Wu, C. D.; Hu, A.; Zhang, L.; Lin, W., A Homochiral Porous Metal-Organic Framework for Highly Enantioselective Heterogeneous Asymmetric Catalysis. *Journal of the American Chemical Society* **2005**, *127*, 8940-8941.

24. Himsl, D.; Hartmann, M. In *Hydrogen Storage in Li-Doped Metal-Organic Frameworks*, DGMK Tagungsbericht, 2010; pp 157-164.

25. Demir, B.; Ahunbay, M. G., Propane/Propylene Separation in Ion-Exchanged Zeolite-Like Metal Organic Frameworks. *Microporous and Mesoporous Materials* **2014**, *198*, 185-193.

26. Wegrzyniak, A.; Jarczewski, S.; Wegrzynowicz, A.; Michorczyk, B.; Kustrowski, P.; Michorczyk, P., Catalytic Behavior of Chromium Oxide Supported on Nanocasting-Prepared Mesoporous Alumina in Dehydrogenation of Propane. *Nanomaterials (Basel)* **2017**, *7*.

27. Pan, Y.; Li, T.; Lestari, G.; Lai, Z., Effective Separation of Propylene/Propane Binary Mixtures by ZIF-8 Membranes. *Journal of Membrane Science* **2012**, *390-391*, 93-98.

28. Kwon, H. T.; Jeong, H. K., In Situ Synthesis of Thin Zeolitic-Imidazolate Framework ZIF-8 Membranes Exhibiting Exceptionally High Propylene/Propane Separation. *Journal of the American Chemical Society* **2013**, *135*, 10763-10768.

29. Lee, M. J.; Kwon, H. T.; Jeong, H. K., Defect-Dependent Stability of Highly Propylene-Selective Zeolitic-Imidazolate Framework ZIF-8 Membranes. *Journal of Membrane Science* **2017**, *529*, 105-113.

30. Hara, N.; Yoshimune, M.; Negishi, H.; Haraya, K.; Hara, S.; Yamaguchi, T., Diffusive Separation of Propylene/Propane with ZIF-8 Membranes. *Journal of Membrane Science* **2014**, *450*, 215-223.

31. Hara, N.; Yoshimune, M.; Negishi, H.; Haraya, K.; Hara, S.; Yamaguchi, T., Effect of Temperature on Synthesis of ZIF-8 Membranes for Propylene/ Propane Separation by Counter Diffusion Method. *Journal of the Japan Petroleum Institute* **2015**, *58*, 237-244.

32. Hara, N.; Yoshimune, M.; Negishi, H.; Haraya, K.; Hara, S.; Yamaguchi, T., Effect of Solution Concentration on Structure and Permeation Properties of ZIF-8 Membranes for Propylene/Propane Separation. *Journal of Chemical Engineering of Japan* **2016**, *49*, 97-103.

33. Krokidas, P.; Castier, M.; Moncho, S.; Brothers, E.; Economou, I. G., Molecular Simulation Studies of the Diffusion of Methane, Ethane, Propane, and Propylene in ZIF-8. *Journal of Physical Chemistry C* **2015**, *119*, 27028-27037.

34. Krokidas, P.; Moncho, S.; Brothers, E. N.; Castier, M.; Economou, I. G., Tailoring the Gas Separation Efficiency of Metal Organic Framework ZIF-8 through Metal Substitution: A Computational Study. *Physical Chemistry Chemical Physics* **2018**, *20*, 4879-4892.

35. Pan, Y.; Lai, Z., Sharp Separation of C2/C3 Hydrocarbon Mixtures by Zeolitic Imidazolate Framework-8 (ZIF-8) Membranes Synthesized in Aqueous Solutions. *Chemical Communications* **2011**, *47*, 10275-10277.

36. Zheng, B.; Pan, Y.; Lai, Z.; Huang, K. W., Molecular Dynamics Simulations on Gate Opening in ZIF-8: Identification of Factors for Ethane and Propane Separation. *Langmuir* **2013**, *29*, 8865-8872.

37. Tanaka, S., et al., Adsorption and Diffusion Phenomena in Crystal Size Engineered ZIF-8 MOF. *Journal of Physical Chemistry C* **2015**, *119*, 28430-28439.

38. Huang, X. C.; Lin, Y. Y.; Zhang, J. P.; Chen, X. M., Ligand-Directed Strategy for Zeolite-Type Metal-Organic Frameworks: Zinc(II) Imidazolates with Unusual Zeolitic Topologies. *Angewandte Chemie - International Edition* **2006**, *45*, 1557-1559.

39. Moggach, S. A.; Bennett, T. D.; Cheetham, A. K., The Effect of Pressure on ZIF-8: Increasing Pore Size with Pressure and the Formation of a High-Pressure Phase at 1.47 Gpa. *Angewandte Chemie - International Edition* **2009**, *48*, 7087-7089.

40. Ma, X.; Liu, D., Zeolitic Imidazolate Framework Membranes for Light Olefin/Paraffin Separation. *Crystals* **2018**, *9*, 14.

41. Phan, A.; Doonan, C. J.; Uribe-Romo, F. J.; Knobler, C. B.; Okeeffe, M.; Yaghi, O. M., Synthesis, Structure, and Carbon Dioxide Capture Properties of Zeolitic Imidazolate Frameworks. *Accounts of Chemical Research* **2010**, *43*, 58-67.

42. Zhang, Z.; Zhao, Y.; Gong, Q.; Li, Z.; Li, J., MOFs for CO_2 Capture and Separation from Flue Gas Mixtures: The Effect of Multifunctional Sites on Their Adsorption Capacity and Selectivity. *Chem Commun (Camb)* **2013**, *49*, 653-661.

43. Zhang, Z.; Xian, S.; Xia, Q.; Wang, H.; Li, Z.; Li, J., Enhancement of CO_2 adsorption and CO_2/N_2 selectivity on ZIF-8 Via Postsynthetic Modification. *AIChE Journal* **2013**, *59*, 2195-2206.

44. Fan, Y.-H.; Zhang, S.-W.; Qin, S.-B.; Li, X.-S.; Qi, S.-H., An Enhanced Adsorption of Organic Dyes onto NH_2 Functionalization Titanium-Based Metal-Organic Frameworks and the Mechanism Investigation. *Microporous and*

Mesoporous Materials **2018**, *263*, 120-127.

45. Ramsahye, N. A., et al., Adsorption and Diffusion of Light Hydrocarbons in Uio-66(Zr): A Combination of Experimental and Modeling Tools. *The Journal of Physical Chemistry C* **2014**, *118*, 27470-27482.

46. Krokidas, P.; Castier, M.; Economou, I. G., Computational Study of ZIF-8 and ZIF-67 Performance for Separation of Gas Mixtures. *The Journal of Physical Chemistry C* **2017**, *121*, 17999-18011.

47. Ma, S.; Zhou, H. C., Gas Storage in Porous Metal-Organic Frameworks for Clean Energy Applications. *Chem Commun (Camb)* **2010**, *46*, 44-53.

48. Lee, Y. R.; Jang, M. S.; Cho, H. Y.; Kwon, H. J.; Kim, S.; Ahn, W. S., ZIF-8: A Comparison of Synthesis Methods. *Chemical Engineering Journal* **2015**, *271*, 276-280.

49. Banerjee, R.; Phan, A.; Wang, B.; Knobler, C.; Furukawa, H.; O'Keeffe, M.; Yaghi, O. M., High-Throughput Synthesis of Zeolitic Imidazolate Frameworks and Application to CO_2 Capture. *Science* **2008**, *319*, 939-943.

50. Sung Park, K., Characterization of Zeolitic Imidazolate Framework–Derived Polyhedral Carbonaceous Material and Its Application to Electrocatalyst for Oxygen Reduction Reaction. *International Journal of Electrochemical Science* **2016**, 9295-9306.

51. Go, Y.; Lee, J. H.; Shamsudin, I. K.; Kim, J.; Othman, M. R., Microporous ZIF-7 Membranes Prepared by in-Situ Growth Method for Hydrogen Separation. *International Journal of Hydrogen Energy* **2016**, *41*, 10366-10373.

52. Zhang, W.; Jiang, X.; Wang, X.; Kaneti, Y. V.; Chen, Y.; Liu, J.; Jiang, J. S.; Yamauchi, Y.; Hu, M., Spontaneous Weaving of Graphitic Carbon Networks Synthesized by Pyrolysis of ZIF-67 Crystals. *Angew Chem Int Ed Engl* **2017**, *56*, 8435-8440.

53. Verploegh, R. J.; Nair, S.; Sholl, D. S., Temperature and Loading-Dependent Diffusion of Light Hydrocarbons in ZIF-8 as Predicted through Fully Flexible

Molecular Simulations. *J Am Chem Soc* **2015**, *137*, 15760-15771.

54. Wang, C.; Yang, F.; Sheng, L.; Yu, J.; Yao, K.; Zhang, L.; Pan, Y., Zinc-Substituted ZIF-67 Nanocrystals and Polycrystalline Membranes for Propylene/Propane Separation. *Chem Commun (Camb)* **2016**, *52*, 12578-12581.

55. Ramachandran, K. I.; Deepa, G.; Namboori, K., *Computational Chemistry and Molecular Modeling: Principles and Applications*, 2008, p 1-397.

56. Marques, M. A. L.; Maitra, N. T.; Nogueira, F. M. S.; Gross, E. K. U.; Rubio, A., Fundamentals of Time-Dependent Density Functional Theory. In *Lecture Notes in Physics*, 2012; Vol. 837, pp 1-559.

57. Elstner, M.; Seifert, G., Density Functional Tight Binding. *Philos Trans A Math Phys Eng Sci* **2014**, *372*, 20120483.

58. Elstner, M.; Seifert, G., Density Functional Tight Binding. *Philosophical Transactions of the Royal Society A: Mathematical, Physical and Engineering Sciences* **2014**, *372*.

59. Wang, C.; Yang, F.; Sheng, L.; Yu, J.; Yao, K.; Zhang, L.; Pan, Y., Zinc-Substituted ZIF-67 Nanocrystals and Polycrystalline Membranes for Propylene/Propane Separation. *Chemical Communications* **2016**, *52*, 12578-12581.

60. Monticelli, L.; Salonen, E., *Biomolecular Simulations: Methods and Protocols*; Humana Press, 2016.

61. Beeman, D., Some Multistep Methods for Use in Molecular Dynamics Calculations. *Journal of Computational Physics* **1976**, *20*, 130-139.

62. Swope, W. C.; Andersen, H. C.; Berens, P. H.; Wilson, K. R., A Computer Simulation Method for the Calculation of Equilibrium Constants for the Formation of Physical Clusters of Molecules: Application to Small Water Clusters. *The Journal of Chemical Physics* **1982**, *76*, 637-649.

63. Lewars, E. G., *Computational Chemistry: Introduction to the Theory and*

Applications of Molecular and Quantum Mechanics, 2011, p 1-664.

64. Andersen, H. C., Molecular Dynamics Simulations at Constant Pressure and/or Temperature. *The Journal of Chemical Physics* **1980**, *72*, 2384-2393.

65. Kowsari, M. H.; Naderlou, S., Understanding the Dynamics, Self-Diffusion, and Microscopic Structure of Hydrogen inside the Nanoporous Li-Lsx Zeolite. *Microporous and Mesoporous Materials* **2017**, *240*, 39-49.

66. Novakovic, S. B.; Bogdanovic, G. A.; Heering, C.; Makhloufi, G.; Francuski, D.; Janiak, C., Charge-Density Distribution and Electrostatic Flexibility of ZIF-8 Based on High-Resolution X-Ray Diffraction Data and Periodic Calculations. *Inorg Chem* **2015**, *54*, 2660-2670.

67. Kwon, H. T.; Jeong, H. K.; Lee, A. S.; An, H. S.; Lee, J. S., Heteroepitaxially Grown Zeolitic Imidazolate Framework Membranes with Unprecedented Propylene/Propane Separation Performances. *J Am Chem Soc* **2015**, *137*, 12304-12311.

68. Aradi, B.; Hourahine, B.; Frauenheim, T., Dftb+, a Sparse Matrix-Based Implementation of the DFTB Method. *Journal of Physical Chemistry A* **2007**, *111*, 5678-5684.

69. Elstner, M.; Porezag, D.; Jungnickel, G.; Elsner, J.; Haugk, M.; Frauenheim, T., Self-Consistent-Charge Density-Functional Tight-Binding Method for Simulations of Complex Materials Properties. *Physical Review B - Condensed Matter and Materials Physics* **1998**, *58*, 7260-7268.

70. Moreira, N. H.; Dolgonos, G.; Aradi, B.; Da Rosa, A. L.; Frauenheim, T., Toward an Accurate Density-Functional Tight-Binding Description of Zinc-Containing Compounds. *Journal of Chemical Theory and Computation* **2009**, *5*, 605-614.

71. Dovesi, R., et al. *Crystal14 User's Manual*, University of Torino, Torino, 2014.

72. Becke, A. D., Density-Functional Thermochemistry. Iii. The Role of Exact Exchange. *The Journal of Chemical Physics* **1993**, *98*, 5648-5652.

73. Lee, C.; Yang, W.; Parr, R. G., Development of the Colle-Salvetti Correlation-Energy Formula into a Functional of the Electron Density. *Physical Review B* **1988**, *37*, 785-789.

74. Gatti, C.; Saunders, V. R.; Roetti, C., Crystal Field Effects on the Topological Properties of the Electron Density in Molecular Crystals: The Case of Urea. *The Journal of Chemical Physics* **1994**, *101*, 10686-10696.

75. Heyd, J.; Peralta, J. E.; Scuseria, G. E.; Martin, R. L., Energy Band Gaps and Lattice Parameters Evaluated with the Heyd-Scuseria-Ernzerhof Screened Hybrid Functional. *Journal of Chemical Physics* **2005**, *123*.

76. Jaffe, J. E.; Hess, A. C., Hartree-Fock Study of Phase Changes in ZnO at High Pressure. *Physical Review B* **1993**, *48*, 7903-7909.

77. Harvey, S. C.; Tan, R. K.-Z.; Cheatham III, T. E., The Flying Ice Cube: Velocity Rescaling in Molecular Dynamics Leads to Violation of Energy Equipartition. **1998**, *19*, 726-740.

78. Chmelik, C.; Kärger, J., The Predictive Power of Classical Transition State Theory Revealed in Diffusion Studies with MOF ZIF-8. *Microporous and Mesoporous Materials* **2016**, *225*, 128-132.

79. Zheng, B.; Huang, K. W.; Du, H., Theoretical Model Estimation of Guest Diffusion in Metal-Organic Frameworks (MOFs). *RSC Advances* **2015**, *5*, 70433-70438.

80. Sant, M.; Papadopoulos, G. K.; Theodorou, D. N., A Second-Order Markov Process for Modeling Diffusive Motion through Spatial Discretization. *Journal of Chemical Physics* **2008**, *128*.

81. Zheng, B.; Wang, L. L.; Du, L.; Pan, Y.; Lai, Z.; Huang, K. W.; Du, H. L., Diffusion as a Function of Guest Molecule Length and Functionalization in Flexible Metal-Organic Frameworks. *Materials Horizons* **2016**, *3*, 355-361.

82. Yang, M.; Wang, L. D.; Chen, G. D.; An, B.; Wang, Y. J.; Liu, G. Q., First-Principles Study on Field Emission of C-Doped Capped Single-Walled Bnnt.

Wuli Xuebao/Acta Physica Sinica **2009**, *58*, 7151-7155.

83. Skoulidas, A. I.; Sholl, D. S., Self-Diffusion and Transport Diffusion of Light Gases in Metal-Organic Framework Materials Assessed Using Molecular Dynamics Simulations. *Journal of Physical Chemistry B* **2005**, *109*, 15760-15768.

84. Novaković, S. B.; Bogdanović, G. A.; Heering, C.; Makhloufi, G.; Francuski, D.; Janiak, C., Charge-Density Distribution and Electrostatic Flexibility of ZIF-8 Based on High-Resolution X-Ray Diffraction Data and Periodic Calculations. *Inorganic Chemistry* **2015**, *54*, 2660-2670.

85. Rowland, R. S.; Taylor, R., Intermolecular Nonbonded Contact Distances in Organic Crystal Structures: Comparison with Distances Expected from Van Der Waals Radii. *Journal of Physical Chemistry* **1996**, *100*, 7384-7391.

VITA

NAME	Miss Benjawan Kaewruksa
DATE OF BIRTH	8 November 1985
PLACE OF BIRTH	Ubonratchathani, Thailand
INSTITUTIONS ATTENDED	2013–2018 Ph.D. (Physical Chemistry), Chulalongkorn University, Thailand 2009–2011 M.Sc. (Physical Chemistry), Chulalongkorn University, Thailand 2005–2008 B.Sc. (Chemistry), Burapha University, Thailand 2001–2004 Leu Kumharn Warinchamlarp high school, Ubonratchathani, Thailand 1998–2000 Tessaban Warin Wichachart secondary school, Ubonratchathani, Thailand 1992–1997 Tessaban Warin Wichachart primary school, Ubonratchathani, Thailand
HOME ADDRESS	104 Tessaban 64 Road, Ubonratchathani 34190, Thailand
PUBLICATION	[1] Kaewruksa, B., and Ruangpornvisuti, V. Theoretical study on the adsorption behaviors of H2O and NH3 on hydrogen–terminated ZnO nanoclusters and ZnO graphene–like nanosheets. J. Mol. Struct. 994, 276–282. [2] Kaewruksa, B.; Wanbayor, R.; Ruangpornvisuti, V., CO–Adsorptions of CO/N2O, NO/NH3, CO2/N2 and Conversion of CO/N2O to CO2/N2 on ZnO Graphene-Like Nanosheet. Journal of Molecular Structure 2012, 1012, 50-55. [3] Kaewruksa, B.; Ruangpornvisuti, V., First Principles Investigation of Oxygen Adsorptions on Hydrogen–Terminated ZnO Graphene–Like Nanosheets. Journal of Molecular Modeling 2012, 18, 1447–1454. [4] Kaewruksa, B.; Pipornpong, W.; Wanno, B.; Ruangpornvisuti, V., Density Functional Studies of Small Gases Adsorbed on the ZnO Sodalite–Like Cage and Its Adsorption Abilities. Computational and Theoretical Chemistry 2013, 1020, 100-107. [5] Kaewruksa, B.; Vchirawongkwin, V.; Ruangpornvisuti, V., DFT Investigation on Molecular Structure of Zirconia Nanoparticle and Its Adsorption Structures with Elementary Gases. Journal of Molecular Structure 2016, 1108, 187–194.

[6] Pipornpong, W.; Kaewruksa, B.; Ruangpornvisuti, V., DFT Investigation on Molecular Structures of Metal and Nonmetal–Doped ZnO Sodalite–Like Cage and Their Electronic Properties. Structural Chemistry 2016, 27, 773–784.
[7] Kaewruksa, B.; Vchirawongkwin, V.; Ruangpornvisuti, V., Adsorption of Propane and Propylene in Zeolitic Imidazolate Framework ZIF–8 Pore: Periodic SCC–DFTB Method. Adsorption 2018, 24, 691–701.

APPENDIX

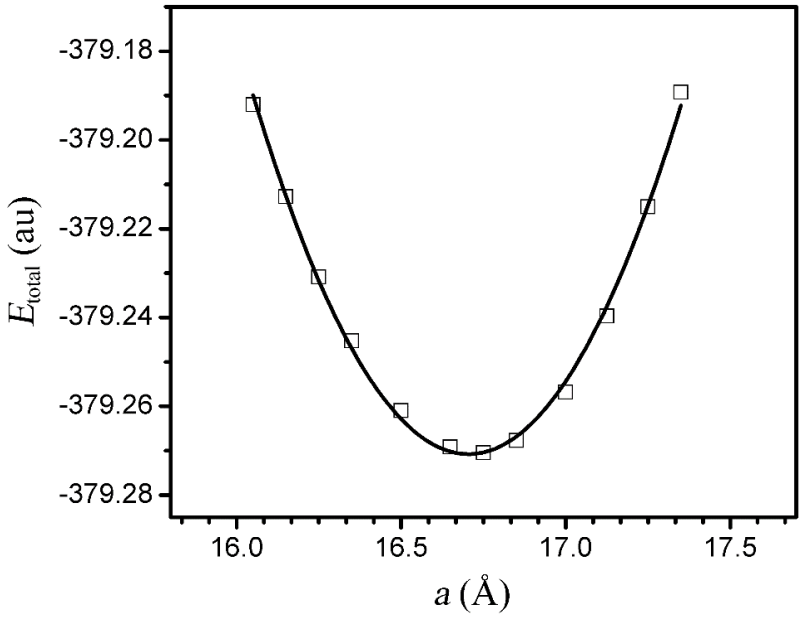

Figure A1 Plot of total energy (au) of the ZIF–8 against lattice parameter a including its quadratic fit (Etotal = 0.18857a2 – 6.30013a – 326.64929). The minimum value derived by equation (dE_total)/da=0, a = 16.7050 Å was obtained.

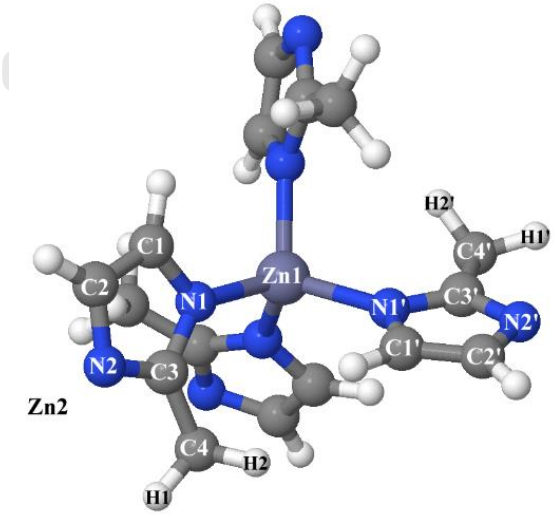

Figure A2 Labeling atoms of ZIF–8 for as referred in Table A1.

Table A1 Selected geometrical parameters of ZIF–8, based on X–ray diffraction and DFTB optimized structures.

Parameters [a]	X–ray [b]	Component [c]	Unit cell [d]
Bond length (Å)			
Zn1–N1	1.989	1.972	1.975
Zn1–N1'	1.989	1.973	1.975
Zn2–N2	1.989	–	1.975
C3–N1	1.340	1.362	1.356
C3–N2	1.340	1.354	1.356
C2–N2	1.379	1.378	1.377
C1–C2	1.360	1.394	1.387
C1–N1	1.379	1.375	1.377
C3–C4	1.494	1.486	1.482
C4–H1	1.026	1.106	1.103
C4–H2	1.030	1.098	1.097
Angle (º)			
C2–C1–N1	108.2	106.8	107.5
C1–N1–Zn1	126.9	126.3	124.6
C3–N1–Zn1	127.2	126.4	127.5
C1–N1–C3	105.8	107.3	107.8
N1–Zn1–N1'	109.4	109.4	109.8
N1–C3–N2	112.0	110.9	109.4
N1–C3–C4	124.0	123.7	125.3
C1–C2–N2	108.2	108.8	107.5
C2–N2–C3	105.8	106.1	107.8
Zn2–N2–C3	127.2	–	127.5
N2–C3–C4	124.0	125.4	125.3
C3–C4–H1	115.8	111.8	111.1
C3–C4–H2	111.1	110.4	110.7

[a] The structure is defined in Figure A2.

[b] Taken from ref. [84].

[c] B3LYP/6–311++g(2d,2p)–optimized structure.

[d] SCC–DFTB optimized unit–cell–size structure.

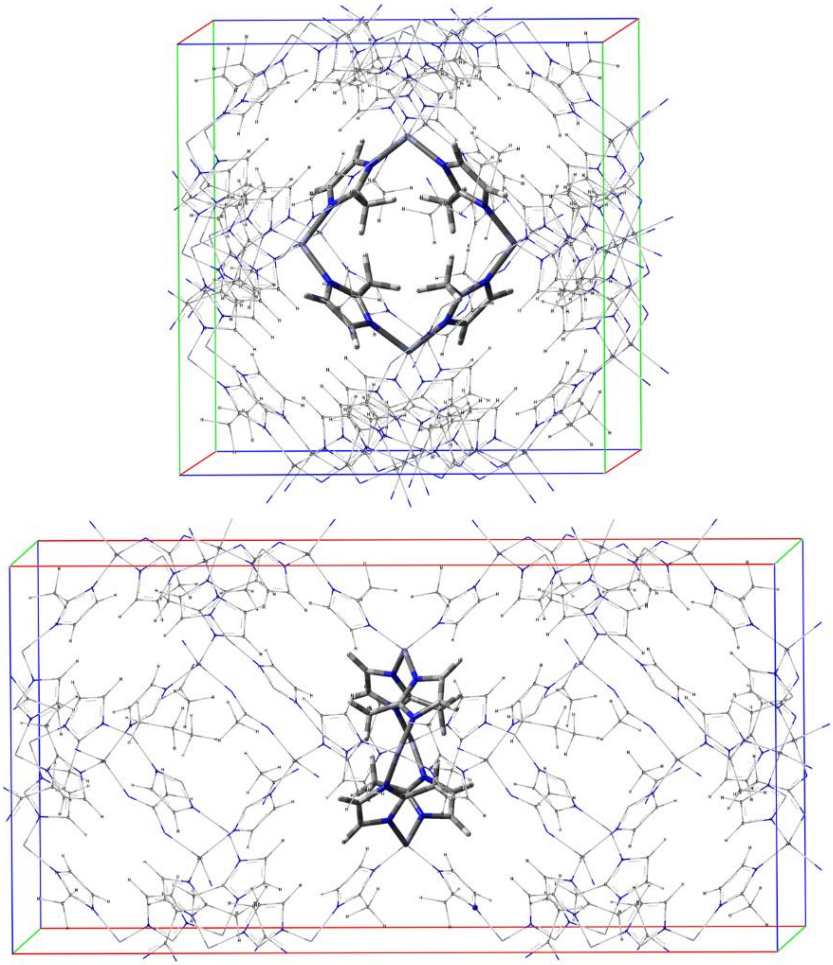

Figure A2 The SCC–DFTB optimized structure of ZIF–8 unit–cell, shown its tetragonal aperture depicted as tube model. The above and bottom graphics are front and side views, respectively. At the corner of the unit-cell cubic box shows hexagonal apertures.

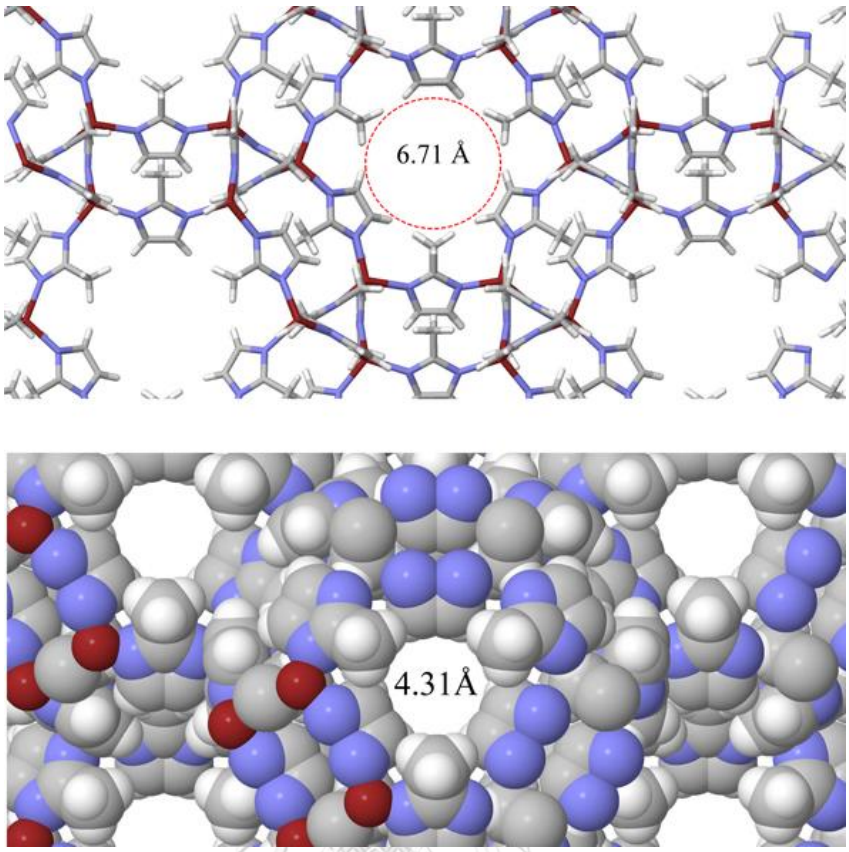

Figure A3 The approximate diameter for hexagonal aperture including van der Waals (VDW) radius of hydrogen atom (1.2 Å [85]) is shown.

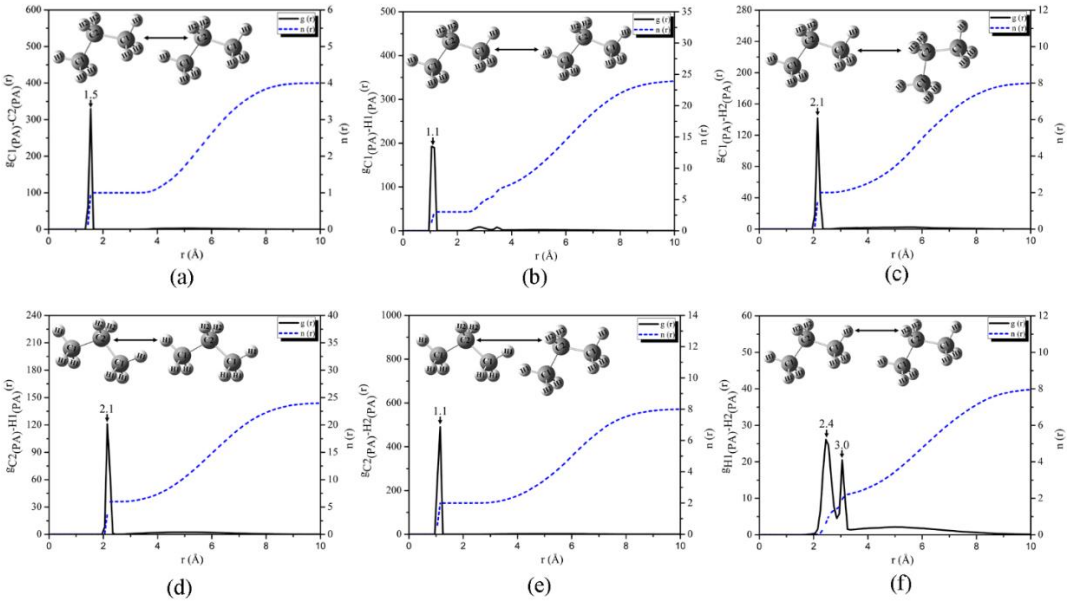

Figure A4 Radial distribution function of propane (4PA) in terms of g(r) (left axis) and n(r) (right axis) in the systems of 4 propane molecules in the ZIF–8 unit–cell.

Table A2 Data extraction from Figure A4.

Type	Peak	Distance	The number of H atom
a	1	1.2–1.4	2.0
	2	3.5–6.0	4.0
b	1	0.9–1.1	2.0
	2	2.5–6.0	28.0
c	1	2.0–2.2	2.5
	2	2.2–8.0	15.0
d	1	2.0–2.2	5.0
	2	2.2–7.0	30.0
e	1	1.0–1.2	2.5
f	1	1.8–3.0	2.5
	2	2.9–3.1	4.0

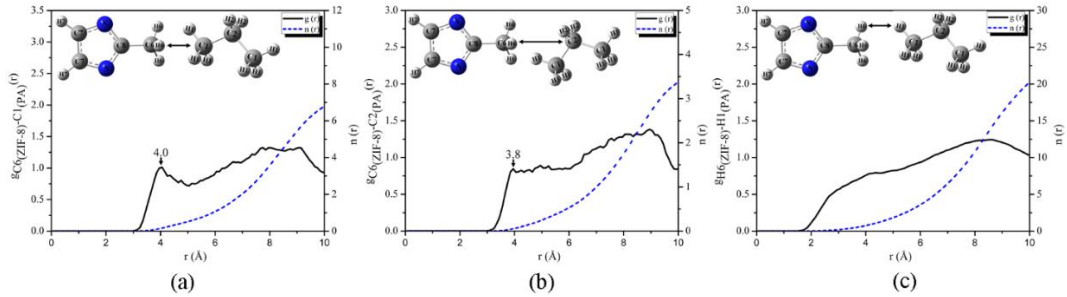

Figure A5 Radial distribution function between ZIF–8 unit–cell and propane (4PA) in terms of g(r) (left axis) and n(r) (right axis) in the systems of 4 propane molecules.

Table A3 Data extraction from Figure A5.

Type	Peak	Distance	The number of H atom
a	1	3.0–5.0	2.5
	2	6.5–10.0	7.0
b	1	3.1–4.1	1.0
	2	4.1–5.1	1.0
	3	6.2–8.0	4.0
c	1	1.9–4.2	10.0
	2	4.2–10.0	20.0

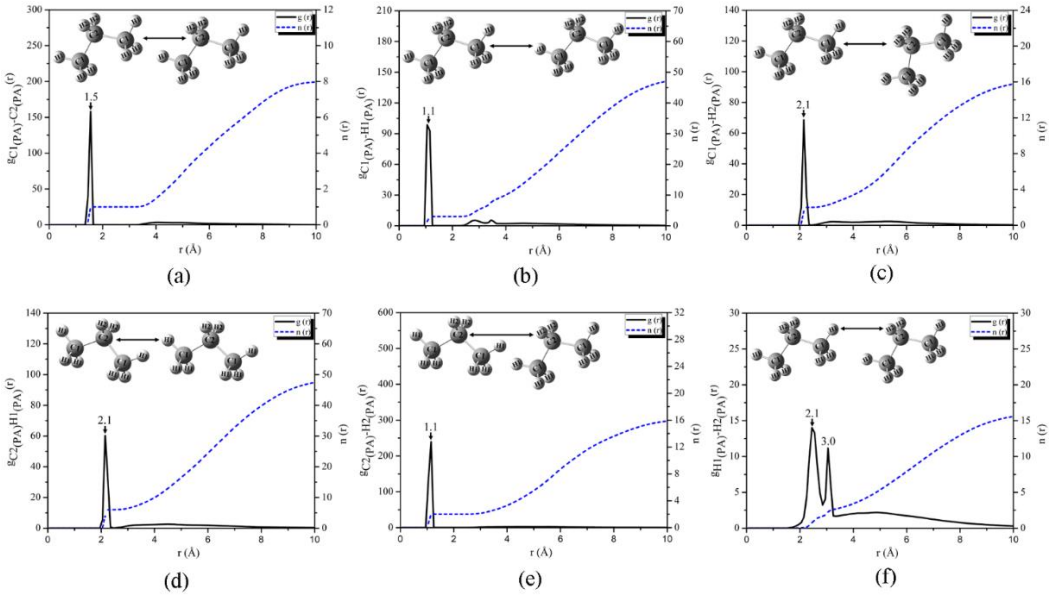

Figure A6 Radial distribution function of propane (8PA) in terms of g(r) (left axis) and n(r) (right axis) in the systems of 8 propane molecules in the ZIF–8 unit–cell.

Table A4 Data extraction from Figure A6.

Type	Peak	Distance	The number of H atom
a	1	1.2–1.6	2.0
	2	3.5–6.0	2.2
b	1	1.0–1.2	2.0
	2	2.5–6.0	28.0
c	1	2.0–2.2	2.5
	2	2.2–7.0	10.5
d	1	1.9–2.1	5.0
	2	3.0–7.0	30.0
e	1	1.0–1.2	2.5
f	1	1.9–2.9	2.0
	2	2.9–3.1	0.5
	3	3.1–10.0	20.0

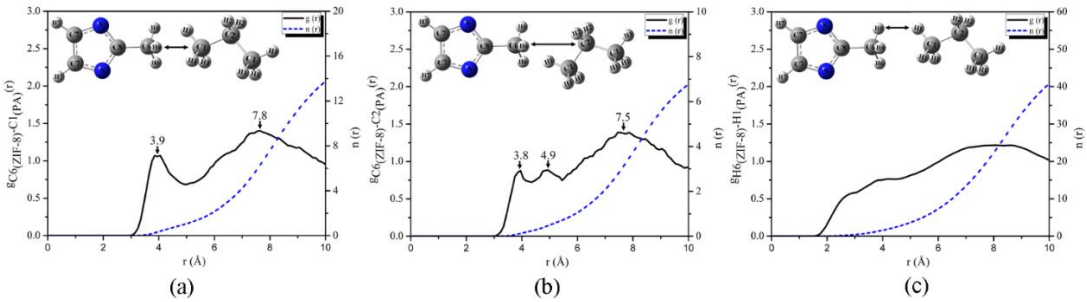

Figure A7 Radial distribution function between ZIF–8 unit–cell and propane (8PA) in terms of g(r) (left axis) and n(r) (right axis) in the systems of 8 propane molecules.

Table A5 Data extraction from Figure A7.

Type	Peak	Distance	The number of H atom
a	1	3.0–4.8	2.5
	2	4.8–10.0	18.5
b	1	3.0–4.5	1.5
	2	4.5–6.2	1.3
	3	6.2–9.0	3.0
c	1	1.8–5.0	8.0
	2	5.0–10.0	24.0

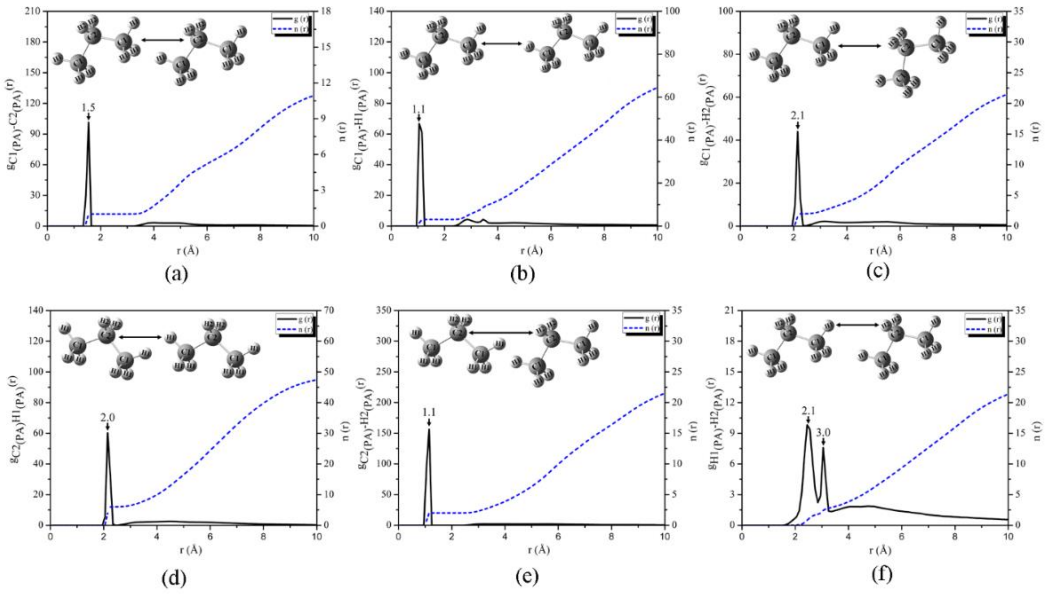

Figure A8 Radial distribution function of propane (12PA) in terms of g(r) (left axis) and n(r) (right axis) in the systems of 12 propane molecules in the ZIF–8 unit–cell.

Table A6 Data extraction from Figure A8.

Type	Peak	Distance	The number of H atom
a	1	1.4–1.6	1.0
b	1	1.0–1.2	2.5
	2	2.5–6.0	17.5
c	1	2.0–2.2	2.0
	2	2.2–8.0	12.0
d	1	2.0–2.2	5.0
	2	2.2–8.0	35.0
e	1	1.0–1.2	2.0
f	1	2.0–2.9	2.2
	2	2.9–3.1	0.3
	3	3.1–10.0	13.8

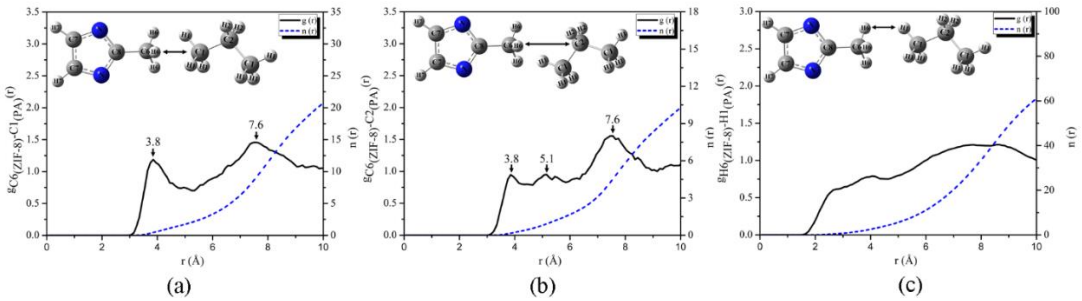

Figure A9 Radial distribution function between ZIF–8 unit–cell and propane (12PA) in terms of g(r) (left axis) and n(r) (right axis) in the systems of 12 propane molecules.

Table A7 Data extraction from Figure A9.

Type	Peak	Distance	The number of H atom
a	1	3.0–5.0	1.5
	2	5.0–10.0	12.5
b	1	2.5–4.2	1.5
	2	4.2–5.2	0.5
	3	5.2–10.0	5.3
c	1	1.9–5.0	5.0
	2	5.0–10.0	35.0

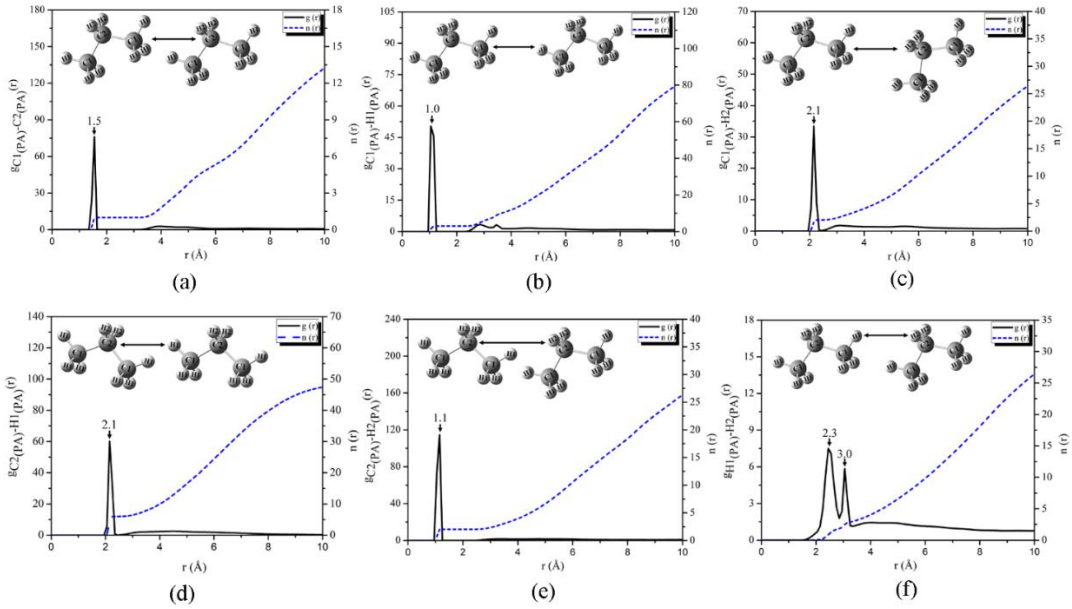

Figure A10 Radial distribution function of propane (16PA) in terms of g(r) (left axis) and n(r) (right axis) in the systems of 16 propane molecules in the ZIF–8 unit–cell.

Table A8 Data extraction from Figure A10.

Type	Peak	Distance	The number of H atom
a	1	1.4–1.6	1.0
b	1	1.0–1.2	4.0
	2	2.5–4.0	4.0
c	1	2.0–2.2	2.0
d	1	2.0–2.2	8.0
e	1	1.0–1.2	3.0
f	1	2.0–2.5	1.8
	2	2.5–3.1	0.2
	3	3.1–8.0	5.2

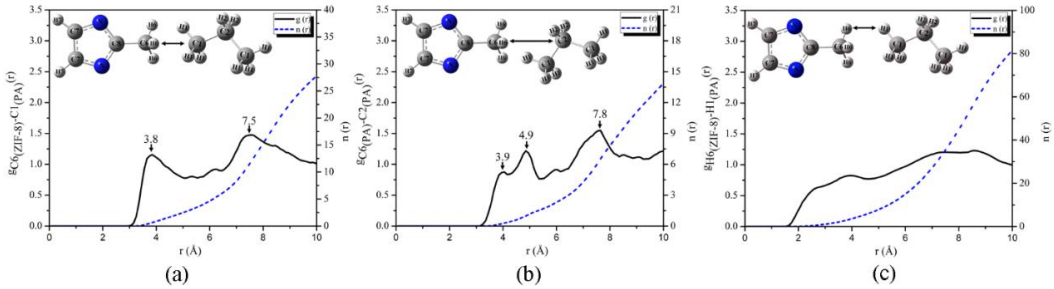

Figure A11 Radial distribution function between ZIF–8 unit–cell and propane (16PA) in terms of g(r) (left axis) and n(r) (right axis) in the systems of 16 propane molecules.

Table A9 Data extraction from Figure A11.

Type	Peak	Distance	The number of H atom
a	1	3.0–5.0	0.8
	2	5.0–10.0	6.2
b	1	3.0–6.0	0.5
	2	6.0–10.0	3.0
c	1	2.0–6.0	4.8
	2	6.0–10.0	15.2

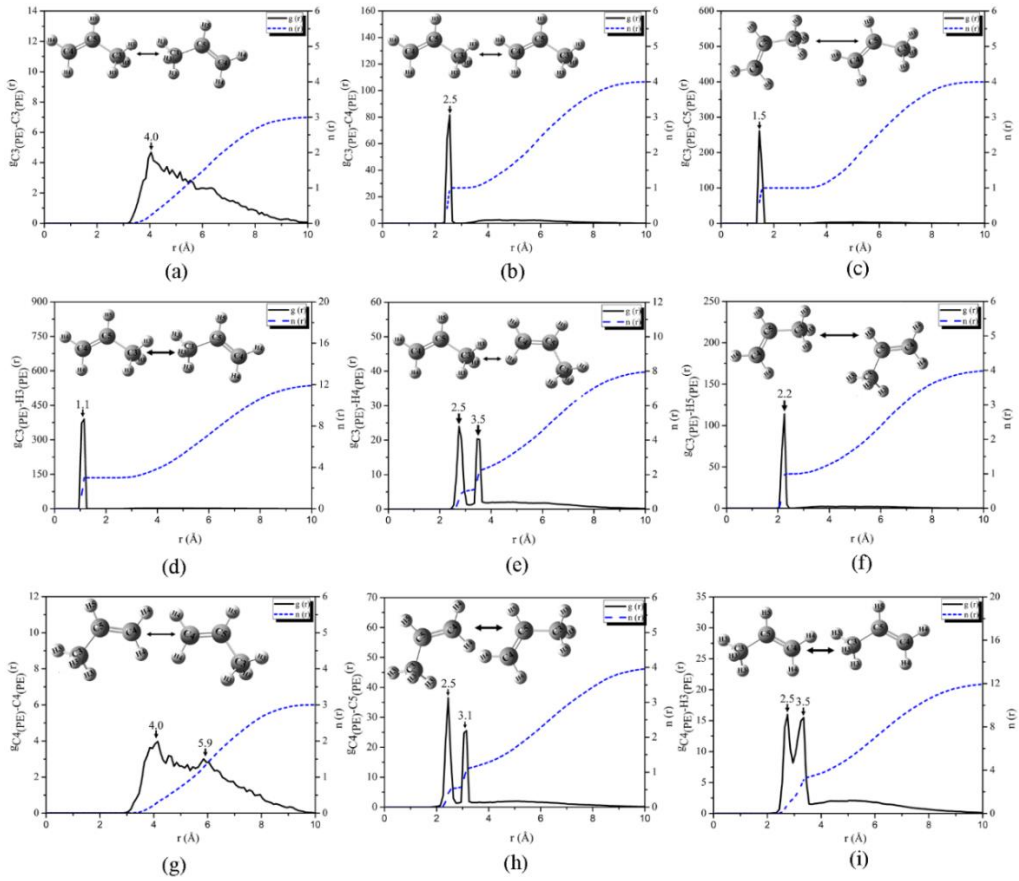

Figure A12 Radial distribution function of propene (4PE) in terms of *g*(r) (left axis) and *n*(r) (right axis) in the systems of 4 propene molecules in the ZIF–8 unit–cell.

Table A10 Data extraction from Figure A12.

Type	Peak	Distance	The number of H atom
a	1	3.1–4.0	3.0
b	1	2.4–2.6	3.0
c	1	1.4–1.6	1.0
d	1	1.0–1.2	3.0
e	1	2.4–3.0	1.0
	2	3.0–3.6	1.0
	3	3.6–8.0	6.0
f	1	2.1–2.3	1.0
g	1	3.0–5.0	0.6
	2	5.0-10.0	2.4
h	1	2.4–2.6	0.5
	2	2.6–3.2	0.5
	3	3.2–8.0	3.0
i	1	2.4–2.6	2.0
	2	2.6–3.6	2.0
	3	3.6–10.0	8.0

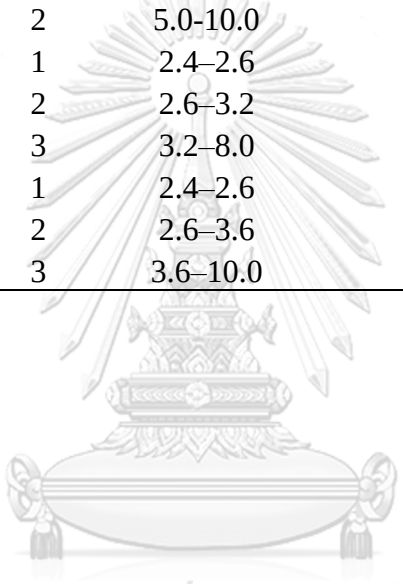

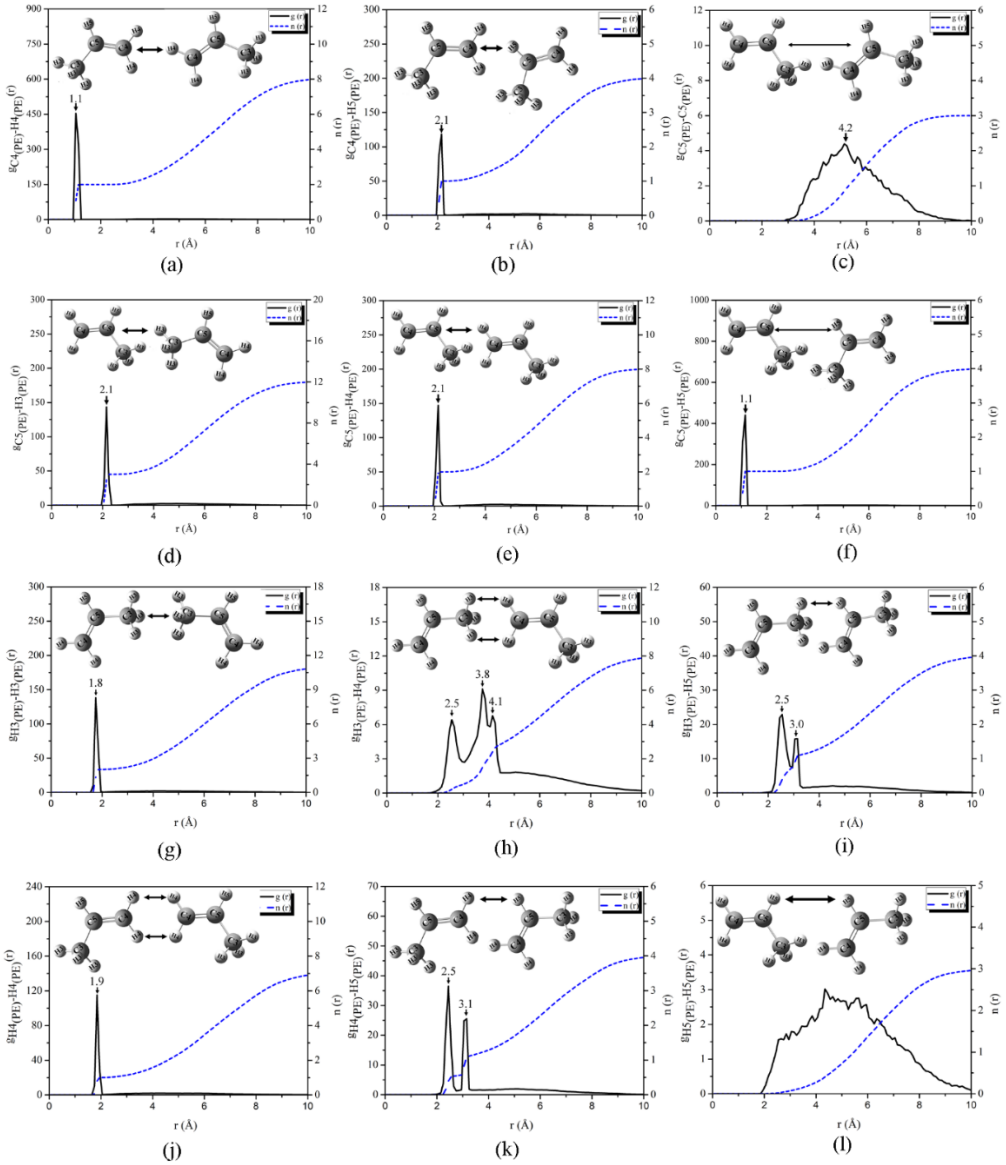

Figure A13 Radial distribution function of propene (4PE) in terms of *g*(r) (left axis) and *n*(r) (right axis) in the systems of 4 propene molecules in the ZIF–8 unit–cell.

Table A11 Data extraction from Figure A13.

Type	Peak	Distance	The number of H atom
a	1	1.0–1.2	2.0
b	1	2.0–2.2	1.0
c	1	3.0–9.0	2.0
d	1	2.0–2.2	2.0
e	1	2.0–2.2	2.0
f	1	1.0–1.2	1.0
g	1	1.7–1.9	1.0
h	1	2.0–3.0	0.5
	2	3.0–4.0	1.5
	3	4.0–4.5	1.0
i	1	2.0–3.0	0.5
	2	3.0–3.5	0.5
	3	3.5–8.0	2.5
j	1	1.8–2.0	1.0
k	1	2.0–3.0	0.5
	2	3.0–3.2	0.5
	3	3.2–8.0	2.5
l	1	2.0–10.0	3.0

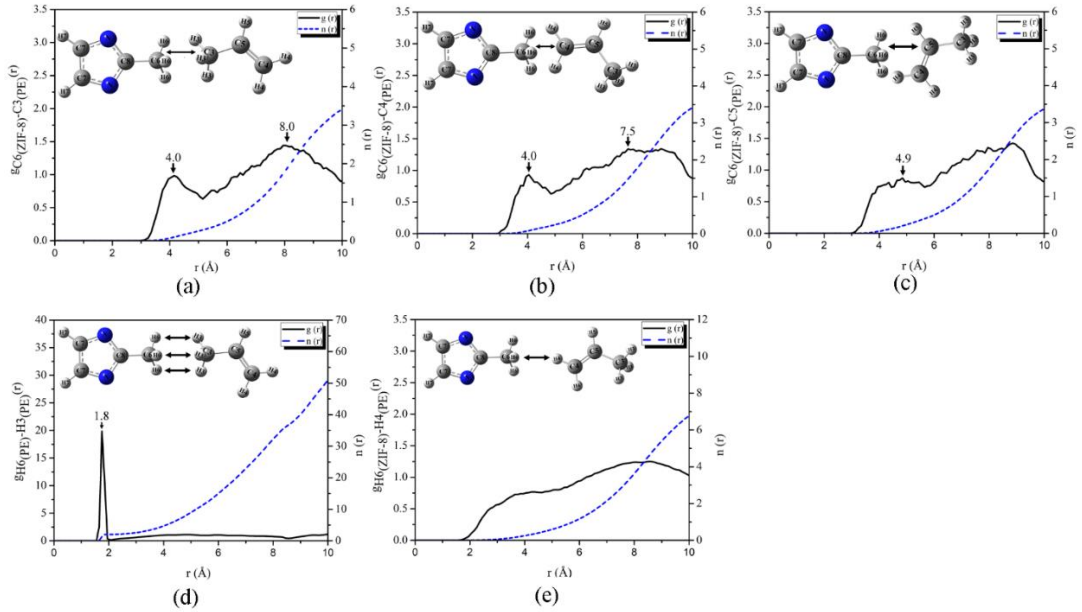

Figure A14 Radial distribution function between ZIF–8 unit–cell and propene (4PE) in terms of g(r) (left axis) and n(r) (right axis) in the systems of 4 propene molecules.

Table A12 Data extraction from Figure A14.

Type	Peak	Distance	The number of H atom
a	1	3.0–5.0	0.2
	2	5.0–10.0	3.3
b	1	3.0–5.0	0.2
	2	5.0–10.0	3.3
c	1	3.0–6.0	0.5
	2	6.0–10.0	3.0
d	1	1.7–1.9	2.0
	2	1.9–8.5	34.0
e	1	2.0–6.0	0.5
	2	6.0–10.0	6.5

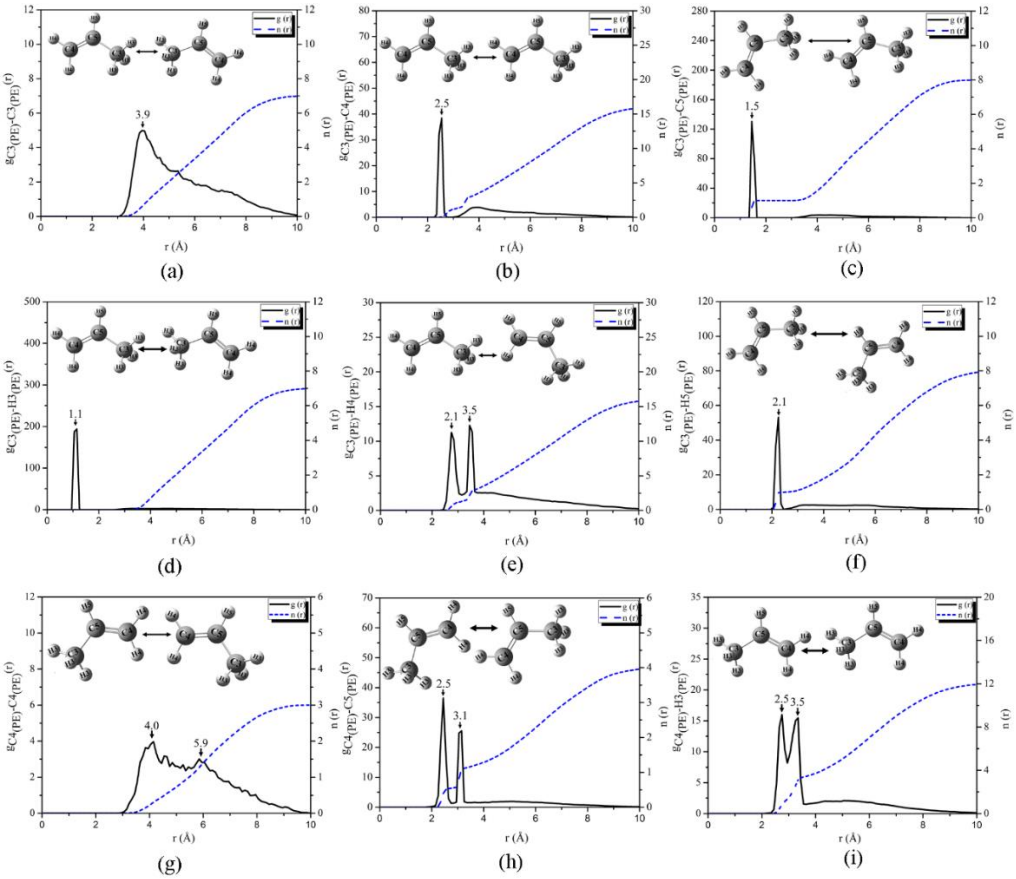

Figure A15 Radial distribution function of propene (8PE) in terms of *g*(r) (left axis) and *n*(r) (right axis) in the systems of 8 propene molecules in the ZIF–8 unit–cell.

Table A13 Data extraction from Figure A15.

Type	Peak	Distance	The number of H atom
a	1	3.0–10.0	7.0
b	1	2.4–3.0	2.0
	2	3.0–8.0	12.0
c	1	1.4–1.6	1.0
d	1	1.0–1.2	1.0
e	1	2.0–2.2	2.0
	2	2.2–3.8	0.5
	3	3.8–10.0	13.5
f	1	2.0–2.2	1.0
	2	2.2–8.0	6.0
g	1	3.0–5.0	0.7
	2	5.0–10.0	2.3
h	1	2.0–3.0	0.5
	2	3.0–3.5	0.5
	3	3.5–8.0	3.0
i	1	2.0–3.0	1.0
	2	3.0–3.5	2.2
	3	3.5–8.0	6.8

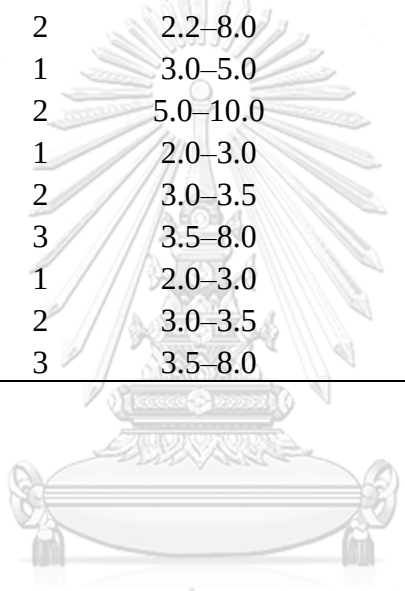

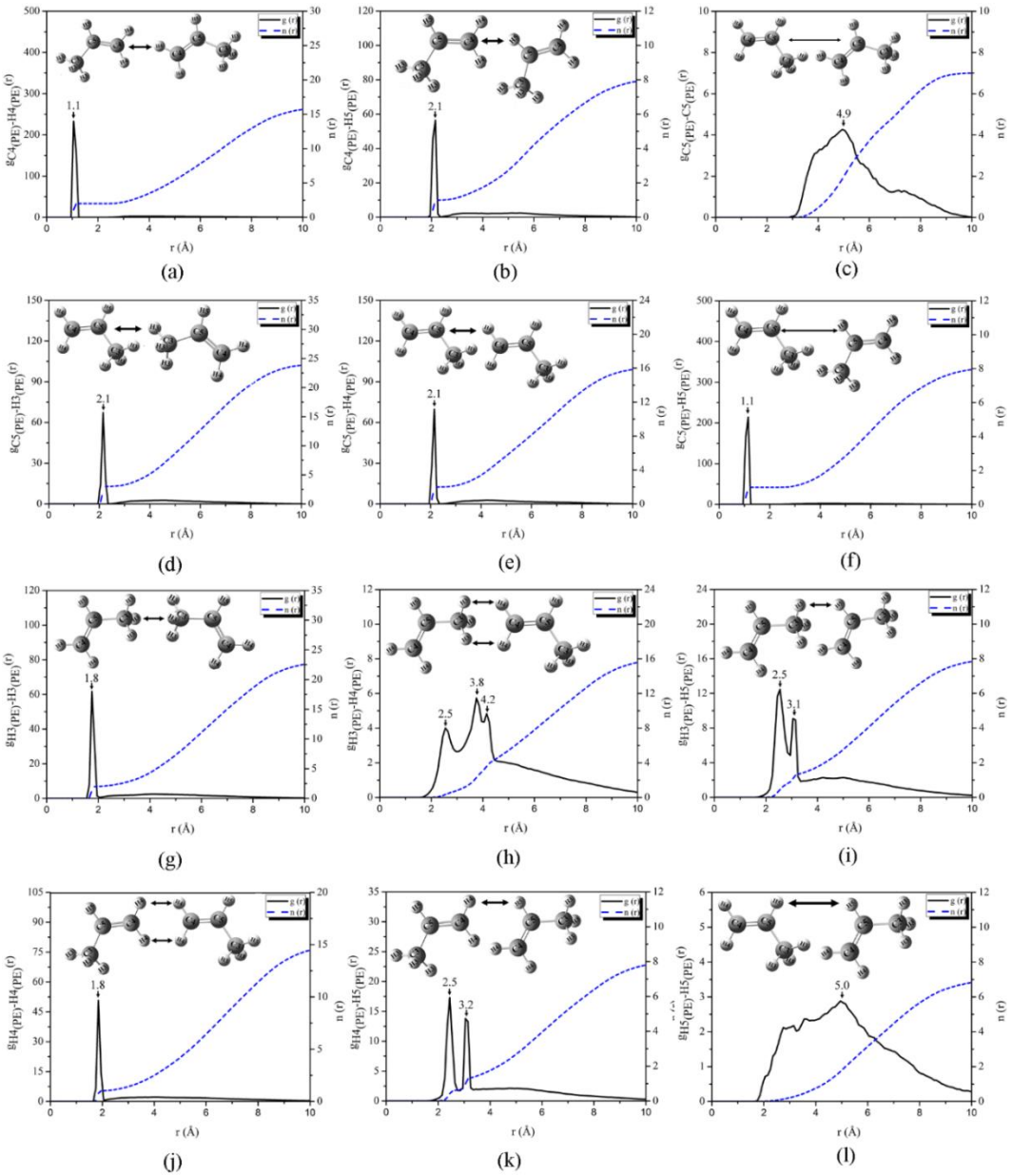

Figure A16 Radial distribution function of propene (8PE) in terms of *g*(r) (left axis) and *n*(r) (right axis) in the systems of 8 propene molecules in the ZIF–8 unit–cell.

Table A14 Data extraction from Figure A16.

Type	Peak	Distance	The number of H atom
a	1	1.0–1.2	2.0
b	1	2.0–2.2	1.0
	2	2.2–8.0	6.0
c	1	3.0–6.8	5.0
	2	6.8–10.0	2.0
d	1	2.0–2.2	2.5
	2	2.2–7.0	15.0
e	1	2.0–2.2	2.0
	2	2.2–8.0	12.0
f	1	1.0–1.2	1.0
g	1	1.7–1.9	2.5
	2	1.9–8.0	16.0
h	1	1.8–3.0	1.0
	2	3.0–4.0	1.0
	3	4.0–4.5	2.0
	4	4.5–10.0	11.0
i	1	2.0–3.0	1.0
	2	3.0–3.5	0.2
	3	3.5–10.0	7.0
j	1	1.7–1.9	1.0
	2	1.9–8.0	12.0

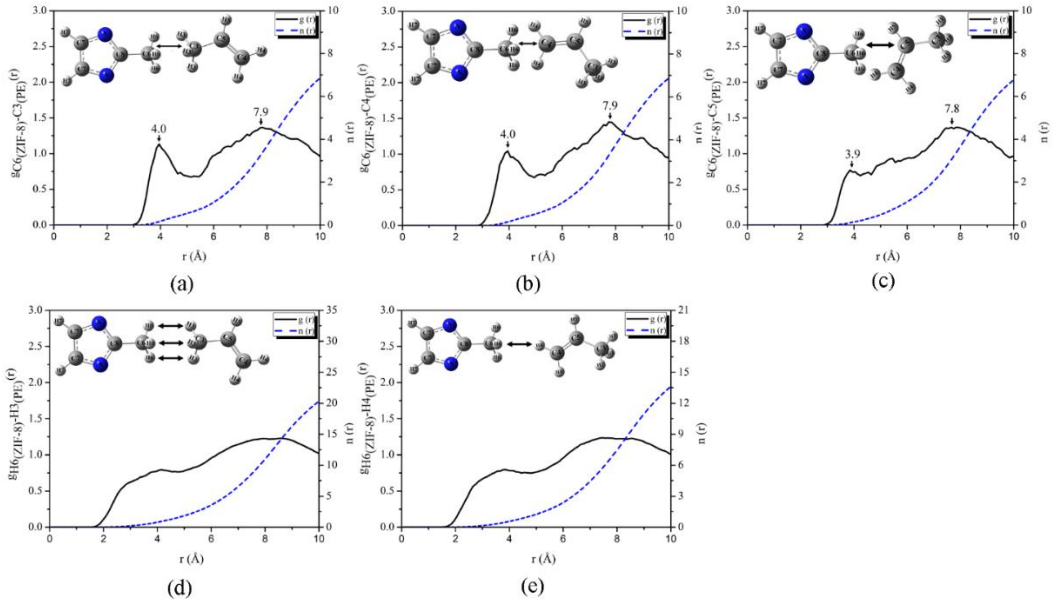

Figure A17 Radial distribution function between ZIF–8 unit–cell and propene (8PE) in terms of g(r) (left axis) and n(r) (right axis) in the systems of 8 propene molecules.

Table A15 Data extraction from Figure A17.

Type	Peak	Distance	The number of H atom
a	1	3.0–5.0	0.5
	2	5.0–10.0	6.5
b	1	3.0–5.0	0.5
	2	5.0–10.0	6.5
c	1	3.0–5.0	0.5
	2	5.0–10.0	6.5
d	1	1.8–5.0	2.0
	2	5.0–10.0	18.0
e	1	1.8–5.0	1.5
	2	5.0–10.0	12.0

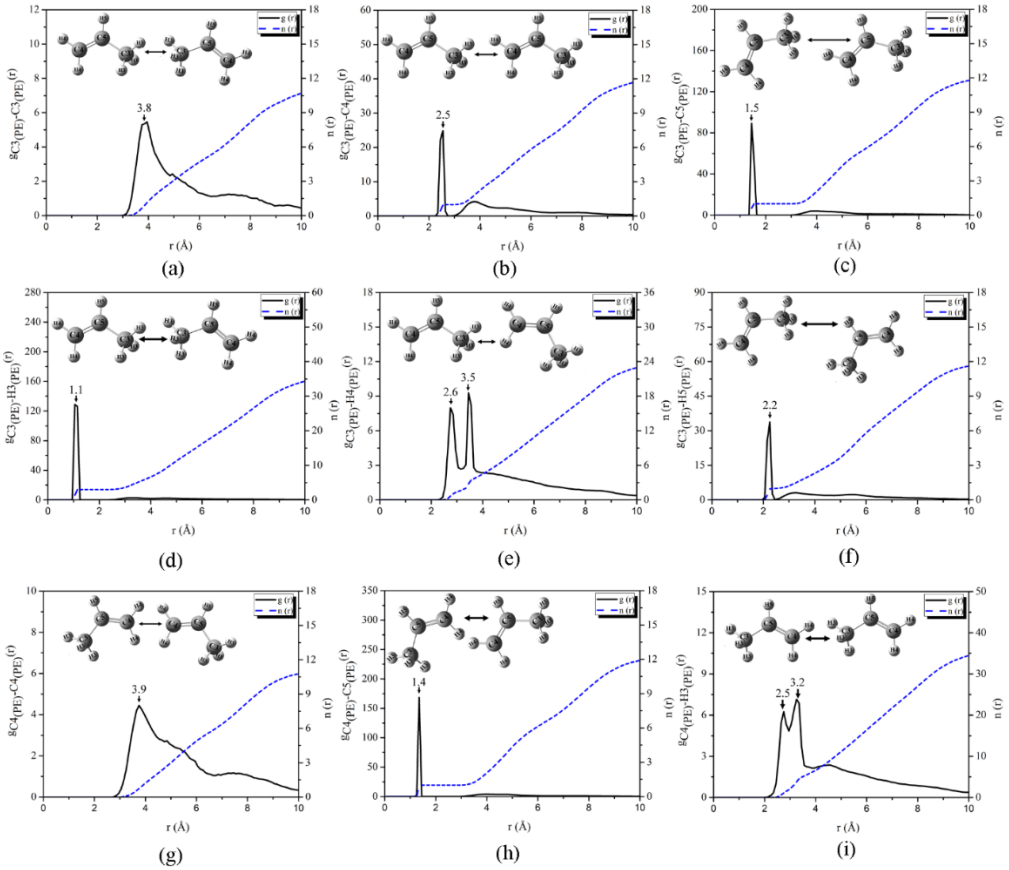

Figure A18 Radial distribution function of propene (12PE) in terms of *g*(r) (left axis) and *n*(r) (right axis) in the systems of 12 propene molecules in the ZIF–8 unit–cell.

Table A16 Data extraction from Figure A18.

Type	Peak	Distance	The number of H atom
a	1	3.0–8.0	5.0
	2	8.0–10.0	6.0
b	1	2.4–2.6	2.0
	2	2.6–10.0	10.0
c	1	1.4–1.6	2.0
	2	1.6–8.0	8.0
d	1	1.0–1.2	5.0
e	1	2.5–3.3	2.0
	2	3.3–3.6	3.0
	3	3.6–10.0	19.0
f	1	2.1–2.3	1.0
	2	2.3–10.0	11.0
g	1	2.4–6.8	6.0
	2	6.8–10.0	5.0
h	1	1.3–1.5	1.0
i	1	2.0–2.6	2.0
	2	2.6-3.3	3.0
	3	3.3–10.0	30.0

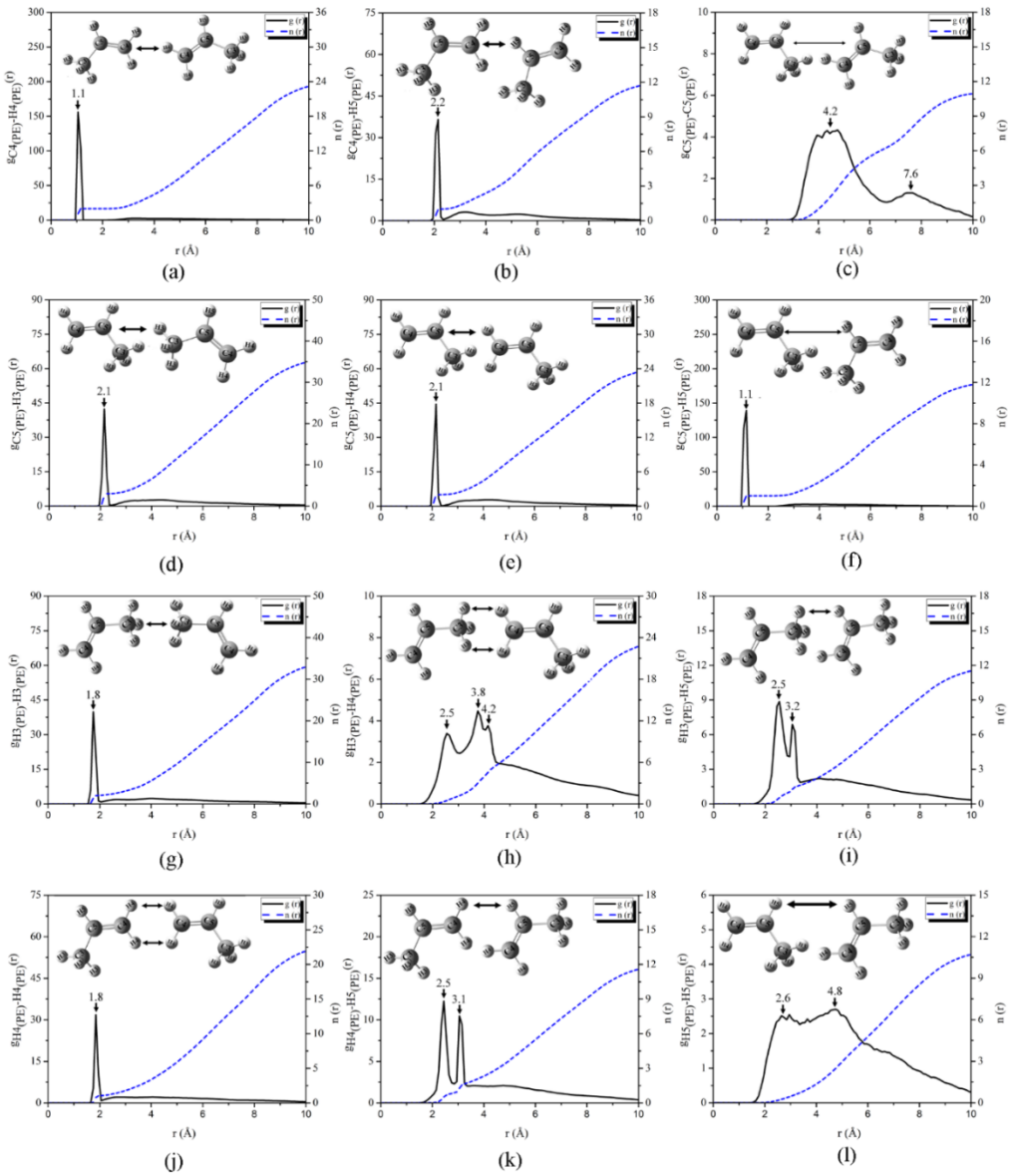

Figure A19 Radial distribution function of propene (12PE) in terms of *g*(r) (left axis) and *n*(r) (right axis) in the systems of 12 propene molecules in the ZIF–8 unit–cell.

Table A17 Data extraction from Figure A19.

Type	Peak	Distance	The number of H atom
a	1	1.0–1.2	2.0
b	1	2.1–2.3	1.0
	2	2.3–10.0	11.0
c	1	3.0–6.5	6.0
	2	6.5–10.0	5.0
d	1	2.0–2.2	2.0
	2	2.2–10.0	33.0
e	1	2.0–2.2	2.0
	2	2.2–10.0	22.0
f	1	1.0–1.2	2.0
g	1	1.7–1.9	2.0
	2	1.9–10.0	31.0
h	1	1.5–3.0	2.0
	2	3.0–4.0	3.0
	3	4.0–4.3	1.0
	4	4.3–10.0	17.0
i	1	2.0–2.6	1.0
	2	2.6–3.3	1.0
	3	3.3–10.0	9.0
j	1	1.7–1.9	1.0
	2	1.9–10.0	21.0
k	1	1.8–2.6	1.0
	2	2.6–3.2	1.0
	3	3.2–10.0	9.0
l	1	1.5–3.5	1.0
	2	3.5–10.0	10.0

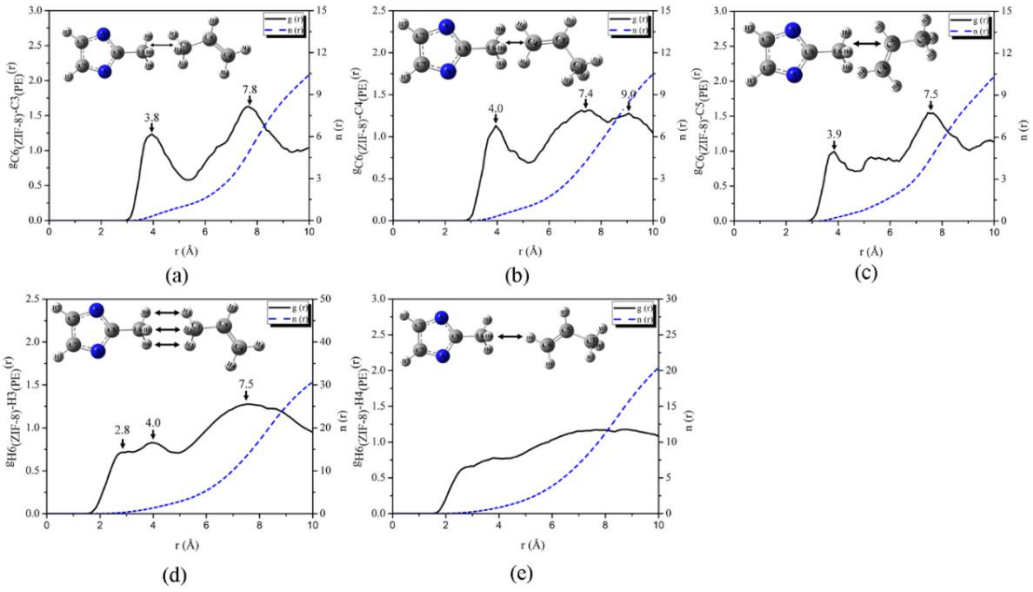

Figure A20 Radial distribution function between ZIF–8 unit–cell and propene (12PE) in terms of g(r) (left axis) and n(r) (right axis) in the systems of 12 propene molecules.

Table A18 Data extraction from Figure A20.

Type	Peak	Distance	The number of H atom
a	1	3.0–5.5	2.0
	2	5.5–10.0	8.0
b	1	3.0–5.5	2.0
	2	5.5–8.0	6.0
	3	8.0–10.0	2.0
c	1	3.0–4.5	1.0
	2	4.5–6.0	1.0
	3	6.0–10.0	8.0
d	1	1.8–3.0	1.0
	2	3.0–5.0	1.0
	3	5.0–10	28.0
e	1	1.8–5.0	2.0
	2	5.0–10.0	18.0

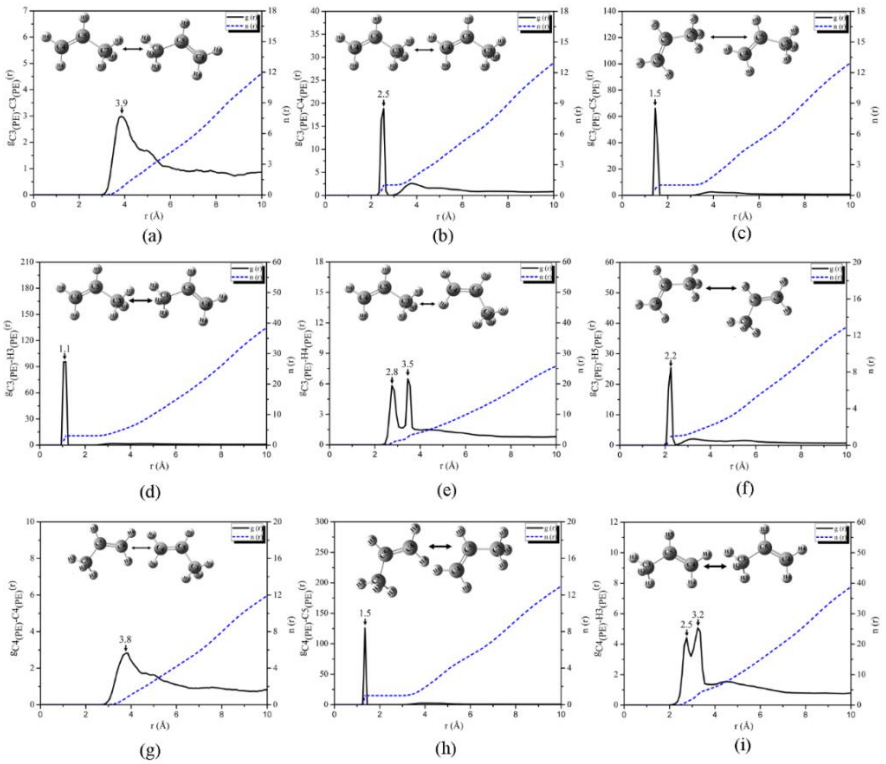

Figure A21 Radial distribution function of propene (16PE) in terms of g(r) (left axis) and n(r) (right axis) in the systems of 16 propene molecules in the ZIF–8 unit–cell.

Table A19 Data extraction from Figure A21.

Type	Peak	Distance	The number of H atom
a	1	3.0–4.2	2.0
	2	4.2–10.0	10.0
b	1	2.0–2.6	1.0
	2	2.6–10.0	12.0
c	1	1.4–1.6	2.0
	2	3.0–8.0	4.0
d	1	1.0–1.2	2.0
e	1	2.5–2.9	2.0
	2	2.9–3.6	1.0
	3	3.6–10.0	22.0
f	1	2.1–2.3	2.0
	2	2.3–10.0	11.0
g	1	3.0–5.0	3.0
	2	5.0–10.0	9.0
h	1	1.4–1.6	1.0
i	1	2.0–2.6	2.0
	2	2.6–3.3	3.0
	3	3.3–10.0	35.0

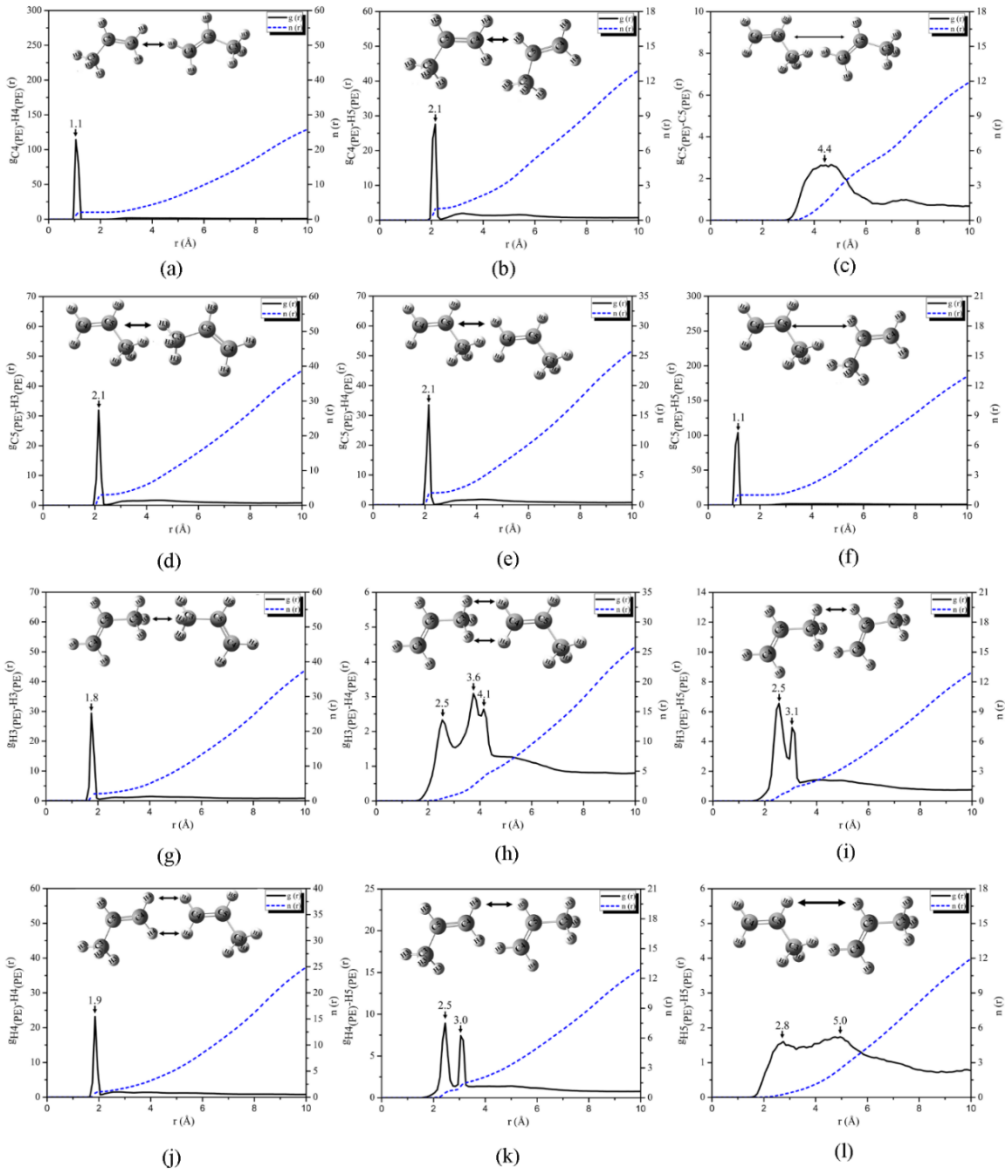

Figure A22 Radial distribution function of propene (16PE) in terms of *g*(r) (left axis) and *n*(r) (right axis) in the systems of 16 propene molecules in the ZIF–8 unit–cell.

Table A20 Data extraction from Figure A22.

Type	Peak	Distance	The number of H atom
a	1	1.0–1.2	1.0
b	1	2.0–2.2	1.0
	2	2.2–10.0	12.0
c	1	3.0–6.2	6.0
	2	6.2–10.0	6.0
d	1	2.0–2.2	1.0
	2	2.2–10.0	38.0
e	1	2.0–2.2	2.0
	2	2.2–10.0	23.0
f	1	1.0–1.2	1.0
g	1	1.7–1.9	1.0
	2	1.9–10.0	35.0
h	1	1.8–3.0	1.0
	2	3.0–3.7	2.0
	3	3.7–10.0	23.0
i	1	1.8–2.6	1.0
	2	2.6–3.3	1.0
	3	3.3–10.0	11.0
j	1	1.8–2.0	1.0
	2	2.0–10.0	24.0
k	1	2.0–2.6	1.0
	2	2.6–3.1	1.0
	3	3.1–10.0	11.0
l	1	1.8–3.0	1.0
	2	3.0–6.0	3.0
	3	6.0–10.0	8.0

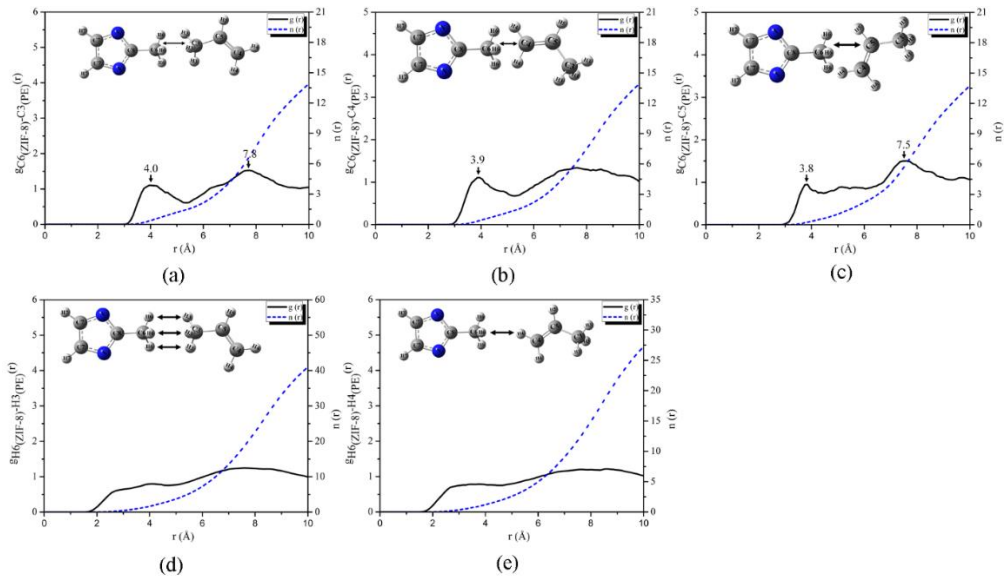

Figure A23 Radial distribution function between ZIF–8 unit–cell and propene (16PE) in terms of g(r) (left axis) and n(r) (right axis) in the systems of 16 propene molecules.

Table A21 Data extraction from Figure A23.

Type	Peak	Distance	The number of H atom
a	1	3.0–5.0	2.0
	2	5.0–10.0	12.0
b	1	3.0–5.0	2.0
	2	5.0–10.0	12.0
c	1	3.0–5.0	2.0
	2	5.0–10.0	12.0
d	1	2.0–5.0	5.0
	2	5.0–10.0	35.0
e	1	2.0–5.0	2.0
	2	5.0–10.0	25.0

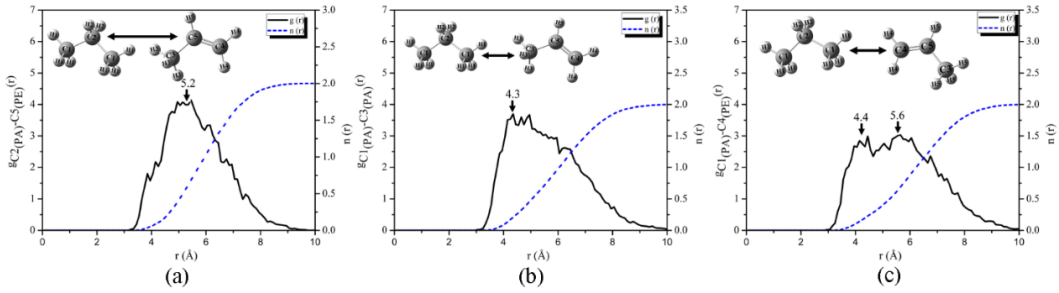

Figure A24 Radial distribution function between 2 propane molecules (2PE) and 2 propene molecules (2PE) in terms of g(r) (left axis) and n(r) (right axis) in the systems of 4 molecules.

Table A22 Data extraction from Figure A24.

Type	Peak	Distance	The number of H atom
a	1	3.0–10.0	2.0
b	1	3.0–10.0	2.0
c	1	3.0–5.0	0.5
	2	5.0–10.0	1.5

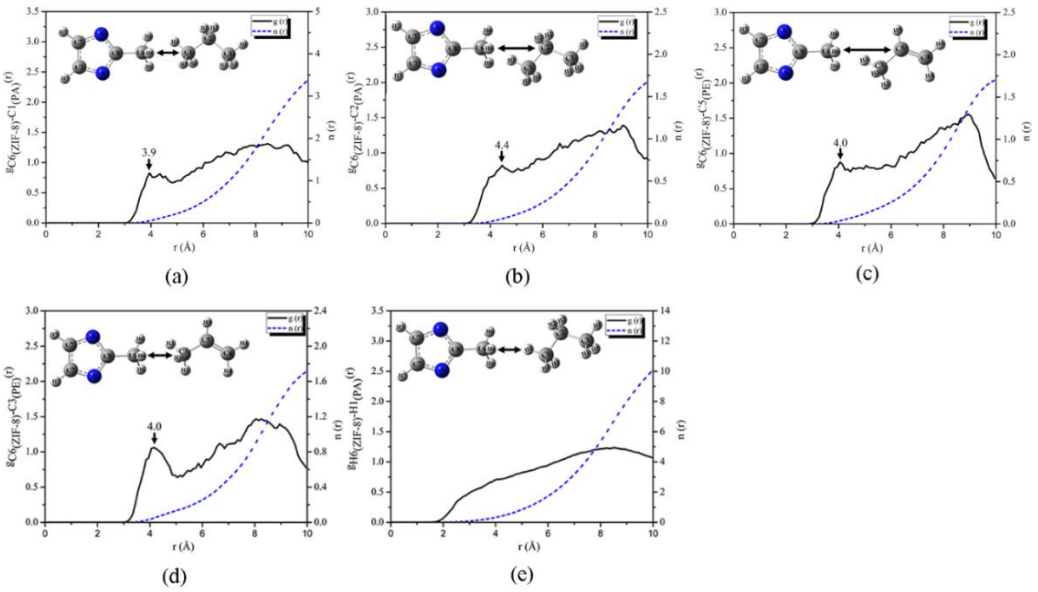

Figure A25 Radial distribution function of 2 propane molecules (2PE), 2 propene molecules (2PE) and ZIF–8 unit–cell in terms of g(r) (left axis) and n(r) (right axis) in the systems of 4 molecules.

Table A23 Data extraction from Figure A25.

Type	Peak	Distance	The number of H atom
a	1	3.0–5.0	0.5
	2	5.0–10.0	3.0
b	1	3.0–5.0	0.5
	2	5.0–10.0	1.0
c	1	3.0–5.0	0.3
	2	5.0–10.0	1.5
d	1	3.0–5.0	0.2
	2	5.0–10.0	1.5
e	1	2.0–6.0	2.0
	2	6.0–10.0	8.0

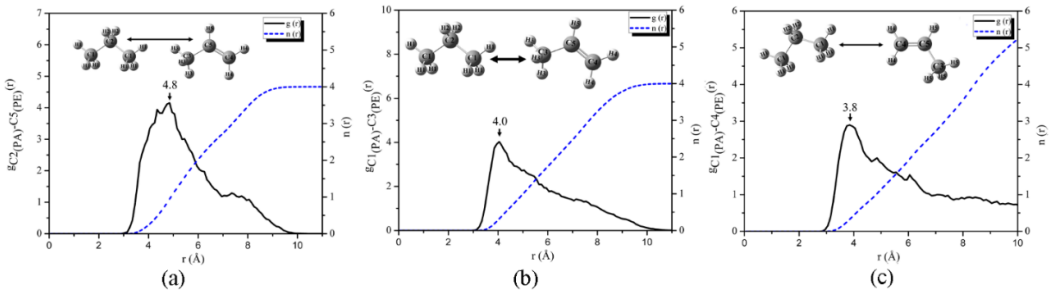

Figure A26 Radial distribution function between 4 propane molecules (4PE) and 4 propene molecules (4PE) in terms of g(r) (left axis) and n(r) (right axis) in the systems of 8 molecules.

Table A24 Data extraction from Figure A26.

Type	Peak	Distance	The number of H atom
a	1	3.0–7.0	3.0
	2	7.0–10.0	1.0
b	1	3.0–10.0	4.0
c	1	3.0–7.0	2.5
	2	7.0–10.0	3.0

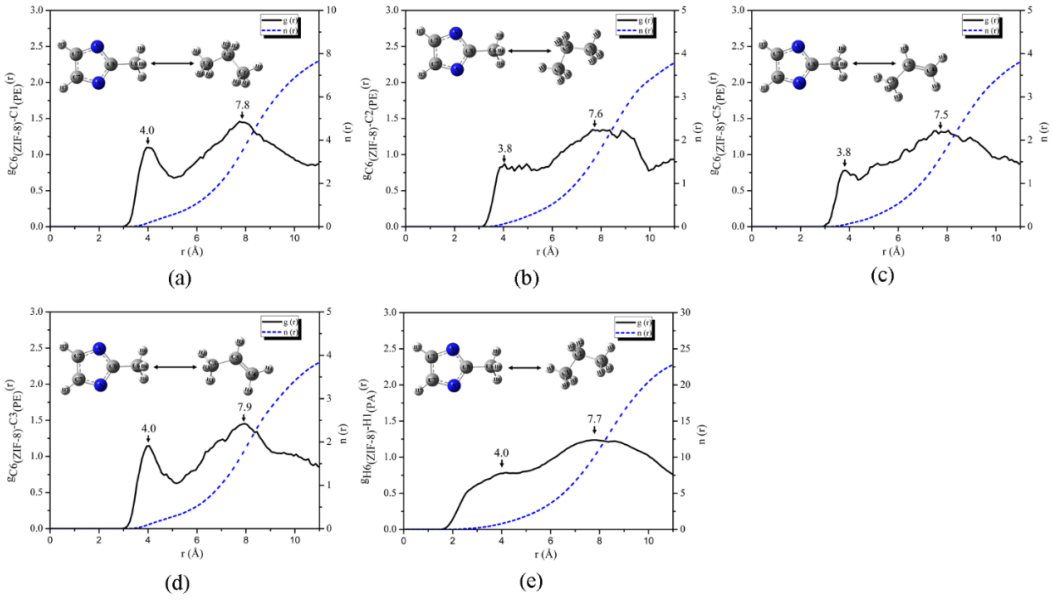

Figure A27 Radial distribution function of 4 propane molecules (4PE), 4 propene molecules (4PE) and ZIF–8 unit–cell in terms of g(r) (left axis) and n(r) (right axis) in the systems of 8 molecules.

Table A25 Data extraction from Figure A27.

Type	Peak	Distance	The number of H atom
a	1	3.0–5.0	1.0
	2	5.0–10.0	7.0
b	1	3.0–5.0	0.5
	2	5.0–10.0	3.5
c	1	3.0–5.0	0.5
	2	5.0–10.0	3.5
d	1	3.0–5.0	0.5
	2	5.0–10.0	3.5
e	1	2.0–5.0	2.0
	2	5.0–10.0	21.0

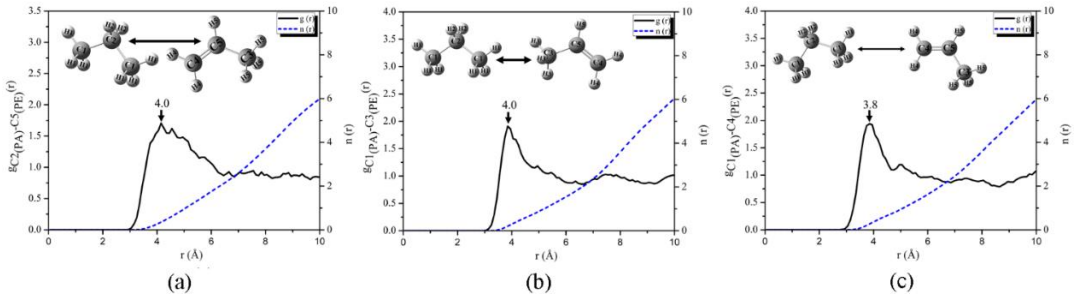

Figure A28 Radial distribution function between 8 propane molecules (8PE) and 8 propene molecules (8PE) in terms of g(r) (left axis) and n(r) (right axis) in the systems of 16 molecules.

Table A26 Data extraction from Figure A28.

Type	Peak	Distance	The number of H atom
a	1	3.0–6.0	2.0
	2	6.0–10.0	4.0
b	1	3.0–6.0	2.0
	2	6.0–10.0	4.0
c	1	3.0–6.0	2.0
	2	6.0–10.0	4.0

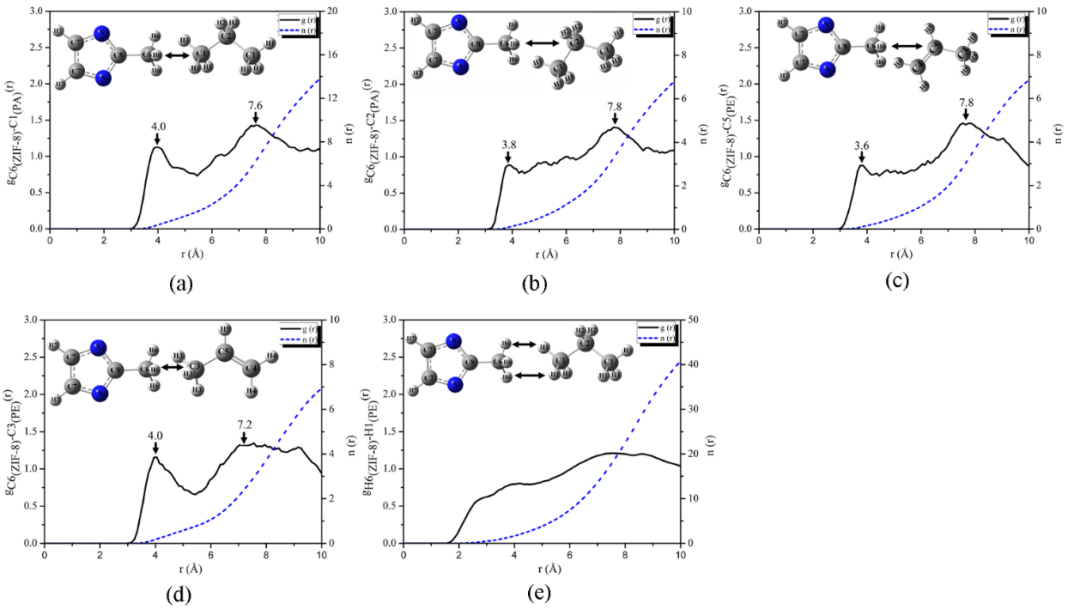

Figure A29 Radial distribution function of 8 propane molecules (8PE), 8 propene molecules (8PE) and ZIF–8 unit–cell in terms of g(r) (left axis) and n(r) (right axis) in the systems of 16 molecules.

Table A27 Data extraction from Figure A29.

Type	Peak	Distance	The number of H atom
a	1	3.0–6.0	2.0
	2	6.0–10.0	12.0
b	1	3.0–6.0	1.0
	2	6.0–10.0	6.0
c	1	3.0–6.0	1.0
	2	6.0–10.0	6.0
d	1	3.0–5.5	1.0
	2	5.5–10.0	6.0
e	1	1.8–5.0	2.0
	2	5.0-10.0	38.0